

Marco Denicolai:

# Tesla Transformer for Experimentation and Research



Lisensiaatintyö / Licentiate Thesis

Työn valvoja: Prof. Tapani Jokinen

Työn ohjaaja: Dos. Martti Aro

Espoossa 30 May 2001.

Author:	Marco Denicolai	
Title of the Thesis:	Tesla Transformer for Experimentation and Research	
Title in Finnish:	Koe- ja tutkimustoimintaan tarkoitettu Tesla-muuntaja	
Date:	30 May 2001	Number of Pages: 96
Department:	Electrical and Communications Engineering	Chair: Electromechanics
Supervisor:	Prof. Tapani Jokinen	
Instructor:	Chief Eng. Martti Aro	
<p>The Tesla Transformer is an electrical device capable of developing high potentials ranging from a few hundreds of kilovolts up to several megavolts; the voltage is produced as AC, with a typical frequency of 50 - 400 kHz.</p> <p>The Tesla Transformer has been known for more than a century to the scientific community and has been used in several applications. Yet some of the effects involved with its operation, which are pretty unique to this kind of device, and the theory underneath them, still deserve a certain amount of research to be fully explained and justified.</p> <p>This work concentrates on the design and construction of a versatile Tesla Transformer that can be easily used for measurements and general research. The task is, therefore, to minimize the number of stochastic and unknown parameters influencing the device functionality.</p> <p>First, the different possibilities to implement a Tesla Transformer and its power supply are explored, pointing out pros and cons of each solution. Then, a medium-sized apparatus is designed and built using off-the-self components. The theory of operation is described using a classical approach, together with some innovative concepts.</p> <p>A model of the transformer is built using a standard simulation package and a set of preliminary measurements of the main components' values. Finally, the model is validated by practical measurements indicating its correctness.</p>		
Keywords:	Tesla coil, Tesla transformer, CCPS, resonance	
Not borrowable till:	Library code:	

Tekijä:	Marco Denicolai	
Työn nimi:	Koe- ja tutkimustoimintaan tarkoitettu Tesla-muuntaja	
Title in English:	Tesla Transformer for Experimentation and Research	
Päivämäärä:	30 May 2001	Sivumäärä: 96
Osasto/Laitos:	Sähkö- ja tietoliikennetekniikka	Professori: Sähkömekaniikka
Työn valvoja:	Prof. Tapani Jokinen	
Työn ohjaaja(t):	Dos. Martti Aro	
<p>Tesla-muuntaja on sähkölaite, joka pystyy tuottamaan suuria potentiaaleja; muutamista sadoista kilovolteista muutamiin megavolteihin. Jännite on vaihtojännite ja sen taajuus on 50 – 400 kHz.</p> <p>Tesla-muuntaja on tiedeyhteisölle tuttu 1900-luvun alusta lähtien ja sitä on käytetty monessa sovelluksessa. Siitä huolimatta monet muuntajan käyttöön liittyvät ainutlaatuiset ilmiöt ja niiden teoria kaipaavat vielä lisätutkimuksia.</p> <p>Tämä työ keskittyy koe- ja tutkimustoimintaan tarkoitettun Tesla-muuntajan suunnitteluun ja rakentamiseen: tavoitteena on pienentää toimintaan vaikuttavien stokastisten ja tuntemattomien parametrien määrää.</p> <p>Aluksi Tesla-muuntajan ja siihen tarvittavan virtalähteen toteuttamisvaihtoehdot on tutkittu, jokaisen hyviä ja huonoja puolia on tarkasteltu. Seuraavaksi keskikokonen Tesla-muuntaja on suunniteltu ja rakennettu käyttämällä yleisesti saatavia komponentteja. Toimintateoria on kuvattu käyttämällä perinteistä lähestymistapaa sekä uusia näkökulmia.</p> <p>Tesla-muuntajasta on rakennettu malli, jonka pohjana on käytetty kaupallista simulaatio-ohjelmistoa sekä pääkomponenttien mittaustuloksia. Lopuksi malli on todettu käyttökelpoiseksi vertailemalla simulaatio- ja mittaustuloksia.</p>		
Avainsanat:	Tesla-muuntaja, teslakuristin, CCPS, resonanssi	
Ei lainata ennen:	Työn sijaintipaikka:	

This page intentionally left blank

## ***PREFACE***

*Undertake something that is difficult; it will do you good. Unless you try to do something beyond what you have already mastered, you will never grow.*

— *Ronald E. Osborn*

This project has truly been a learning experience, being the first three lessons learned *patience, patience* and again *patience*.

Special thanks (in no particular order) go to all those who contributed to the accomplishment of this work:

- Mika Salkola, for initially turning my attention to Tesla Coils.
- My two kids, Taneli and Matias, for helping me winding Thor's secondary coil (about 1000 meters of copper wire).
- Martti Aro and Jari Hällström for their help and directions to get around problems.
- The High Voltage Institute staff at the HUT for their help in practical matters.
- Malcolm Watts, Antonio Carlos M. de Queiroz and Terry Fritz for helping me understanding the theory of operation of the Tesla Coil.
- Paul Nicholson and all members of the Tesla Secondary Simulation Group for their excellent research work in simulating the secondary coil.
- Bill Wysock for supplying the bulky primary capacitor and the rotating spark gap.
- Imatran Voiman Säätiö, for supporting this work by granting me a scholarship.
- All members of the Tesla mailing List for their support and interest during all the phases of Thor's development.

And, last but not least, thanks to my wife Kaija for understanding me when I was transporting the big toroid on the top of my car, during my neverending coil winding sessions, and for her support during all these "Tesla years".

*Marco Denicolai*

*Espoo, Finland, 24 May, 2001*

This page intentionally left blank

## ***LIST OF SYMBOLS AND ACRONYMS***

<b>AC</b>	Alternate Current
<b>BJT</b>	Bipolar Junction Transistor
<b>CCPS</b>	Capacitor Charging Power Supply
<b>DC</b>	Direct Current
<b>EMF</b>	ElectroMagnetic Force
<b>IC</b>	Integrated Circuit
<b>IGBT</b>	Insulated Gate Bipolar Transistor
<b>GTO</b>	Gate Turn-Off Thyristor
<b>HDPE</b>	High-Density Polyethylene
<b>HUT</b>	Helsinki University of Technology
<b>HF</b>	High Frequency
<b>H.P.</b>	Horse Power
<b>HV</b>	High Voltage
<b>H/D</b>	Height/diameter ratio
<b>KAPTON<sup>1</sup></b>	Polyimide
<b>MOS</b>	Metal Oxide Semiconductor
<b>MOSFET</b>	Metal Oxide Semiconductor Field Effect Transistor
<b>MTO</b>	MOS Turn-Off Thyristor
<b>MYLAR<sup>2</sup></b>	Polyester
<b>OPAMP</b>	Operational Amplifier
<b>PCB</b>	Printed Circuit Board
<b>PTFE</b>	Polytetrafluorethylene
<b>PVC</b>	Polyvinyl Chloride
<b>Q</b>	Quality-factor, a 'figure of merit' of an oscillating circuit
<b>RF</b>	Radio Frequency
<b>R.P.M.</b>	Revolutions Per Minute
<b>TC</b>	Tesla Coil, Tesla Transformer, resonance transformer
<b>TEFLON<sup>3</sup></b>	Polytetrafluorethylene
<b>THOR</b>	The Tesla Coil built within this thesis
<b>VARIAC</b>	Variable transformer

---

<sup>1</sup> Kapton is a registered trademark of DuPont

<sup>2</sup> Mylar is a registered trademark of DuPont

<sup>3</sup> Teflon is a registered trademark of DuPont

This page intentionally left blank

# CONTENTS

<b>LIST OF FIGURES.....</b>	<b>VII</b>
<b>LIST OF TABLES.....</b>	<b>IX</b>
<b>1. INTRODUCTION.....</b>	<b>1</b>
1.1. Structure of this thesis .....	1
1.2. Nikola Tesla .....	1
1.3. The Tesla Coil .....	2
1.4. Applications .....	3
1.4.1. Testing of insulating materials .....	3
1.4.2. Testing of insulators .....	4
1.4.3. Generation of high-voltage pulses .....	4
1.4.4. Research on lightning discharges .....	4
1.5. Previous work.....	4
1.6. Project goals .....	6
<b>2. TESLA COIL TOPOLOGIES AND VARIATIONS.....</b>	<b>8</b>
2.1. Simplified theory of operation .....	8
2.2. Alternative coupling schemes .....	10
2.2.1. 3-coils, inductive coupling .....	10
2.2.2. 3-coils, series feed .....	10
2.3. Static vs. rotary spark gap .....	11
2.4. AC vs. DC power supply.....	11
2.5. DC power supply topologies .....	12
2.5.1. Conventional stabilized DC power supply .....	13
2.5.2. DC power supply employing a high-voltage switch element .....	14
2.5.3. High-frequency converter .....	15
2.6. Effect of increased pulse rate .....	16
2.7. Pulsed vs. continuous wave.....	16
2.8. Tesla Coil physical dimensions.....	17
<b>3. DESIGN SPECIFICATION AND MAIN SOLUTIONS.....</b>	<b>18</b>
3.1. Excitation mode and topology.....	18
3.2. Spark gap selection.....	18
3.3. Power supply selection.....	18
3.4. Power supply requirements .....	20
3.5. Tesla Coil dimensions .....	22
3.6. Material selection .....	22
<b>4. TESLA COIL DESIGN .....</b>	<b>24</b>
4.1. General .....	24
4.2. Secondary design.....	25
4.3. Top terminal design.....	26
4.4. Primary capacitor choice .....	26
4.5. Primary design.....	27
4.6. Filter design.....	28
<b>5. POWER SUPPLY DESIGN .....</b>	<b>29</b>
5.1. System design.....	29
5.2. High-frequency converter.....	30
5.2.1. Theory of operation .....	30

5.2.2.	Bridge switch design.....	34
5.2.3.	Resonant load design .....	36
5.2.4.	Step-up transformer design.....	36
5.3.	High voltage probe .....	41
5.4.	Controller.....	42
5.5.	Module interconnection and auxiliary circuitry.....	44
5.6.	Assembly and mechanics.....	44
<b>6.</b>	<b>TESLA COIL MODELING AND MEASUREMENTS .....</b>	<b>48</b>
6.1.	Detailed theory of operation .....	48
6.1.1.	Air-coupled resonant circuits.....	48
6.1.2.	Conditions for maximum voltage gain .....	51
6.1.3.	Conditions for complete energy transfer.....	55
6.1.4.	Inductance and capacitance of a close-wound solenoid.....	58
6.2.	Measurement results .....	63
6.2.1.	Secondary circuit components .....	63
6.2.2.	Primary circuit components .....	64
6.2.3.	Secondary voltage waveform.....	66
6.3.	Simulation model.....	68
6.3.1.	Secondary coil simulation.....	68
6.3.2.	Spark gap simulation .....	71
6.3.3.	Overall simulation model .....	73
6.4.	Comparison of measurement against simulation results .....	75
<b>7.</b>	<b>CONCLUSIONS AND FUTURE WORK.....</b>	<b>77</b>
7.1.	Conclusions .....	77
7.2.	Future work.....	78
	<b>REFERENCES .....</b>	<b>79</b>

## LIST OF FIGURES

Figure 1: Portrait of Nikola Tesla.....	2
Figure 2: “Apparatus for transmitting electrical energy” [Tes14].....	2
Figure 3: Tesla’s first air-cored transformer [Tes91].....	5
Figure 4: Another version of Tesla’s air-cored transformer [Tes94]. .....	5
Figure 5: Tesla Coil basic schematic diagram.....	8
Figure 6: Inductively coupled primary and secondary circuits in a TC.....	9
Figure 7: Top terminal voltage for a single spark gap pulse. ....	9
Figure 8: From left to right, basic TC, 3-coil inductively coupled TC and 3-coil series feed TC. ....	10
Figure 9: MicroSim model of a conventional DC power supply. ....	13
Figure 10: MicroSim simulation results for the conventional power supply.....	14
Figure 11: Power supply employing a high-voltage switch. ....	14
Figure 12: Power supply employing a high-frequency converter. ....	16
Figure 13: Series-loaded resonant converter.....	19
Figure 14: Maximum available pulse peak voltage vs pulse rate. ....	21
Figure 15: Maximum power provided to the Tesla Coil vs pulse rate.....	21
Figure 16: Power supply architecture.....	29
Figure 17: Basic block diagram of one converter module. ....	30
Figure 18: Series-loaded resonant converter.....	31
Figure 19: MicroSim simulation of the SLR converter. ....	32
Figure 20: SLR converter simulation waveforms. ....	32
Figure 21: Converter full-bridge schematic diagram. ....	35
Figure 22: Simulation of transformer primary voltage and current at charge beginning (left) and end (right). ....	38
Figure 23: Simulation of the transformer current (lower trace) and of its voltage integrated over time (upper trace). ....	39
Figure 24: High voltage probe schematic diagram. ....	42
Figure 25: CCPS controller module schematics. ....	43
Figure 26: CCPS modules’ interconnection.....	44
Figure 27: The CCPC rack housing. ....	45
Figure 28: One of the plug-in converter modules. ....	45
Figure 29: Resonant load PCB assembly. ....	46
Figure 30: The resonant load assembled in its plug-in frame. ....	46
Figure 31: Primary winding organization. ....	47
Figure 32: Secondary winding organization. ....	47
Figure 33: Inductively coupled primary and secondary circuits in a TC. ....	48
Figure 34: $G/G_L$ gain vs. tuning ratio $T$ for different $m$ values [Phu91].....	52
Figure 35: $K_1$ gain vs. tuning ratio $T$ for different $m$ values.....	53
Figure 36: Total energy transfer after 10 primary cycles (see cursor) with $k=0.161$ , in correspondence of the second notch. ....	57
Figure 37: Energy transferred and transfer time vs. coupling coefficient. ....	58
Figure 38: Modeling of the secondary coil capacitances [Nic00].....	59
Figure 39: Primary circuit resonance frequency vs. primary coil tap position.....	64
Figure 40: Primary and secondary coils coupling coefficient vs. primary elevation. ....	65
Figure 41: Primary coil inductance vs. tap position.....	66
Figure 42: Typical secondary voltage waveform, with four beats. ....	67
Figure 43: Zoomed first two beats from Figure 42. ....	67

Figure 44: Another secondary voltage waveform sample. ....67  
Figure 45: A third secondary waveform sample, with three beats only. ....67  
Figure 46: Secondary voltage waveform when leaders are produced. ....68  
Figure 47: Secondary voltage waveform with a ground discharge. ....68  
Figure 48:  $C_{int}(x,y)$  for  $y=10$  vs. coil position.....68  
Figure 49:  $C_{ext}(x)$  vs. coil position.....68  
Figure 50: Module and phase of the secondary coil base impedance vs. frequency. ....69  
Figure 51: Voltage gain of the secondary coil vs. frequency. ....70  
Figure 52: Voltage and current distribution (module) of the secondary coil at 66.49 kHz....70  
Figure 53: Voltage and current distribution (phase) of the secondary coil at 66.49 kHz.....70  
Figure 54: Voltage gradient of the secondary coil along its height. ....71  
Figure 55: Spark gap simulation model. ....72  
Figure 56: Transfer function of the spark gap simulation model ( $I_{scale}=0.01, R_{scale}=1$ ). ....73  
Figure 57: Thor's overall simulation model.....74  
Figure 58: Measured secondary voltage waveform (unloaded condition). ....76  
Figure 59: Simulated secondary voltage waveform. ....76

**LIST OF TABLES**

Table 1: Absolute maximum ratings for the IRG4PH40UD device .....	34
Table 2: Transformer design specification.....	37
Table 3: Characteristics of the U100/57/25-3C90 core .....	37
Table 4: Maximum gain as a function of tuning ratio and coupling coefficient [Phu91].....	55
Table 5: Some of the values of k that ensure complete energy transfer if T=1 [Deq02] .....	56
Table 6: Primary circuit resonance frequencies .....	64
Table 7: Primary and secondary coils coupling coefficient .....	65
Table 8: Primary coil inductance vs. tap position.....	66
Table 9: Predicted and measured secondary resonance frequencies.....	71
Table 10: Predicted equivalent reactances at 66.49 kHz.....	71

This page intentionally left blank

# 1. INTRODUCTION

The Tesla Transformer is a fascinating device capable of creating spectacular effects: by generating high-voltage pulses with several megavolts of amplitude, it emits electrical discharges that easily extend for several meters and remind natural lightning.

The Tesla Transformer has been known for more than a century to the scientific community and also used in several applications. A significant amount of papers, articles and books have been written about its theory of operation and its practical construction.

Still, nearly every university high-voltage laboratory and technology museum strives to own a Tesla Transformer, because some of the effects involved with its operation are pretty unique to this kind of device and the theory underneath them still deserves a certain amount of research to be fully explained and justified.

On January 1999 the construction of a medium-sized Tesla Transformer was started at the High Voltage Institute of the Helsinki University of Technology (HUT). The Tesla Transformer to be built was named “Thor”, after the god from the Nordic mythology who was capable of emitting lightning from its powerful hammer.

## 1.1. Structure of this thesis

Chapter 1 provides the reader with the minimal amount of background needed to understand the context of this thesis and the reasons why this project was undertaken. First a basic biography of Nikola Tesla, the inventor of the Tesla Transformer, is presented. Then an introduction to the Tesla Transformer and its main applications is given. Finally, the previous work in this area is concisely reviewed and the project goals are stated.

Chapter 2 is a review of the different possibilities to build a Tesla Transformer, with a discussion of the benefits and penalties implied by each solution. Reading of this chapter helps to understand the choices made in Chapter 3 for building Thor and its power supply.

Chapter 4 reports the mathematical procedure used to design the main components of Thor (primary coil, secondary coil, etc.) and Chapter 5 is a detailed description of Thor’s switching power supply. In Chapter 6 the theory of operation of the Tesla Transformer is described in detail: a simulation model is built and its validity is tested against actual measurements. Finally, Chapter 7 lists the conclusions and outlines the research plans for the future.

## 1.2. Nikola Tesla

Nikola Tesla was born in Smijlan, Croatia in 1856. He attended the Technical University of Graz, Austria, and the University of Prague (1879-1880). His first employment was in a government telegraph engineering office in Budapest, where he made his first invention, the loudspeaker. In 1882 Tesla went to work in Paris for the Continental Edison Company, and constructed his first induction motor.

Tesla moved to America in 1884. In May 1885, George Westinghouse, head of the Westinghouse Electric Company in Pittsburgh, bought the patent rights to Tesla's polyphase system of alternating-current dynamos, transformers, and motors. In 1887 Tesla established his own laboratory in New York City, where he performed countless experiments including work on a carbon button lamp, on the power of electrical resonance, and on various types of lighting. Tesla also invented the fluorescent lights and a new type of steam turbine.

A controversy between alternating current and direct current advocates raged in 1880s and 1890s, featuring Tesla and Edison as leaders in the rival camps.

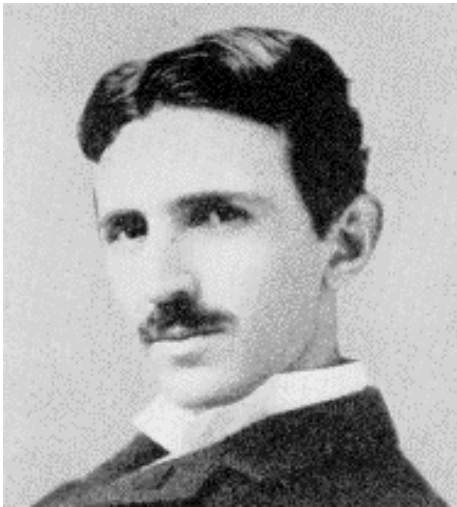


Figure 1: Portrait of Nikola Tesla.

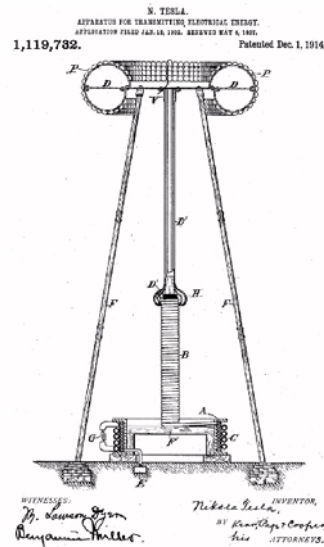


Figure 2: “Apparatus for transmitting electrical energy” [Tes14].

In Colorado Springs, where he stayed from May 1899 until early 1900, Tesla made what he regarded as his most important discovery - terrestrial stationary waves. By this discovery he proved that the earth could be used as a conductor and would be as responsive as a tuning fork to electrical vibrations of a certain pitch. In this period he also conducted the majority of experiments intended to develop a way to wirelessly transmit electrical energy to consumer appliances.

Tesla had a way of intuitively sensing hidden scientific secrets and employing his inventive talent, but was quite impractical in financial matters. Returned to New York in 1900, because of a lack of funds, his ideas kept remaining in his notebooks, which are still today examined by engineers for unexploited clues. He died in 1943, the holder of more than 100 patents.

### 1.3. The Tesla Coil

Among Tesla’s inventions, the resonance transformer occupies a place of its own. Originally named as “Apparatus for transmitting electrical energy” in its patent [Tes14] dated 1914 (Figure 2), it was intended for transferring electrical energy without wires to lamps and possibly other devices. Following the original Tesla’s concept, the emission of electrical discharges from the top of the transformer was an unwanted effect that he considered as the release of a “security valve”. The Tesla resonance transformer is nowadays better known as Tesla Coil or simply resonance transformer. In the rest of this paper the Tesla Coil will be referred to as TC.

A TC is an electrical device capable of developing high potentials typically ranging from a few hundreds of kilovolts up to several megavolts. The voltage produced is AC, being the voltage frequency typically 50 - 400 kHz. TCs are typically operated in pulsed mode, with pulse widths varying from some nanoseconds up to several hundreds of microseconds according to the particular application.

In its simpler configuration, a TC is composed by two air-cored coils, named primary and secondary coils. While in conventional metal- and ferrite-core transformers the primary and secondary voltage ratio is directly related to the windings number of turns ratio, the output voltage of a TC it is related to primary and secondary inductance ratio.

Different groups of people have been interested in Tesla Coils during all the past century:

- In the first half of the 20<sup>th</sup> century industry have manufactured small-sized TCs to generate high-voltage for a number of classical applications (X-ray generators, electrocution and coagulation for veterinary purposes, etc.). Nowadays the TCs used in most of these applications have been replaced by conventional technology using discrete electronic components.
- Research groups have replicated Tesla's original TC designs and produced new ones, according to the increasing number of materials becoming available (plastics and insulators in general). Many attempts have been made to complete the rudimental measurements Nikola Tesla originally performed and provide a robust and proven mathematical model covering all operational principles of TCs.
- The spectacular leader inception produced by TCs, that closely remind downsized natural lightning, has attracted the film industry from its very beginning. TCs are still today manufactured and used to produce special effects in movies and theatre shows.
- TCs have fascinated a number of hobbyists all around the world that have engaged in building low-cost, small- and medium-sized TCs in their garages. These individuals have had an enormous influence in the demolition and replacement of existing theories about TC operational principles.

## ***1.4. Applications***

Nowadays, applications for Tesla Coils fall within the following categories.

### ***1.4.1. Testing of insulating materials***

Insulation materials used in high-voltage switched-mode power supplies are exposed to high frequency high voltages. Traditional tests performed with high DC voltages might not reveal the true aging effects occurring during rated operation; successful experiments have been conducted using high-frequency, high-voltage power sources [Har98].

Cored transformers are not preferred for generating high test voltages at high frequencies, since they must employ ferrite instead of iron and therefore are quite costly for the power required by these applications. Furthermore, the reactive power needed by the capacitive load of the sample under test has to pass also through the transformer and be supplied to it.

Ferrite-cored resonance transformers have small dimensions but a comparatively high stray capacitance that is in the order of the sample capacitance. The ferrite core also produces high flux non-linear effects that result in unacceptable harmonics.

The Tesla Coil avoids non-linear effects because it is air-cored. As the size of its coils is bigger, the distance between its windings can be bigger as well, so that the stray capacitance becomes smaller. Options are available to increase the test voltage level and to modify the voltage frequency.

### **1.4.2. Testing of insulators**

Although it is difficult to control the generated wave-shapes, the damped high frequency oscillations of Tesla Coils are somewhat similar to typical transient disturbances found in power systems (e.g. caused by switching operations or by arcing to ground).

Manufacturers of ceramic insulators are still using TCs as a test source in routine tests for puncture withstand. They are also employed for generic insulator testing [Phu91] and synthetic testing of circuit breakers [Dam87].

### **1.4.3. Generation of high-voltage pulses**

Sources of short high-voltage pulses with high repetition rate are considered to be of interest for a number of problems. For instance, they can be used to generate electromagnetic radiation to measure objects to a high precision or powerful microwave pulses with 3-cm wavelength [Gub97].

Numerous papers have been published with particular emphasis on the use of a TC in relativistic electron beam generators [Hof75, Mat82]: its main advantages over the Marx generator are high repetition rates of operation and low cost because of the lower number of capacitors used.

Tesla Coil use is also reported in a series of compact and portable devices to drive cold-cathode e-beam tubes and X-ray tubes [Mes95]; applications include express spectral analysis of minerals and jewels, as well as rapid radiography on-field.

### **1.4.4. Research on lightning discharges**

Research on natural lightning has been motivated by the desire to prevent spectacular accidents, such as occurred in 1969 during the launch of Apollo 12 [God70] and in 1987 during the launch of Atlas-Centaur 67 [Bus87].

While cloud-to-ground lightning has been studied more extensively, cloud-to-cloud and cloud-to-air discharges still need to be understood more thoroughly as they are more difficult to be measured [Uma87]. Field observations of lightning can reveal directly little of the physics of the phenomenon; the propagation process and the leader velocity are best studied by scaling of laboratory sparks [Les77, Les81]. In pre-war work Allibone and Meek had succeeded to demonstrate the existence of a laboratory analogue to the lightning stepped leader discovered by Schonland in 1933 [Wat96].

## **1.5. Previous work**

The first record of Tesla's air-cored transformer is dated 1891 and appeared in one of his patents [Tes91], where the high voltage developed was intended to be used for electric lighting. The circuit converted low frequency currents into "currents of very high frequency and very high potential" which then supplied single terminal lamps (Figure 3). A much more refined version of the same circuit appeared in a subsequent patent [Tes94], where the spark gap had been moved in parallel to the feeding power supply and the primary capacitor had been split in two (Figure 4). Nikola Tesla, as he quoted in some of his patents, tested a huge number of circuitual variations along several years, but patented only a few of them.

The first mathematical analysis of Tesla's air-cored transformer is due to Oberbeck [Obe95]: he treated the transformer as two air-coupled resonant circuits and covered thoroughly the case where the two circuits are tuned to resonate at the same frequency. In a later paper, dated 1904, Drude [Dru04] pointed out the conditions required to achieve the

maximum voltage at the secondary circuit (that is, a unitary tuning ratio but a coupling coefficient of 0.6).

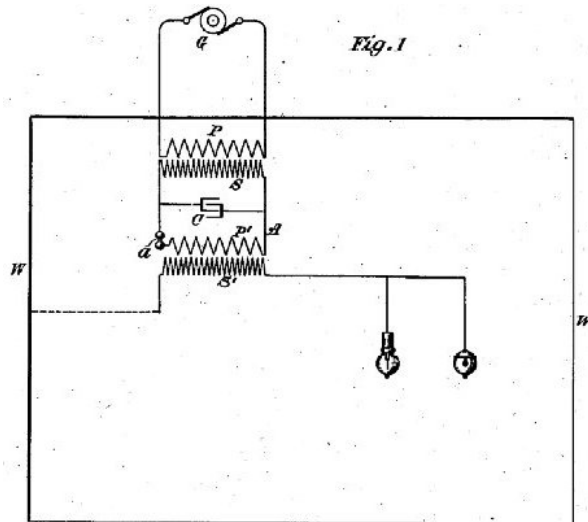


Figure 3: Tesla's first air-cored transformer [Tes91].

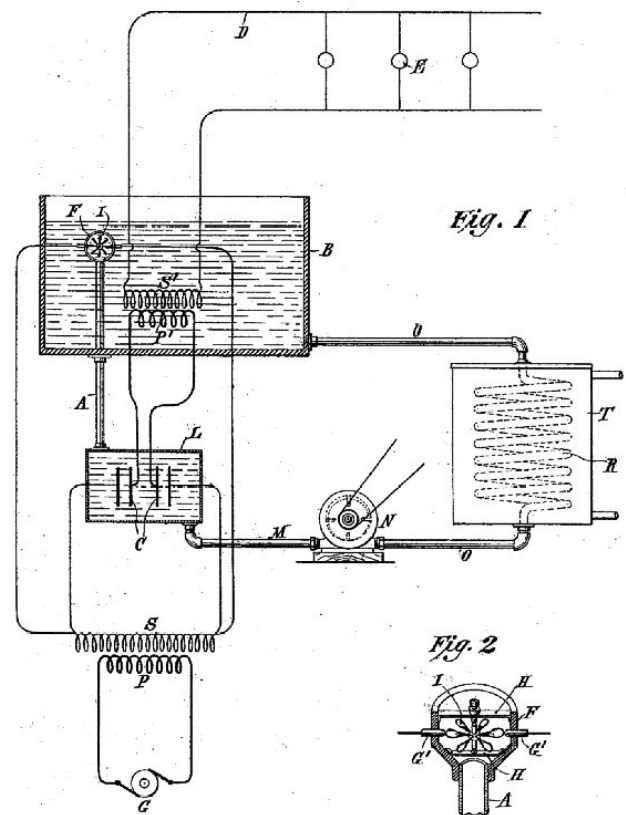


Figure 4: Another version of Tesla's air-cored transformer [Tes94].

A series of presentations of the air-coupled resonant circuits theory appeared in a number of books and papers all along the last century. These analysis are basically similar to each other, differing only in the level of detail or the degree of clearness. Some of the classical references are listed below:

- Terman [Ter43], with a pragmatic view of the influence of Q factor and coupling coefficient on the energy transfer efficiency.
- Smythe [Smy50], giving a thorough (but someway complicated) analysis of lossy and lossless circuits.
- Craggs & Meek [Cra54], providing straightforward results.

As only the case of ideal (i.e. lossless) circuits could be solved in a closed form, the lossy case was always tabulated or presented as family of curves [Ter43], only recently produced by using computer algorithms ([Hof75, Mat82, Hit83]).

The search for an optimal working point of the Tesla Coil evolved along two axis, targeting either the maximum output voltage or a complete energy transfer from the primary to the secondary circuits. In 1988, Reed [Ree88] observed that an 18% increase in voltage could be obtained by using a tuning ratio less than unity and a suitable amount of coupling. Reed's work was generalized in 1991 by Phung et al. [Phu91] that provided a set of equations

in order to calculate all tuning ratio and coupling coefficients pairs that achieved a (local) maximum output.

In 1966, Finkelstein [Fin66] identified the general conditions required for a complete energy transfer from the primary to the secondary circuits: in all cases, a unitary tuning ratio was required. The Drude's conditions turned out to achieve complete energy transfer in the least time, but other values of coupling coefficient could also be used, while the transfer completion got simply moved to a later time instant.

Finkelstein's work was continued and extended to three coupled resonance circuits by Bieniosek [Bie90] and eventually generalized to any number of circuits by de Queiroz [Deq00, Deq01]. The importance of these works is that they can be easily applied to the particular case of the Tesla Coil (two-circuit case) in order to obtain complete energy transfer and, therefore, a better efficiency.

The previous work dealing with Tesla Coils provides only partial views of the whole theory of operation involved. All the papers aimed at maximizing the voltage developed at the top terminal, or at achieving a complete energy transfer, use a simple lumped-element model for the secondary circuit. In some rare case the coil and its top load have been modeled using transmission line theory [Cor87, Cor99]. Both approaches have shown (or pretended to show) a good match with experimental results, while starting from a controversial view of the phenomena. This difference of view has started a long debate among different parties, involving merely hobbyists and being ignored by the scientific community.

Descriptions of TC construction details can only be found in material written by hobbyists and justification of the solutions adopted is often missing or based on rules-of-the-thumb. A reference that encompasses all the parts of a TC, following the energy transformations from the power supply to the leader inception into free air is missing.

## 1.6. Project goals

The goal of this project is to design and build a medium-sized Tesla Coil suitable for performing experiments and measurements in a rational and controlled manner. This can be achieved if the following requirements are satisfied:

- The TC is constructed according to design drawings; dimensions are well known and an accurate modeling is possible.
- The TC size is sufficient to easily allow for insertion of measurement transducers (current probes, field probes, etc.) without being noticeably disturbed by the losses introduced by them.
- The characteristics of all components have been (directly or indirectly) measured in advance.
- A model of the whole TC has been created and used for simulations, and the experimental data match simulation results.
- The power supply used to feed the TC allows charging the primary capacitor to a repeatable, predefined potential within a known time: practical experience suggests that a target voltage of 10 to 20 kV might be appropriate. The charging voltage is independent from the capacitor discharge frequency (pulse repetition rate) to allow a separated regulation of these two parameters.
- The pulse repetition rate is stable, extending over the 200 Hz typically found in today's TC designs up to at least 500 Hz. Nikola Tesla used a pulse rate of over 2400 Hz in his own experiments, together with an average power of about 15 kVA [Tes78, Hul93].

For instance, a subsequent research work could investigate on the elongation of the ramified discharges emitted by the TC and its relationship to the operational parameters, as it is well known that these discharges are noticeably longer than what is expected based on simple considerations.

## 2. TESLA COIL TOPOLOGIES AND VARIATIONS

In the literature, the name “Tesla Coil” has been traditionally used for quite a range of different devices, being the only common thread that air-coupled resonant circuits were involved and a high-voltage was developed. The purpose of this chapter is to give an overview of the many ways a Tesla Coil can be built, pointing out the major pros, cons or simply the consequences caused by adopting different solutions for each component.

First, a simplified theory of operation of the TC is presented, together with the typical three feeding topologies. Then the choice for the TC power supply is analyzed and different solutions for its implementation explored. Finally, the effect of the excitation method (pulsed or continuous) and the influence of the TC physical size are discussed.

### 2.1. Simplified theory of operation

A Tesla Coil can be built using only a few basic components (Figure 5). A transformer generates a high voltage (typically 5 – 30 kV) from the mains that charges the primary capacitor C through the primary coil LP. LP is composed by a few turns (5 – 20) of heavy copper wire having a very low resistance.

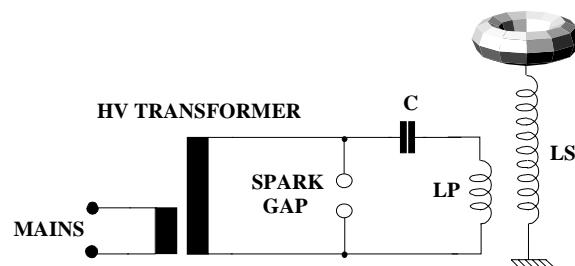


Figure 5: Tesla Coil basic schematic diagram.

When C is sufficiently charged, the potential difference between the spark gap electrodes becomes sufficient for the gap to fire and allow current to pass through. While the gap is conducting, C is connected in parallel to LP and gets discharged into it. C and LP form a parallel resonant circuit with a resonance frequency defined by their capacitance and inductance values.

The magnetic field generated by LP is partly induced into the secondary coil LS. LS is composed by about 1000 turns of thin copper wire and its top lead is connected to a spherical or toroidal terminal with a capacitance of typically 15 – 30 pF. LS and its top terminal form a resonant circuit. If its resonance frequency is near to the one of the primary circuit, an extremely high potential is developed at the top terminal.

As the secondary can easily reach potentials ranging from 100 kV to several MV, the electric field generated is usually sufficient to breakdown the surrounding air dielectric releasing a leader inception. Once the capacitor C gets completely discharged, the spark gap stops conducting and the same process already described repeats again.

The operation of a TC is governed by the mathematical laws describing two air-cored, inductively coupled resonant circuits [Ter43, Smy50]. The first circuit is formed by the primary capacitor C and primary coil LP connected in series through the spark gap, while the second circuit is constituted by the secondary coil LS in series with the top terminal acting as a capacitance connected to ground (Figure 6).

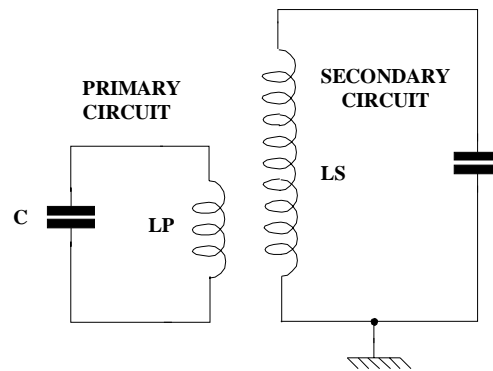


Figure 6: Inductively coupled primary and secondary circuits in a TC.

As the spark gap closes, the energy stored in the primary capacitor C feeds LP; the primary circuit oscillates close to its resonance frequency defined by the values of C and LP<sup>4</sup>. Part of this energy is magnetically coupled into the secondary LS that, in turn, oscillates close to its own resonance frequency too. The amplitude of the resultant oscillation is at a maximum when these two are in phase; this produces the phenomenon of beats<sup>5</sup> like those observed in water and sound waves (see the example in Figure 7).

The energy transfers back and forth from one circuit to the other with this beat frequency until it is entirely dissipated in resistive and RF losses; at this time the current in the primary circuit is minimal and the spark gap opens.

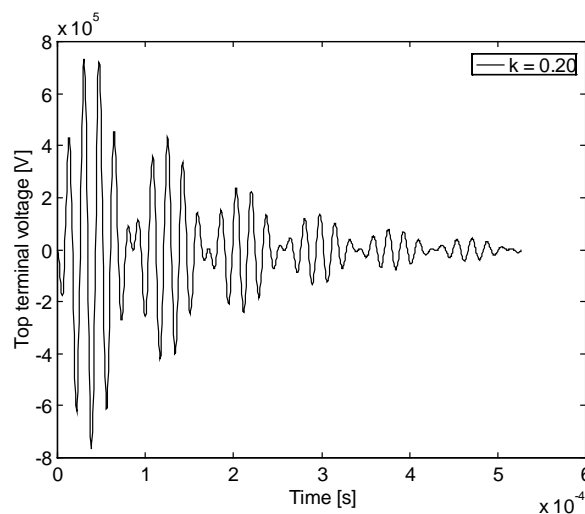


Figure 7: Top terminal voltage for a single spark gap pulse.

The ratio between the voltage applied to LP and the one developed on LS is not dependent on the turn ratio between primary and secondary coils but is instead directly proportional to the square root of the ratio of LS and LP inductance. The coupling coefficient between the two coils is also quite different from the usual values of 0.9 - 1 used in traditional iron-core transformers: typical values range from 0.1 to 0.6.

<sup>4</sup> The oscillation frequency depends also on other parameters because the primary is magnetically coupled to the primary. A complete treatment of this matter can be found in Chapter 6.1.1.

<sup>5</sup> Within this thesis, the term *beat* is used for an amplitude modulated carrier to indicate an interval between two successive points where the signal amplitude is zero. For instance, six beats can be identified in Figure 7.

## 2.2. Alternative coupling schemes

In the basic 2-coil TC presented in Figure 5, the energy from the primary circuit is transferred to the secondary by inductive coupling. A series of different solutions for transferring the primary circuit energy have been investigated by Nikola Tesla himself and replicated during the years with success by experimenters.

### 2.2.1. 3-coils, inductive coupling

This connection scheme is known among hobbyists as “magnifier” and employs what Nikola Tesla named as the “extra coil”. The basic idea (Figure 8) is to move the most of the traditional secondary coil relatively far away from the magnetic field generated by the primary; the secondary is reduced to a few turns tightly coupled to the primary (coupling coefficient used is about 0.6).

The voltage rise-up in the reduced secondary is now governed by the turn ratio, as in a usual transformer. The top of the secondary is used to series feed the “extra coil”, where the voltage built is still due to resonant charging.

In several TCs, the top terminal height practically limits the potential they can develop: the terminal can easily arch to the nearby primary coil or directly to the floor. Using this TC configuration, the top terminal (together with the extra coil) can be elevated far from any grounded point thus avoiding any leader inception to ground.

Anyway, the assembly is made more difficult by the need to provide high inductive coupling between primary and secondary while still keeping a good insulation between the two of them. The tight coupling requires a rugged and fast rotary spark gap to avoid dissipating all the energy in losses during transfers between primary and secondary circuits.

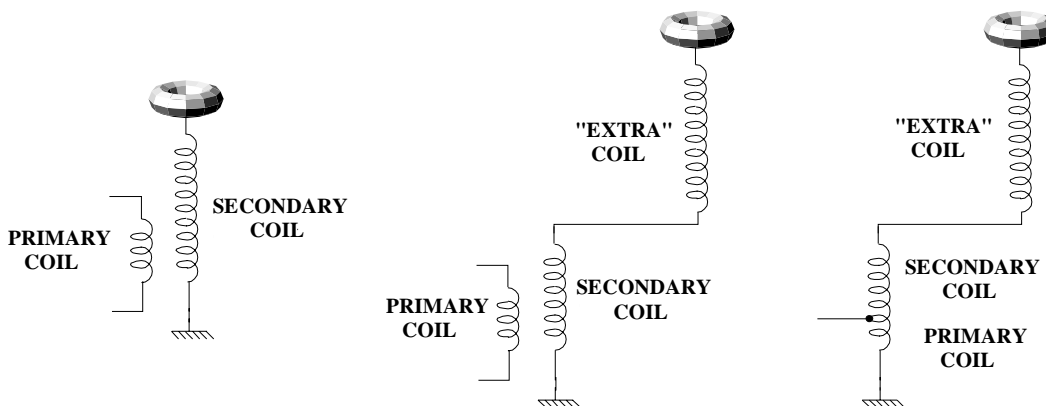


Figure 8: From left to right, basic TC, 3-coil inductively coupled TC and 3-coil series feed TC.

### 2.2.2. 3-coils, series feed

This connection scheme differs from the previous as the primary coil is connected in series and also inductively coupled to the secondary; primary and secondary therefore implement an autotransformer that series feeds the extra coil. The two windings don't need anymore to be insulated but the requirements for the spark gap are still quite strict.

### 2.3. *Static vs. rotary spark gap*

The simplest solution for the spark gap is a static couple of electrodes separated by a suitable dielectric (usually a dry gas mixture including SF<sub>6</sub>, Nitrogen, etc.). Spark-over occurs when a voltage threshold is exceeded and the arc self-extinguish when the current passing through the gap decreases below a certain value.

Commercial spark gaps usually employ also a trigger electrode to provide an initial ionization of the dielectric and facilitate its breakdown between the two main electrodes. This way it is possible to control the exact spark repetition rate, as required by radars, lasers, etc. Strict constraints are placed on the triggering pulse rise time, duration and amplitude, usually required to be 100% of the switched voltage.

The high current flowing in the primary circuit of a typical middle-sized TC is capable of quickly warm-up these static spark gaps: water or other kind of cooling is thus required. Using a series of multiple static gaps results in an even heat distribution and can partly reduce this problem; the spread between the minimum and maximum triggering voltage is anyway worsened by the connection.

For an optimal Tesla Coil performance, the gap is also required to stop conducting without re-igniting; the ionized dielectric gas mixture must be renewed after each pulse, maintaining a suitable pressure inside the gap. Vacuum or sealed static spark gaps are not suitable for TC use because they require a recovery time of several milliseconds between pulses.

Commercial static spark gaps are expensive to purchase and also to operate, while their construction with conventional amateur techniques is almost impossible. In practice, simple two or multiple electrode spark gaps with air dielectric are viable for small-sized TCs where switched power doesn't exceed 2 kW. Ionized air is removed from the gap by using compressed air or vacuum suction.

Rotary spark gaps represent a solution to several of the above mentioned problems: being engineered in different configurations, they basically consist of a set of stationary electrodes and a set of rotating ones. When a rotating electrode comes in proximity of the static ones their clearance is at a minimum and spark-over occurs.

Rotary spark gaps can be easily manufactured by using brushless motors or DC motors when a variable pulse rate is required. Static electrodes are cooled by providing them with proper heat sinks, while moving electrodes usually don't get even sensibly warm. By using fast rotating speeds there is no need of removing ionized dielectric and high pulse rates can be easily achieved.

### 2.4. *AC vs. DC power supply*

The basic TC described in Figure 5 employs an AC power supply; the rate of the pulses generated by the spark gap closures is related to its triggering voltage. If this voltage is slightly lower than the supplied peak voltage, the pulse rate is equal to the AC supply frequency (50 or 60 Hz) as there is only one pulse for each cycle.

A decrease in the spark gap triggering voltage allows for a higher pulse rate but the TC operation gets much more complicated. Note that when the spark gap is closed the power supply is effectively short-circuited. At spark gap opening the primary capacitor charging voltage depends on several factors:

- The power supply current capabilities.
- The instantaneous voltage value available from the mains (i.e. the temporal "phase" of the previous pulse).

- The spark gap triggering voltage, together with its intrinsic level of randomness.

The resulting functional mode makes performance optimization problematic. Practical experience indicates that if the power used is higher than a few kilowatts, the use of rotary spark gaps becomes mandatory. This adds one more uncertainty factor to the three listed above: the temporal phase of the AC supply voltage in respect to the gap electrodes spark-over.

On the other hand, the use of a rotary spark gap provides also a mechanism to control the TC performance better than with a static one. This can be achieved in several ways:

1. The pulse rate dictated by the rotating spark gap is sensibly higher than the AC supply frequency (e.g. 400 - 700 Hz). This way the phase relation between gap and supply voltage becomes irrelevant, as the pulses are on average uniformly distributed.
2. The rotary spark gap employs a synchronous motor fed from the same AC voltage used for the power supply. Gap and supply are thus in phase and a pulse rate equal to an integer multiple of the supply frequency can be achieved. The phase angle can be precisely set for the pulses to be distributed in an optimal area of the supply voltage half cycle.
3. The power supply is replaced by an alternator driven by the same motor used for the spark gap [Gla48]. The system can be designed so that the generated AC voltage frequency is exactly equal to the gap pulse rate. Because the alternator and gap rotors are mounted on the same motor shaft, a constant phase angle between them is ensured.

While the above solutions allow for reaching a stable and optimal performance point, the resulting amplitude of each single pulse is still not a constant; measurements of the coil parameters are very difficult as each pulse should be analyzed as a unique entity.

A great simplification is introduced by using a stabilized DC power supply together with a rotary spark gap. The pulse rate is solely defined by the spark gap rotation rate, provided that the power supply is capable of providing enough current to charge the primary capacitor between pulses. All pulses have the same amplitude, as the capacitor gets always charged to the same voltage, while the spark gap phase and rotating speed do not need anymore to be precisely controlled.

Under these conditions, parameter measurement is facilitated, at the expense of higher complexity required for the design of a DC power supply.

## 2.5. DC power supply topologies

It is essential to excite the primary circuit with pulses having known amplitude; the primary capacitor must always get charged to a stable, predefined voltage without fluctuations due to the pulses phase or repetition rate. This way, measurements can be concentrated only on tracking and modeling various parameters object of study without unnecessary complications.

This requirement, together with the high desired pulse rate of 500 Hz, put a special emphasis on the selection of the power supply design. The requirements to be satisfied can be specified as follows:

1. The primary capacitor must get charged before each pulse to an exact, known voltage.
2. This charging voltage must be adjustable, in order to obtain a range of different operating conditions.
3. Maximum desired charging voltage is about 20 kV.

4. Maximum desired pulse rate is 500 Hz.
5. Estimated maximum power required is about 10 kW (for a primary capacitor of 0.1  $\mu\text{F}$ ).

### 2.5.1. Conventional stabilized DC power supply

A stabilized DC power supply employing a full-bridge rectifier is modeled in Figure 9 using MicroSim<sup>6</sup>. V1, V2 and V3 represent the secondary of a 10 kV three-phase distribution transformer. L1, L2 and L3 are three current limiting inductors equivalent to the actual ones inserted in series with the transformer primary phases. Capacitor C1 provides charge storage sufficient for pulse rates up to 800 Hz, with a maximum voltage decrease of less than 0.7 % for each pulse. L4 has got the function of limiting the current drained from C1 during the time the spark gap conducts, as well as charging the primary capacitor C2 through diode D7. The TC primary winding is not taken into account in this model, as it doesn't noticeably influence the capacitor charge profile.

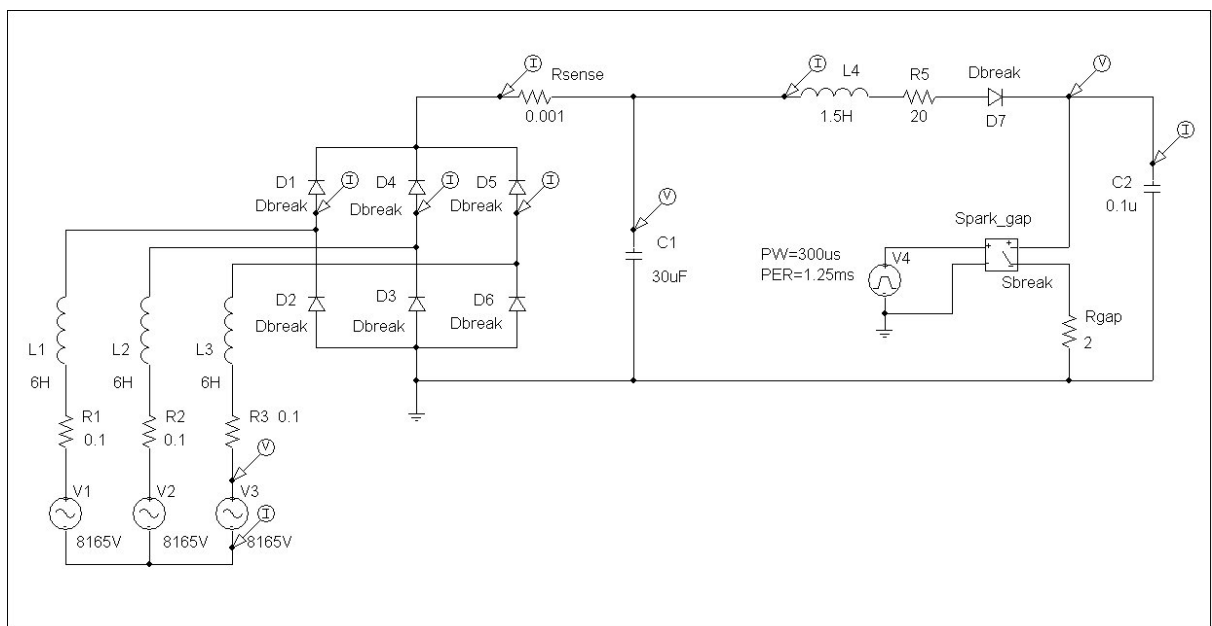


Figure 9: MicroSim model of a conventional DC power supply.

The presence of L4 and D7 realizes a resonant charging scheme that allows voltage developed on C2 to rise up to about 30 kV. Figure 10 is the result of a simulation run at a pulse rate of 800 Hz. L1, L2 and L3 limit the power consumed to about 20 kVA; the available power supply voltage on C1 assumes a value of about 10 kV at regime condition. Regulation of pulse energy (i.e. C2 charging voltage) is performed by a 30 A three-phase variac (not shown) feeding the transformer primary.

In spite of the simplicity of this approach, the following shortcomings must be considered:

- The 30 A three-phase variac, together with L1, L2, L3 and L4 constitute a set of bulky components requiring a lot of space and possibly also custom manufacture.
- C1 is an expensive, heavy and large component.
- The final charging voltage on C2 is partly affected also by the time the spark gap remains closed: this is a parameter that can be hardly controlled.

<sup>6</sup> MicroSim was an original trademark of MicroSim Corporation, which merged with Orcad in 1998, which in turn was acquired by Cadence Corporation in 1999.

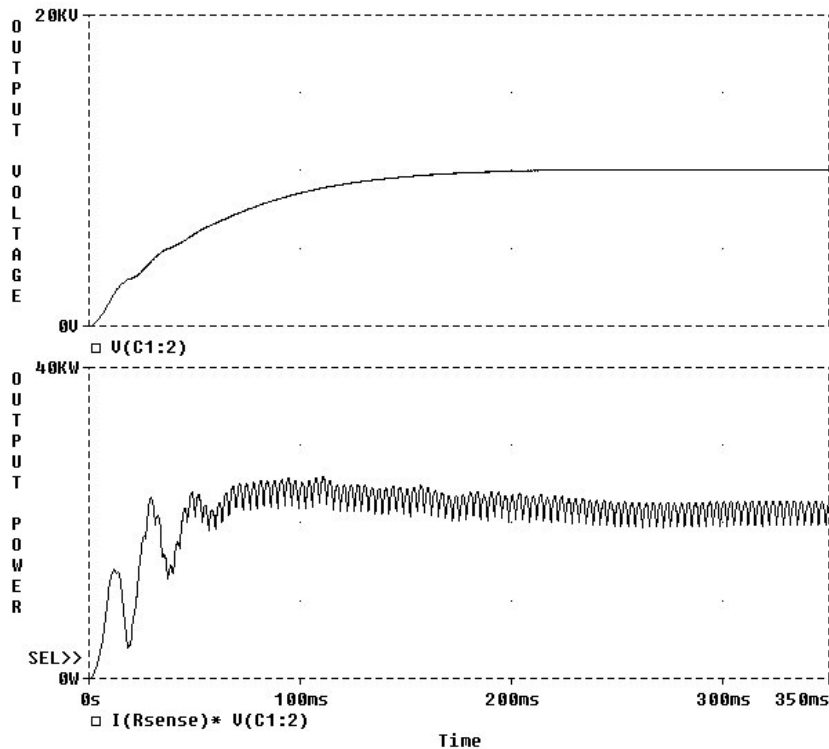


Figure 10: MicroSim simulation results for the conventional power supply.

### 2.5.2. DC power supply employing a high-voltage switch element

With the conventional stabilized DC power supply seen in the previous chapter, the primary capacitor got charged to a voltage related to the supply output voltage. The capacitor charging voltage was varied by changing the power supply output voltage through a variac connected on the mains side.

A different approach is to keep the power supply voltage constant and to charge the primary capacitor through a high-voltage switch that has to be opened when the capacitor reaches the desired voltage (Figure 11).

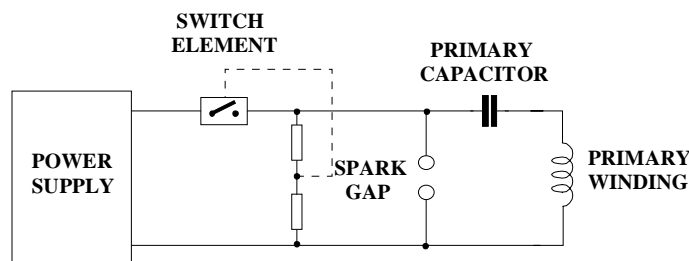


Figure 11: Power supply employing a high-voltage switch.

As the switch opening/closing frequency is at least equal to the maximum pulse rate (500 Hz), it cannot be inserted on the primary side of a conventional transformer because it would introduce high-frequency components in the original 50 Hz sinewave. This would, in turn, generate high losses and heat the transformer core.

Inserting the switch element on the secondary (high voltage) side means that a hold-off voltage of at least 15 kV is required, with an estimated maximum current of about 10 A. Solid state devices currently available on the market (thyristor, triac, BJT, MOSFET, GTO,

IGBT, MTO) have no problem to switch currents of several thousands of Amperes but are limited to a maximum operating voltage of 9 kV. The only possible solution is thus to connect several under-rated devices in series in order to increase their hold-off voltage.

Traditionally, the series operation of high-voltage devices has been challenging in two respects [Pal95]:

1. Switching control signals have to be level shifted across a high voltage barrier still ensuring a very low stray capacitance to ground, due to the high  $dv/dt$  encountered. This problem is widely known and it is usually solved with magnetic or optical methods.
2. A reasonable voltage distribution must be ensured in the transient and steady state, so that some devices are not stressed by over-voltage. Uneven voltage distribution is due to each device exhibiting slightly different characteristics.

Recent literature about operation of series connected devices with increased blocking voltage is mostly devoted to the solution of the voltage distribution problem. Several viable strategies are presented:

- Utilization of snubbers to slow down all the devices to the speed of the slowest device [Che96, Pod91, Oka97].
- Master-slave approaches where the devices are sequentially turned on and off [Bur96, Gui93].
- Active control of the device voltage or current with a local feedback loop influencing the device control signal [Bru98, Ger96, Pal95, Pal96, Pal97, Pal98].
- Overdrive of the device control signal in order to eliminate differences due to parameter spread [Ber96].

Uniform voltage sharing still remains a difficult task to be accomplished. All the proposed methods are more or less in the experimental stage and there is no established solution ready for the industry.

Devices such as BJTs and thyristors require complicated and very inefficient methods of driving due to their low gain and minority carrier device characteristics. In addition, thyristors become difficult to control due to loss of gate control during turn-off and require additional forced-commutation circuitry [Mit95]. Power MOSFET devices can be driven with low power voltage pulses but in high-voltage applications exhibit increased  $R_{DS(on)}$  (on-state, Drain-to-Source equivalent resistance) resulting in lower efficiency due to the increased conduction losses [Tak95].

The IGBT combines the low conduction loss of a BJT with the switching speed of a power MOSFET and, at operating frequencies between 1 and 50 kHz, offers an attractive solution over traditional BJTs, MOSFETs and thyristors. Instead, GTOs and MTOs are limited to switching frequencies below 500 Hz [Ber96].

### **2.5.3. High-frequency converter**

The two solutions previously seen in Chapters 2.5.1 and 2.5.2 rely on a more or less stabilized DC high-voltage to be generated from a conventional 50 Hz transformer through rectification. A high-frequency converter, instead, focuses on charging the primary capacitor with high voltage pulses.

The AC mains voltage is rectified to obtain an approximately stable DC voltage (Figure 12) that is then applied to a step-up transformer through a bridge of solid-state switches (MOSFET, BJT or other). The pulses generated at the transformer secondary are rectified and

used to charge the primary capacitor. The charge cycle is continuously monitored by the power supply controller; when the desired voltage is reached the bridge switch is turned off and the charge cycle is terminated. If the primary capacitor voltage drifts significantly from the setpoint, the charging is restarted in order to maintain an almost stable voltage.

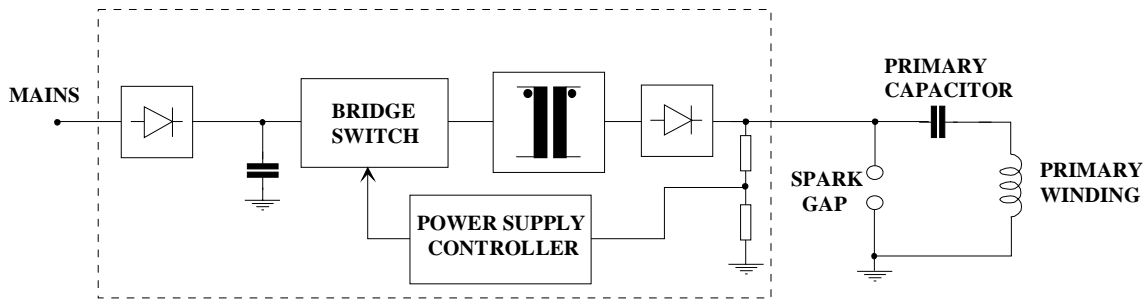


Figure 12: Power supply employing a high-frequency converter.

## 2.6. Effect of increased pulse rate

Pulse rates practically achievable with rotary or static spark gaps (below 1 kHz) don't affect the potential developed in the secondary circuit, as the energy of one pulse is completely dissipated before the following pulse. On the other hand, if higher pulse rates could be realized, a constructive potential build-up at the secondary would require the oscillations generated by each pulse to be perfectly in phase with each other.

If the TC is allowed to emit leaders into air, increased pulse rate results in elongated leaders extending many times over the typical distance expected to be achieved for the secondary potential developed. This effect has only been partly studied; the mechanism involved is probably an extension of the streamer-leader event chain [Lar98, Gir00].

If, instead, the TC sparks over to a grounded target, increased pulse rate produces a brighter discharge, as the energy per time unit employed is directly proportional to the pulse repetition rate.

## 2.7. Pulsed vs. continuous wave

All Tesla Coils described in the previous chapters use a spark gap to discharge a capacitor into the primary coil and thus generate oscillations in the primary circuit in a discontinuous, pulsed way. A natural extension of this principle is having the primary coil directly driven by a power oscillator. In this case the potential developed at the secondary is no more a series of high voltage pulses but instead a continuous AC voltage, that can be used for a wide range of applications.

While the pulsed TC (also called *disruptive* TC) is fed with a high power pulse derived from a capacitor discharge, the continuous wave TC is fed by a continuous oscillation with sensibly smaller instant power. Oscillators operating in Class A, B or C can be used, with different performance [Cor87].

With Class A and B oscillators the efficiency achieved is low. The maximum voltage rise at the secondary is obtained when the primary equivalent impedance is equal to the secondary equivalent impedance. In this condition the power delivered to the secondary is maximum and equal to 50% of the total power. The coupling required to match the impedance of the two circuits is usually very loose, well under 0.1. With increasing coupling the secondary voltage drops down because the coupled primary resistance reduces the secondary Q value.

With Class C oscillators a higher efficiency can be reached (about 80%); the primary circuit impedance rises between the current pulses and the secondary Q keeps high values. This means that a higher value of coupling can be used (typically 0.2), reducing losses and increasing efficiency. A higher coupling coefficient, in turn, produces the beat envelope typical of air-core inductively coupled circuits (Figure 7); this beat can be removed by tuning secondary and primary to slightly different frequencies.

TC oscillators usually employ triode or tetrode vacuum tubes, for the high voltage and relatively high currents required. Solid state devices like IGBTs and FETs don't provide the same power switching capabilities but can be run in Class D with an efficiency of about 90%.

Oscillator driven TCs allow to generate a continuous AC voltage instead of the pulsed AC obtained with spark gap driven TCs. Anyway, they are much more sensible to losses, loading in the secondary circuit and capacitive proximity effects. For the same power supply and coil configuration, they don't allow to generate peak potentials as high as with the pulsed-mode operation. More, from a visual point of view, leaders into air generated by oscillator driven TCs are not so spectacular as the lightning-like leader inceptions generated in pulsed-mode.

## 2.8. Tesla Coil physical dimensions

The performance of a Tesla Coil, intended as the peak potential developed at the secondary top terminal, is related to a number of factors including losses in components, losses in connections, component value selection and operational environment conditions (moisture, elevation from ground, etc.). Some of these factors are directly influenced by the TC physical dimensions:

1. Inductance of primary and secondary coils. Potential developed is directly proportional to the square root of the secondary and primary coils inductance ratio.
2. Resistive losses in the primary coil.
3. Resistive losses in the secondary coil.
4. Internal capacity of the secondary coil. Coils shaped with lower height to width ratio exhibit a lower self-capacitance.
5. Distance between top terminal and primary coil. A taller secondary allows for the top terminal to sustain higher potentials before arching to the primary or to the floor.
6. Top terminal size. The minimum radius of curvature of the top terminal influences directly its leader inception threshold voltage: a bigger radius results in a higher threshold potential. On the other hand, a higher radius usually produces also a larger terminal and, therefore, a higher capacitance to ground. Because an increase in top terminal capacitance results in a reduction of the voltage developed at the secondary<sup>7</sup>, top terminal size selection is actually a tradeoff.

Thus, the geometry of the secondary coil is a compromise between the above factors and is partly driven also by empirical evidence. In general, bigger TCs imply a smaller voltage transformation ratio; on the other hand, they are capable of handling a higher top terminal potential and therefore suitable to produce a higher voltage.

Practical experience suggests that the power required for a satisfactory performance of a TC is not linearly proportional to the size of its secondary coil but the dependency is instead at least quadratic. For example, a TC featuring a doubled secondary height is likely to require four times the power originally used.

---

<sup>7</sup> See Chapter 6.1.1.

### 3. **DESIGN SPECIFICATION AND MAIN SOLUTIONS**

Having analyzed the different TC implementation possibilities in the previous chapter, it is now easier to justify the choices made within this project for the TC major components. In this chapter, the power supply topology and its power requirements are selected, a design for the spark gap is chosen and an approximate size for the TC is planned. Finally, materials are selected for the construction and assembly of the coils and other components exposed to high thermal or electrical stress.

#### 3.1. **Excitation mode and topology**

As seen in Chapter 2.7, continuous wave TCs are extremely sensitive to losses, capacitive proximity effects and loading of the top terminal; they also don't allow to reach potentials as high as in pulsed mode. The Tesla Coil object of this project is thus chosen to work in pulsed mode, using a spark gap.

3-coil TCs require a high-speed, high-performance rotary spark gap and for inductive feed also proper insulation between primary and secondary. They imply an increased engineering difficulty and are much more complex to be modeled for including three resonant circuits. The coupling scheme chosen for Thor is therefore the basic 2-coil (Figure 5), for its simplicity. The 2-coil configuration also relaxes the requirements on the spark gap quench time duration that otherwise would have required a high electrode rotational speed.

#### 3.2. **Spark gap selection**

The major weakness of a not-triggered static spark gap is the tolerance in its threshold voltage and, therefore, the amount of uncertainty implied by its operation. On the other end, triggered spark gaps are considerably expensive and their lifetime is limited.

As this project aims at exploring the TC properties independently of the characteristics of the spark gap, spreading of the threshold voltage and timing errors have to be reduced to a minimum. Using a rotary spark gap, the triggering voltage tolerance can be eliminated by setting the electrode clearance to a minimum that guarantees dielectric breakdown in every condition. A precise timing can be easily achieved by employing a speed control for the spark gap motor.

Therefore, a rotary spark gap is selected, employing a 1 h.p. AC motor running at 2850 r.p.m. (230 VAC, 50 Hz) and controlled by a frequency inverter. The rotor is composed by a LE-grade phenolic disk, measuring 30 cm in diameter and one cm thick. Twelve double-sided electrodes are mounted on the rotating disk; the entire assembly is dynamically balanced to within one gram, to avoid dangerous oscillations that could damage the rotor. The maximum break rate is thus  $2850 / 60 * 12 = 570$  breaks/second.

Four stationary electrode assemblies are arranged as two pairs for the above rotary disk assembly, on separate supporting fiberglass insulators, with brass cooling fins. All electrodes are screw-in 2% thorium doped tungsten electrodes, 0.5" in diameter.

#### 3.3. **Power supply selection**

The conventional stabilized power supply has been modeled in detail in Chapter 2.5.1 and requires a lot of bulky components. A three-phase 10 kV 20 kVA transformer, a 20 kW

variac, a 1.5 H 30 kV inductor plus a triple limiting inductor demand for a lot of space; regulation of the primary capacitor charging voltage still cannot guarantee repeatability.

A power supply employing a high-voltage switch element demands for a particular effort in designing and optimizing a voltage sharing strategy: ready-made solutions are not currently available. Devices to be connected in series with blocking voltages greater than 3 kV are available only for currents of several hundreds of amperes. They are large and expensive, require special mounting mechanics and are definitively wasted for an application using at most 10 A of current.

The high-frequency converter is a solution often reported in the literature for capacitor charging. All components are readily available on the consumer market, except the transformer that must be custom-wound. Schematics can be easily derived from existing low-power designs, as the topology remains the same. The high-voltage secondary affects only in a very small part the overall design and the ratings of a few components.

By choosing this solution there is no need of big current limiting inductors, variacs or heavy and life-dangerous filtering capacitors. The primary capacitor charging voltage can be easily regulated from a low potential point minimizing losses and without danger of electrical shock.

One circuit topology that may be utilized is the series-loaded resonant converter [Lip91, Nel90, Nel92]. In this circuit (Figure 13) four switching devices and the resonant components L and C are connected to the low voltage side of the transformer; only the rectifiers on the transformer secondary must have high voltage ratings. By closing in proper order the switches in pairs, pulses of alternate polarity are applied to the transformer. Using a high turn ratio, high voltage pulses are generated at the secondary, increasing the capacitor charge.

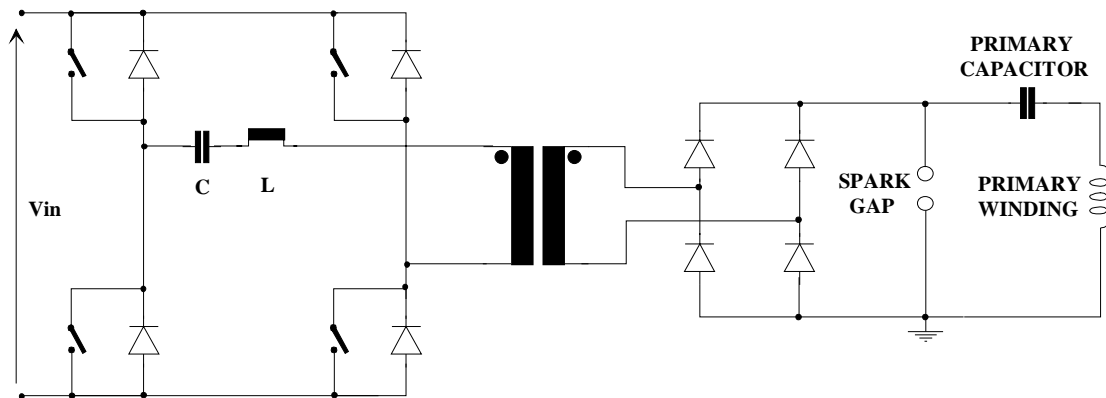


Figure 13: Series-loaded resonant converter.

The leakage inductance of the transformer may be utilized as the resonance inductor L. The switching frequency may be held constant at a value such as one-half of the circuit resonant frequency; alternatively the switching frequency may be started at a low value and then increased to approximately the resonance value during the charge cycle. When the desired capacitor voltage is reached, a command is sent to turn off all switches.

One characteristic of this circuit which makes it attractive for capacitor charging is its ability to operate under short circuit conditions, such as that represented by the capacitor at charging start. Operation at high switching frequencies can reduce the size and weight of the transformer. Regulation can be improved by the utilization of control techniques like pulse-width modulation or constant on-time control.

Solid state devices for the switches can be selected according to the same considerations reported in Chapter 2.5.2: in this case there is no need for series connection of several devices as the required voltage and current ratings are widely supported. Integrated circuits are readily available for driving the switching devices (e.g. IR2110 from International Rectifier) and also for regulating switching frequency and duty-cycle (e.g. UC3860 from Unitrode Integrated Circuits) [Lip91]. The input voltage  $V_{in}$  can be derived by rectifying and filtering the 230 V mains or the three-phase 400 V lines for increased power demand.

### 3.4. Power supply requirements

The selection of the maximum output voltage for the power supply is constrained by the following issues:

- Engineering problems with cabling and connectors' insulation due to corona effect. For potentials over 5 kV DC, custom molded cable assemblies or pricey military-rated connectors must be used. The connectors' size also grows considerably together with the voltage rating.
- Design problems for rotating spark gaps with threshold voltages below 10 kV DC. As the total air gap must be less than 2.5 mm, electrode clearances must be below 1 mm, imposing strict requirements on the rotating assembly precision and rigidity.
- Insulation requirements for the power supply step-up transformer. It must be remembered that this component is not available off-the-shelf and has to be custom manufactured in a reasonably easy way.

A careful consideration of the above listed facts indicates that a maximum output voltage of 20 kV DC might be an appropriate choice. A preliminary investigation on the characteristics of solid-state components currently used by the industry suggests that an output power of 5 kW can be easily reached without resorting to exoteric devices.

If the primary capacitor  $C_p$  is charged to a voltage  $V$ , the pulse discharge energy into the primary coil is approximately (ignoring losses):

$$E = 0.5 \cdot C_p V^2 \quad (3-1)$$

If the pulse rate is  $N$  pulses/second, the power required is:

$$P = N \cdot 0.5 \cdot C_p V^2 \quad (3-1)$$

This assumes that the capacitor  $C_p$  is always completely discharged, meaning that its energy is dissipated into leader discharges and/or losses in the primary and secondary circuits. The maximum power available  $P_{max}$  (5 kW) imposes a limit on the capacitor charging voltage as the pulse rate rises. From Equation (3-1) we have:

$$V = \sqrt{\frac{2P_{max}}{NC_p}} \quad (3-2)$$

On the other hand, even at slow pulse rates, the primary capacitor voltage cannot exceed the maximum voltage available from the power supply (20 kV). Aware of that, we can use

Equation (3-2) and Equation (3-1) to plot the available charging voltage (Figure 14) and power (Figure 15) at different pulse rates, assuming a primary capacitor value of  $0.1 \mu\text{F}$ .

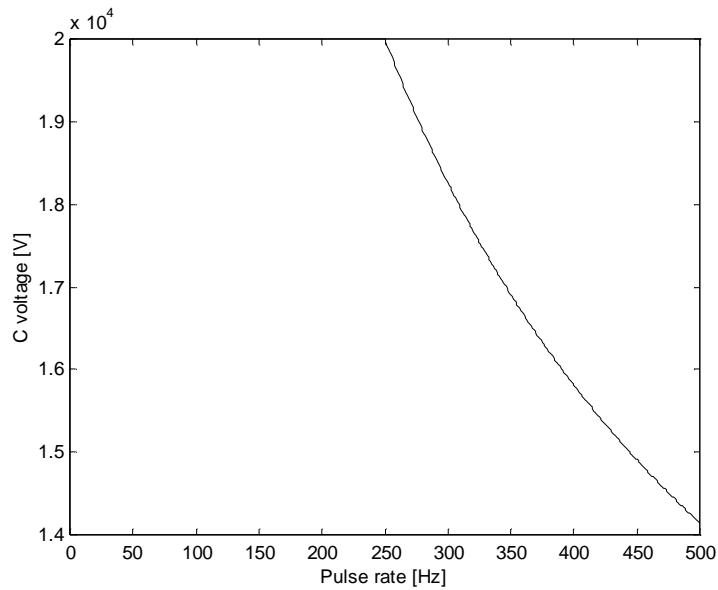


Figure 14: Maximum available pulse peak voltage vs pulse rate.

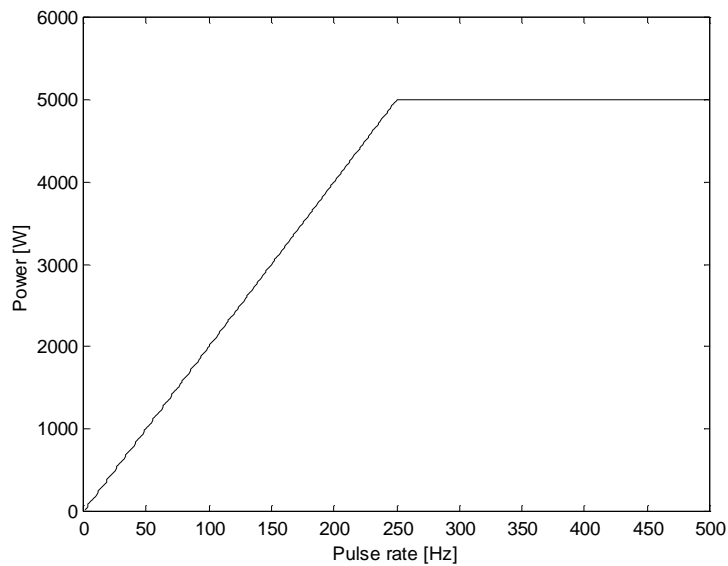


Figure 15: Maximum power provided to the Tesla Coil vs pulse rate.

The maximum power available is reached for a pulse rate:

$$N_{\max} = \frac{2P_{\max}}{C_p V^2} = \frac{2 \cdot 5000}{0.1 \cdot 10^{-6} \cdot 20000^2} = 250 \text{ Hz} \quad (3-2)$$

For pulse rates  $N > N_{\max}$  the available voltage is decreased, constrained by the power maximum rating. In practice, this accounts for the power supply fixed rate of charging the

primary capacitor (see Chapter 5.2.1): as the pulse rate grows, a point is reached when the supply hasn't got enough time to fully charge the capacitor.

As the maximum charging voltage can be provided up to 250 Hz, and at a top break rate of 500 Hz the capacitor can still be charged to 14.1 kV, the maximum power selection of 5 kW proves to be sufficient to fulfil the requirements imposed by this project.

### 3.5. *Tesla Coil dimensions*

As previously mentioned in Chapter 2.8, the process of selecting the physical dimensions for a TC is a compromise between several factors and is mainly driven by practical experience. To be immune from unwanted side effects and, at the same time, allow to display all phenomena involved with sufficient magnitude, a middle-sized Tesla Coil is planned, with a secondary height of about 1.5 meters.

To ensure a low self-capacitance, also aware of the dimensions of other TCs reviewed, a height-to-width ratio of 4:1 is selected, resulting in a secondary outer diameter of approx. 400 mm. A TC of this size should be relatively insensitive to field distortion and capacitive proximity effects caused by probing sensors and other objects nearby the secondary coil.

The output of a TC is a combination of three effects:

- An electromagnetic field and an electrostatic field generated respectively by the secondary and by its top terminal.
- Leader inceptions into free air.
- Discharges to solid grounded points.

The above three effects are usually all present in every TC run, randomly mixed with each other; the mechanisms employed by them are all different and concur to make TC modeling a difficult task. By using different setups it is possible to separate these three energy transfer forms, having one of them predominant among the others and thus simplifying the modeling process.

A large toroidal top terminal is used to increase the leader inception threshold voltage, thus preventing leader formation and allowing to precisely measure the electromagnetic field generated. When using a suitable grounded spherical terminal in proximity of the toroid, it is possible to ensure that all leaders will result into a controlled discharge to ground. If leaders into air have to be investigated, an artificial protuberance on the toroid surface has the effect to offer a preferential point for leader formation and concentration. Practical experience suggests a top terminal with outer diameter equal to the secondary height (i.e. 1.5 m).

### 3.6. *Material selection*

The component that is exposed to the highest electrical stress is the secondary coil, with an electric field that can easily reach 500 kV/m and local spots of maximum field density prone to breakdown. The support material used for the secondary winding must have low HF losses, high dielectric strength and must not be hygroscopic; still it must be available in tubes with diameter approx. 400 mm. HDPE, used for industrial water pipes, is a perfect candidate as long as the antistatic type is avoided (for its high losses). This plastic is easily machineable and offers good mechanical properties, although it can't be glued but must be welded if joining is required. The secondary coil can be wound with enameled copper wire, preferably of Grade 2 for the improved mechanical resistance of its insulating coating.

The primary coil must withstand the primary capacitor discharge current without heating and offer negligible losses; it must be easily wound as a spiral but still has to be enough stiff

to maintain its final shape. Annealed copper tubing fulfills all the above requirements. Use of copper bars is not justified as the skin effect practically limits the current path to the conductor surface.

In general, for all large assembly and frame components, plastic should be preferred to metal, to reduce eddy-current losses. All hygroscopic materials should be avoided and only plastics with good dielectric characteristics should be used.

The remaining assembly components can then be manufactured from stock PVC, suitable for its wide availability in different shapes at low price, its excellent mechanical properties and the possibility to be easily glued.

## 4. TESLA COIL DESIGN

This chapter goes in an ordered manner through the design phases of the Thor components. Starting from the calculation of the secondary coil and its top terminal, a suitable primary coil is produced. Finally a low pass filter is designed, to act as a transient protection between the power supply and the TC primary circuit.

### 4.1. General

The general design procedure of a Tesla Coil is only partly influenced by the power supply choice. The supply voltage value affects clearances and engineering techniques used during the practical construction phases and a Tesla Coil of a chosen size will usually require a minimum power to obtain a satisfactory performance. If the above criteria are satisfied, there is a relative freedom in choosing a power supply solution.

The procedure applied in the following chapters relies quite strongly on practical experience. In several phases of the design, some of the parameters have been chosen according to empirical evidence, without a theoretical justification.

The reasons for this way of doing are basically three:

- Parasitics: due to material dielectric losses, influence of nearby objects, parasitic inductance and capacitance, the performance of the actual TC always drifts, in a certain extent, from the one calculated. Typically, the voltage magnification factor at the secondary top terminal is lower than the one expected and the secondary resonance frequency is slightly different from the one calculated. Therefore, also a design based on exact formulae must in practice allow for a certain amount of tuning to be performed “on field”.
- Engineering problems: designing an optimized TC on paper is pretty far from actually having it reliably working. Dielectric strength of materials employed for the construction and of the surrounding air places a serious limitation on the Tesla Coil geometry.
- Some of the design parameters are actually freely selectable (e.g. the secondary coil height).

Based on the considerations above, it is possible to undertake the Thor’s design procedure and relative component value calculation going through the following ordered phases:

1. Choice of the desired secondary coil height and diameter: this has been done in Chapter 3.5 according to practical experience.
2. Calculation of secondary coil wire gauge, secondary self-capacitance and inductance.
3. Choice of a proper secondary top terminal and calculation of its capacitance. A toroid shape provides the best electric field distribution in order to direct most of the streamers in a horizontal direction and reduces strikes to ground or to the primary. Practical experience indicates that a toroid outer diameter equal to the secondary height should provide the best performance.
4. Calculation of the secondary resonance frequency.
5. Specification of the primary coil physical size: this is influenced by the secondary diameter and by the empirical target to use 5 - 20 turns.

6. Calculation of the primary coil inductance and of the primary capacitor required to achieve a resonance frequency equal to the one of the secondary circuit.

#### 4.2. Secondary design

The desired secondary coil height is 150 cm and to maintain a diameter/height ratio of 1:4 a suitable coil diameter is 40 cm. Supposing to wind all the 150 cm length with about 1000 turns of wire, the wire gauge is:

$$G = \frac{H}{N} = \frac{1500}{1000} = 1.5 \text{ mm} \quad (4-1)$$

The actual number of turns obtained can be estimated as about 97% of the theoretical, i.e. 970 turns. According to an equation due to Wheeler [Whe28], the secondary inductance is:

$$L_s = \frac{R^2 N^2}{2540 \cdot (9R + 10H)} \quad (4-2)$$

where:

- $L_s$  secondary inductance [mH]
- $R$  secondary radius [cm]
- $H$  secondary height [cm]
- $R$  secondary radius [cm]
- $N$  number of turns

In our case:

$$L_s = \frac{20^2 \cdot 970^2}{2540 \cdot (9 \cdot 20 + 10 \cdot 150)} = 88.2 \text{ mH}$$

The secondary self capacitance is estimated by a formula due to Medhurst [Med47]:

$$C_s = KD \quad (4-3)$$

where:

- $C_s$  secondary self capacitance [pF]
- $D$  secondary diameter [cm]
- $K$  a constant depending on the H/D ratio from the Table V at page 84 of [Med47]

In our case the H/D ratio is 3.75 that corresponds to  $K = 0.695$  (interpolated). Thus:

$$C_s = 0.695 \cdot 40 = 27.8 \text{ pF}$$

The self-resonance frequency of the secondary without top load is given by:

$$f_{\text{su}} = \frac{1}{2\pi\sqrt{L_s C_s}} = \frac{1}{2\pi\sqrt{88.2 \cdot 10^{-3} \cdot 27.8 \cdot 10^{-12}}} = 101.6 \text{ kHz} \quad (4-4)$$

The length of wire needed to wind the secondary is:

$$l_s = 2\pi RN = 2\pi \cdot 20 \cdot 970 = 1219 \text{ m} \quad (4-5)$$

And its resistance is:

$$R_s = \rho \frac{l_s}{\pi \left(\frac{G}{2}\right)^2} = 0.017 \frac{1219}{\pi \left(\frac{1.5}{2}\right)^2} = 11.7 \Omega \quad (4-6)$$

### 4.3. Top terminal design

The selected top terminal is a toroid with an outer diameter  $d_1$  equal to the secondary height and a cross section diameter  $d_2$  big enough to provide a large radius of curvature. The toroid capacitance is calculated from the following empirical equation (courtesy of Mr. Bert Pool).

$$C_{\text{top}} = 2.8 \cdot \left(1.2781 - \frac{d_2}{d_1}\right) \sqrt{0.1217 \cdot d_2 \cdot (d_1 - d_2)} \quad (4-7)$$

where:

$C_{\text{top}}$  toroid capacitance [pF]

$d_1$  toroid outer [cm]

$d_2$  toroid cross section diameter [cm]

In our case, these dimensions are chosen to be  $d_1 = 150$  cm,  $d_2 = 20$  cm and we have:

$$C_{\text{top}} = 2.8 \cdot \left(1.2781 - \frac{20}{150}\right) \sqrt{0.1217 \cdot 20 \cdot (150 - 20)} = 57 \text{ pF}$$

The self-resonance frequency of the secondary with the top load mounted drops down to:

$$\begin{aligned} f_s &= \frac{1}{2\pi\sqrt{L_s(C_s + C_{\text{top}})}} = \\ &= \frac{1}{2\pi\sqrt{88.2 \cdot 10^{-3} \cdot (27.8 \cdot 10^{-12} + 57 \cdot 10^{-12})}} = 58.2 \text{ kHz} \end{aligned} \quad (4-8)$$

### 4.4. Primary capacitor choice

Capacitance values for the primary capacitor usually vary between 0.05  $\mu\text{F}$  and 0.2  $\mu\text{F}$ . The capacitor choice influences both the primary resonance frequency and the maximum available

pulsed power for the Tesla Coil. Practical experience suggests that a viable value for the primary capacitor is 0.1  $\mu\text{F}$ .

#### 4.5. Primary design

The shape chosen for the primary coil is the flat Archimedes spiral, for the simplicity of its manufacturing and because it allows to maximize its distance from the top of the secondary coil.

As the secondary coil is supposed to be freely movable inside the primary coil, the inside diameter of the primary inner turn must be equal to the secondary outer diameter plus some clearance, which is chosen to be 7.5 cm.

Optimal performance can be achieved if secondary and primary circuits have got the same resonance frequency (Chapter 6.1.1). Given that the value selected for the primary capacitor is 0.1  $\mu\text{F}$ , from Equation (4-8) the primary inductance value required is:

$$L_p = \frac{1}{C_p} \left( \frac{1}{2\pi f_s} \right)^2 = \frac{1}{0.1 \cdot 10^{-6}} \left( \frac{1}{2\pi \cdot 58.19 \cdot 10^3} \right)^2 = 74.8 \mu\text{H} \quad (4-9)$$

The material chosen for the primary coil is copper pipe of 8 mm diameter. As practical experience suggests, the spacing between turns is kept close and chosen to be 22 mm. The resulting inductance is given by the following formulas, adapted from [Whe28]:

$$W_p = (N_p - 1)(S_t + D_t) + D_t \quad (4-10)$$

where:

- $W_p$  width of windings on one side [cm]
- $N_p$  number of turns
- $S_t$  turn spacing [cm]
- $D_t$  pipe outer diameter [cm]

$$R_{av} = \frac{D_i + W_p}{2} \quad (4-11)$$

where:

- $W_p$  width of windings on one side [cm]
- $D_i$  inner diameter [cm]
- $R_{av}$  average radius [cm]

$$L_p = \frac{R_{av}^2 N_p^2}{20.32 \cdot R_{av} + 27.94 \cdot W_p} \quad (4-12)$$

where:

- $L_p$  primary inductance [ $\mu\text{H}$ ]

$W_p$  width of windings on one side [cm]

$R_{av}$  average radius [cm]

$N_p$  number of turns

In our case, the iterative application of the above three formulas indicated that a turn number  $N_p$  between 8 and 9 should result in a proper inductance value. For 9 turns, the resulting inductance is:

$$W_p = (9 - 1)(2.2 + 0.8) + 0.8 = 24.8 \text{ cm}$$

$$R_{av} = \frac{40 + 7.5 + 7.5 + 24.8}{2} = 39.9 \text{ cm}$$

$$L_p = \frac{39.9^2 \cdot 9^2}{20.32 \cdot 39.9 + 27.94 \cdot 24.8} = 85.8 \mu\text{H}$$

To provide sufficient flexibility for tuning, the primary coil is manufactured with 9.5 turns of copper pipe.

#### 4.6. Filter design

Practical experience suggests the addition of a low-pass filter between the power supply and rotating spark gap, in order to protect it from the transients generated by the primary circuit. Following a usual rule-of-the-thumb, a capacitance of about 500 pF between each of the power supply poles and ground, followed by an inductance of about 2 mH in series with each power wire should be useful and sufficient.

The components used for Thor's filter have been selected according to availability criteria. A series of two 1000 pF ceramic capacitors (for a resulting 500 pF), rated for 15 kV AC, have been inserted between each power supply pole and ground.

Two filter inductors are also placed in series between the two power supply wires and the spark gap. Each inductor features 15 turns of HV rated wire (Belden 8866) wound on a toroidal core with an outer diameter of 130 mm. The toroids are made out of wound amorphous magnetic tape (VITROPERM<sup>8</sup> 500 F), allowing for an exceptionally good performance: the typical permeability  $\mu_r$  is 17000, while the saturation flux density is 1 T.

<sup>8</sup> VITROPERM is a registered trademark of Vacuumschmelze GmbH.

## 5. POWER SUPPLY DESIGN

This chapter describes the power supply built to feed Thor and the relevant phases of its design. First, the general functional architecture of the device is presented and then all building blocks are described one by one.

The high-frequency converter, composed by a bridge switch and a resonant load, has a central role; after explaining its theory of operation, the required current and voltage ratings for the major components are derived. In the schematic analysis that follows, these ratings are used to justify the component selected for the bridge switch design. A particular emphasis has also been placed upon the resonant load transformer; its uncommon design and construction are described in detail.

The schematics of the HV metering board and of the controller supervising the whole power supply are analyzed. Finally, a description of the interconnection of these modules and of the power supply general assembly and mechanics is given.

### 5.1. System design

The Thor's power supply is used to charge the primary capacitor with high voltage pulses. Such a device is not capable of providing a regulated DC voltage as expected from usual stabilized supplies and, therefore, can be merely regarded as a Capacitor-Charging Power Supply (CCPS).

A scalable, modular architecture allows simplifying the problem of the construction of the 20 kV 5 kW step-up transformer and the selection of electronic components suitable to drive it. A subdivision of the power supply into four identical blocks reduces the requirements to four 5 kV 1.25 kW modules, which can be implemented with off-the-shelf components. The outputs of the four modules are then connected in series to provide the full operational voltage (Figure 16).

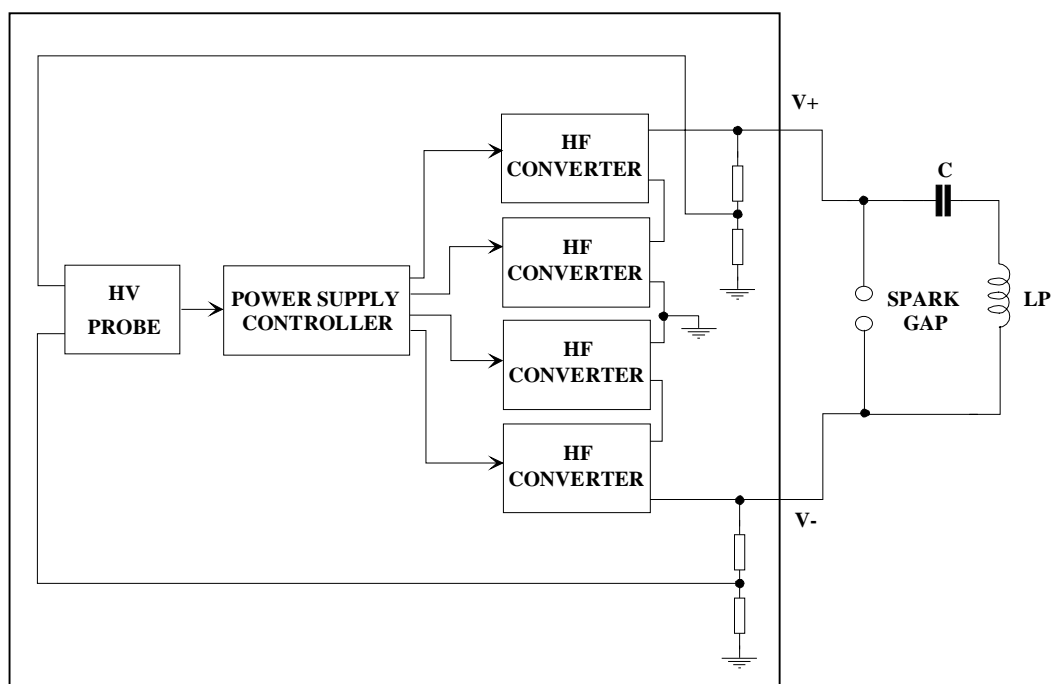


Figure 16: Power supply architecture.

The design is scalable, as more converter modules can be added in series to reach a higher charging voltage, being their output floating in respect to ground. The CCPS output is internally center-tapped to ground: one of the output leads, therefore, can be at a maximum potential of +10 kV while the other one can be at a minimum potential of –10 kV (in respect to ground). This strategy increases safety and allows to reduce to one half (10 kV DC) the insulation requirements of assemblies and wiring.

A high voltage probe module samples the charging voltage and converts it to a 0 to 3 V range. A single controller module drives all of the four converters; it is responsible of synchronizing the charge with external events and suspending the charging pulses when a predetermined voltage is reached. Galvanic isolation at several points is either required or desirable in order to reduce noise and interference.

## 5.2. High-frequency converter

The converter modules are fed with 560 V DC obtained by rectifying 400 V AC from the mains. A full-bridge switch drives a step-up transformer with a 9:1 turns ratio in order to reach a rectified output voltage of about 5 kV DC. The switch commutation is externally driven by the controller module, according to the capacitor charge state.

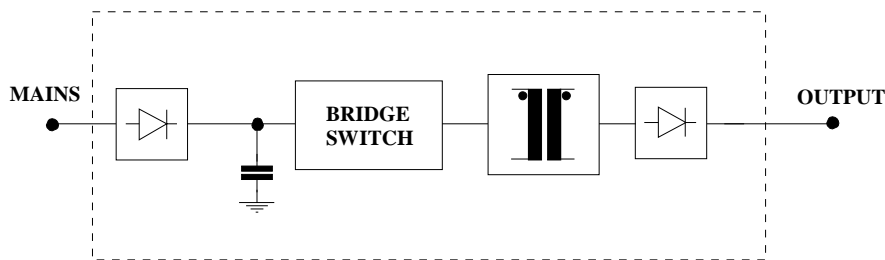


Figure 17: Basic block diagram of one converter module.

The topology selected for the converter is the series-loaded resonant (SLR) [Moh89, Lip91, Nel90]. In this configuration (Figure 18) the switches and resonant components L and C are connected to the low voltage side of the transformer; therefore, only the rectifiers on the transformer secondary must have high voltage ratings. By closing in proper order the switches in pairs, pulses of alternate polarity are applied to the transformer. Using a high turn ratio, high voltage pulses are generated at the secondary, increasing the capacitor charge.

### 5.2.1. Theory of operation

The characteristic impedance  $Z_0$  of the bridge load (Figure 18) is given by:

$$Z_0 = \sqrt{\frac{L}{C_{eq}}} \quad (5-1)$$

And its resonance frequency  $f_0$  by:

$$f_0 = \frac{1}{2\pi\sqrt{LC_{eq}}} \quad (5-2)$$

$C_{eq}$  is the series combination of capacitors  $C$  and  $C'_c$ , where  $C'_c$  is the capacitance  $C_c$  referred to the primary:

$$C'_c = \left( \frac{N_2}{N_1} \right)^2 C_c = 81 \cdot C_c \quad (5-3)$$

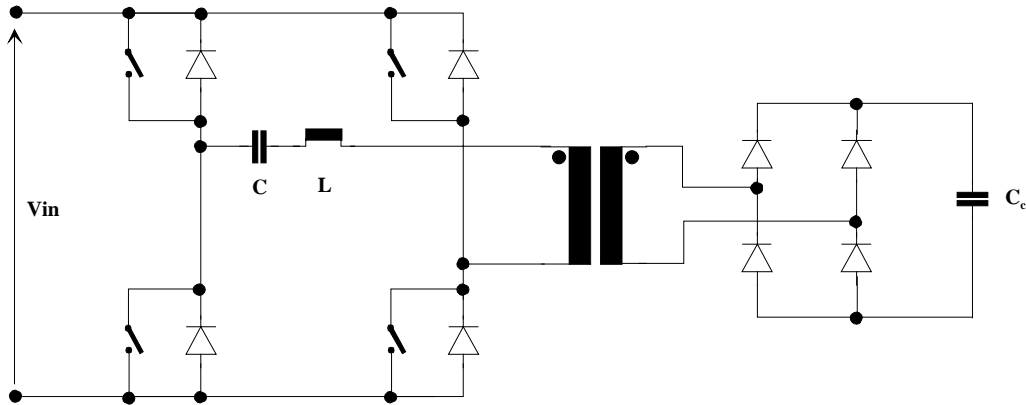


Figure 18: Series-loaded resonant converter.

As usually in high-voltage applications,  $C_c$  ( $0.1 \mu\text{F}$  in our case) is at least one order of magnitude greater than  $C$ . Then its contribute is negligible and:

$$C_{eq} = \frac{1}{\frac{1}{C} + \frac{1}{C'_c}} \approx C \quad (5-4)$$

Therefore,  $Z_0$  and  $f_0$  are uniquely defined by  $C$  and  $L$ . Operating the circuit at a frequency  $f_s < f_0/2$ , all switches and anti-parallel diodes turn on and off at zero current [Moh89]. Using a frequency  $f_0/2 < f_s < f_0$  the diodes' turn off and the switches' turn on happens at a current greater than zero. Conversely, for  $f_s > f_0$ , the diodes turn on and the switches turn off at a current greater than zero. Operation at a frequency slightly less than  $f_0/2$  presents several advantages:

- Because the commutation of switches and diodes happens when the current is zero, switching losses are reduced to a minimum and no snubbers are required.
- For the same reason, switch commutation time and diode reverse recovery time are not critical.
- At this frequency (or at a lower one) the converter behaves as a constant current source [Moh89], providing an inherent overload protection capability together with the best output characteristic for a CCPS.

All of the above advantages are lost for  $f_s > f_0/2$ , while for  $f_s$  increasingly lower  $f_0/2$  the average current supplied gets accordingly lower, thus increasing the capacitor charge time.

Operation of the SLR converter can be accurately simulated with MicroSim (Figure 19) using actual component values. The switches commutation sequence is as follows:

1. S1 and S4 close at time 0.
2. S1 and S4 open at time  $1 / (2 \cdot f_0)$ .
3. Negative current flows back through D1 and D4, reaching zero at time  $1 / f_0$ .

4. S3 and S2 close at time  $k + 1 / f_0$ .
5. S3 and S2 open at time  $k + 1 / f_0 + 1 / (2 f_0)$ .
6. Negative current flows back through D3 and D2, reaching zero at time  $k + 1 / f_0 + 1 / f_0$ .
7. The switching cycle is repeated.

K is the dead time between phase 3 and phase 4: when  $k = 0$  then  $f_s = f_0/2$ , while for  $k > 0$  is  $f_s < f_0/2$ .

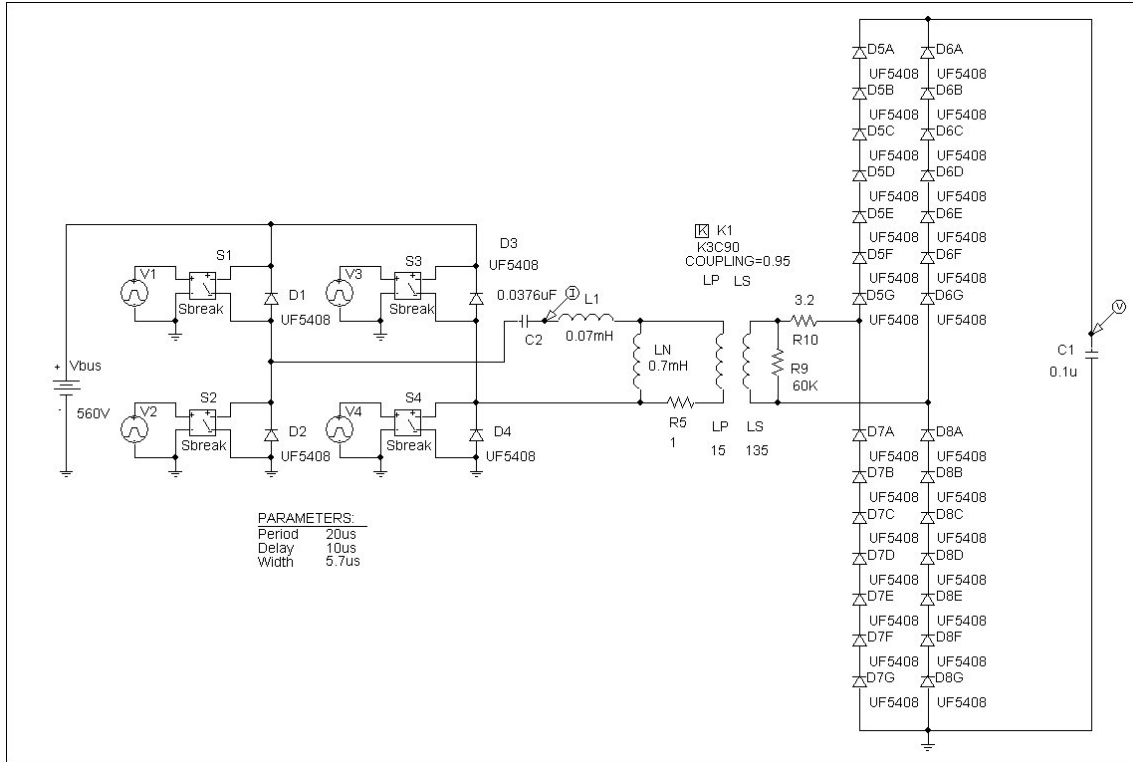


Figure 19: MicroSim simulation of the SLR converter.

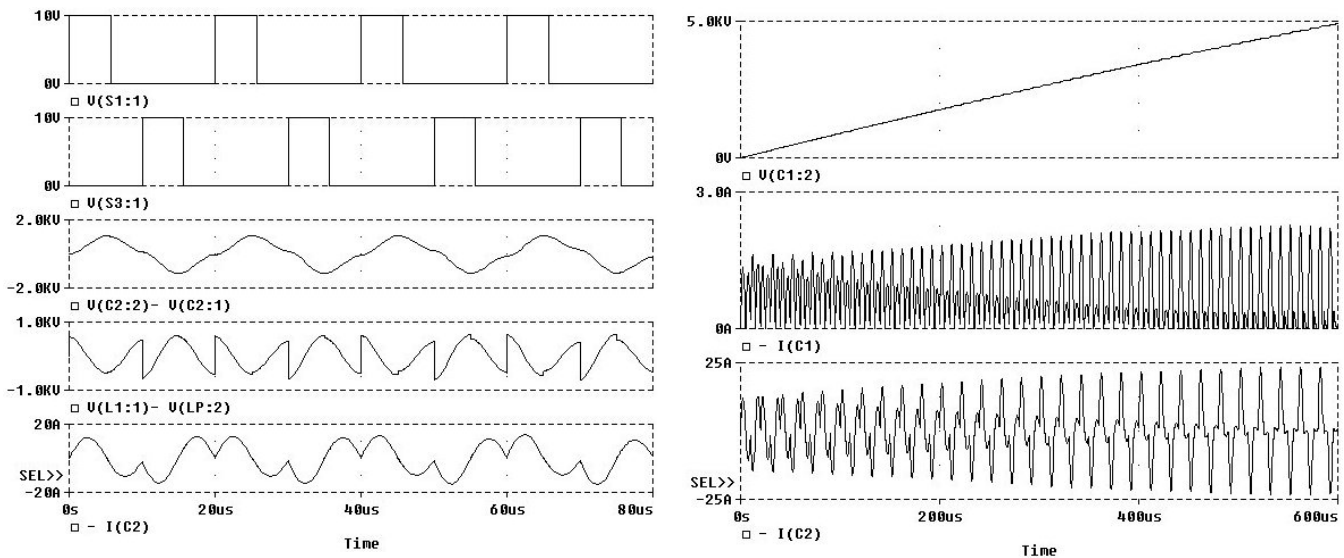


Figure 20: SLR converter simulation waveforms.

With the component values used in the simulation  $f_0 \approx 100$  kHz,  $1/(2f_0) \approx 5$   $\mu$ s and  $k$  is chosen to be zero. As it can be seen from the simulation results (Figure 20), the current flowing in the series-resonant load C2 and L1 is a series of sinusoids and the switches are commutated when the current crosses zero. Voltage on the capacitor under charge increases at a constant rate, as the pulsed charging current average value is constant during all the cycle.

The maximum peak reverse current flowing through the diodes D1–D4 when one switch pair is open is given by:

$$I_{\text{OFF max}} = -\frac{V_{\text{in}}}{Z_0} \quad (5-5)$$

The above value is assumed at the charge beginning and drops down to zero at the charge end; this is due to the voltage reversal effect across the load terminals, caused by the voltage present on the capacitor under charge. Conversely, the maximum peak current flowing in the load C2 and L1 when a switch pair is closed is given by:

$$I_{\text{ON max}} = \frac{2V_{\text{in}}}{Z_0} = -2I_{\text{OFF max}} \quad (5-6)$$

This value is reached only at the end of the charge and is due to the energy accumulated in the resonant load C2 and L1; at charge beginning is  $I_{\text{ON}} = -I_{\text{OFF max}}$ . The SLR converter switches must be capable to stand  $I_{\text{ON max}}$ , while the diodes can be dimensioned to operate at  $I_{\text{OFF max}}$  only. With the component values used in the simulation is:

$$I_{\text{OFF max}} = -\frac{V_{\text{in}}}{Z_0} = -\frac{V_{\text{in}}}{\sqrt{\frac{L_1}{C_2}}} = \frac{560}{\sqrt{\frac{0.07 \cdot 10^{-3}}{0.0376 \cdot 10^{-6}}}} = -13 \text{ A} \quad (5-7)$$

$$I_{\text{ON max}} = -2I_{\text{OFF max}} = 26 \text{ A} \quad (5-8)$$

The RMS capacitor charging current can be calculated directly from the capacitor charging rate displayed in Figure 20 as:

$$I_{\text{C rms}} = \frac{C_1 \Delta V}{\Delta t} = \frac{0.1 \cdot 10^{-6} \cdot 5000}{600 \cdot 10^{-6}} = 833 \text{ mA} \quad (5-9)$$

The RMS current in the resonant load and transformer primary  $I_{1 \text{ rms}}$  can be calculated by balancing the average power between capacitor ( $P_{\text{C av}}$ ) and load ( $P_{\text{L av}}$ ):

$$P_{\text{C av}} = \frac{I_{\text{C rms}} \cdot \Delta V}{2} = \frac{833 \cdot 10^{-3} \cdot 5000}{2} = 2083 \text{ W} \quad (5-10)$$

$$I_{1 \text{ rms}} = \frac{P_{\text{L av}}}{V_{\text{in}}} = \frac{P_{\text{C av}}}{V_{\text{in}}} = \frac{2083}{560} = 3.7 \text{ A} \quad (5-11)$$

The theoretical power achieved with these components is:

$$P = \frac{0.5 \cdot C_1 \cdot (\Delta V)^2}{\Delta t} = \frac{0.5 \cdot 0.1 \cdot 10^{-6} \cdot 5000^2}{600 \cdot 10^{-6}} = 2083 \text{ W} \quad (5-12)$$

The calculated power capacity is more than sufficient to ensure an actual value surely greater than the targeted 1.25 kW.

### 5.2.2. Bridge switch design

The bridge switch module includes four IGBT solid-state switches, their drive circuitry plus additional components generating 560 V, 15 V and 5 V DC.

The IGBT is a relatively new power semiconductor device, which provides the best features of both the MOSFET and the BJT [Tak95]. Among its advantages:

- Low-power, voltage-driven gate turn-on and turn-off. Gate impedance as high as a MOSFET.
- Low conduction losses.
- Positive temperature coefficient. The device will not experience thermal run-away typical of BJTs.
- Possibility to use either integrated or external anti-parallel diode.

The traditional disadvantage of the IGBT is its slow turn-off speed that results in the well-known current tail. For this application, as the SLR converter commutations take place always when the load current is zero, the slow turn-off doesn't represent a problem. The IGBT used is the IRG4PH40UD type, which features an integrated anti-parallel diode with a relatively fast and soft reverse recovery characteristic. The manufacturer recommends it for hard-switching operation up to 40 kHz, but for resonant-mode operation guarantees 200 kHz functionality.

Table 1: Absolute maximum ratings for the IRG4PH40UD device

Parameter	Value
Collector-to-Emitter breakdown voltage	1200 V
Continuous collector current	30 A
Pulsed collector current	120 A
Diode continuous forward current	8 A
Diode maximum forward current	130 A

Even if the commutations take place at zero current, unwanted spikes and noise in general are present in many nodes of the schematics, due to:

- Parasitic capacities  $C_{ce}$ ,  $C_{gc}$  and  $C_{ge}$  internal to the IGBTs.
- PCB traces impedance.
- Reverse recovery time of the anti-parallel diodes.
- Electromagnetic radiation and coupling within the converter PCB.

The most significant source of unwanted noise is, anyway, the Tesla transformer itself. When the spark gap conducts and the charged capacitor is quickly discharged on the primary

coil, high voltage transients are generated on the capacitor. These transients propagate through the step-up transformer as a sudden change of load impedance, which in turn causes high-current spikes in the IGBT bridge. Therefore, a particular attention is required for protecting the switch bridge from failure.

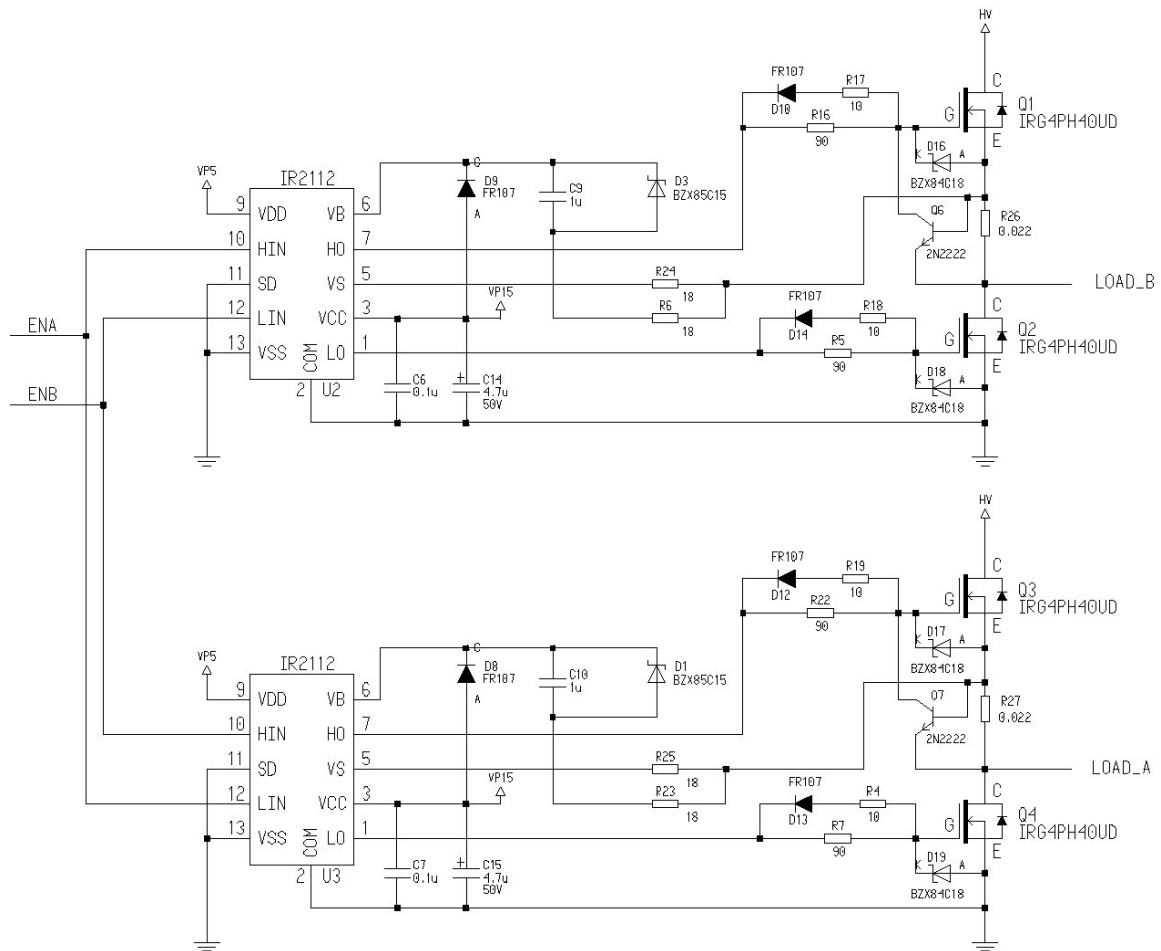


Figure 21: Converter full-bridge schematic diagram.

The gate charging current (at turn on) is limited by a 90 ohm resistor to decrease the  $dv/dt$  of the collector-to-emitter voltage during switching. Conversely, turn-off happens through a 10 ohm resistor that provides a low gate-to-emitter impedance, protecting the IGBT from spurious commutation. A zener diode between gate and emitter limits the gate drive voltage to a maximum of 18 V, clipping all spikes that could potentially damage the IGBT junction. Short traces and SMD zeners are used in order to minimize parasitic inductances and decrease response time. Transistors Q6 and Q7 (see Figure 21) limit the maximum current in each of the bridge legs to 33 A; in the remote case of simultaneous turn-on of both IGBTs belonging to the same bridge leg, this protection gives time to a fuse to safely blow open, avoiding damages to PCB traces and other components.

An IR2112 driver chip controls each IGBT pair, providing a gate charging voltage of 15 V. In order to operate the bridge in the SLR converter mode, signal ENA enables Q6 and Q4 while signal ENB enables Q2 and Q3. The IR2112 is fully operational up to 600 V and has got separate CMOS Schmitt-triggered inputs for the bridge low and high side. The floating voltage required to turn on the high side IGBT is provided by charging C9 and C10 to 15 V when the corresponding IGBT on the low side is conducting. Zeners D3 and D1 together with resistors R6 and R23 prevent C9 and C10 to overcharge as a result of ground bounce.

Resistors R24 and R25 reduce possible oscillations of the IR2112 pin VS below ground and above HV. Without the protection circuitry described above and a careful PCB layout avoiding long traces and ground loops, destruction of the IGBTs and/or the IR2112s is almost certain within a few seconds of operation together with the Tesla transformer.

The 560 V DC (HV in Figure 21) is derived by rectifying the 3-phase mains and filtered by a 235  $\mu\text{F}$  800 V electrolytic capacitor bank. The capacitor bank terminals cannot be connected to the mains neutral pole, and the converter ground cannot be heartened. All the bridge switch circuitry is subjected to potentials ranging from +400 V to -400 V in respect to the neutral pole and special measurement techniques must be employed, including insulation transformers and differential probes.

Galvanic isolation at the two bridge control inputs is provided by the HCPL-2430 high-speed logic optocoupler, followed by a tiny logic block built around a 74HCT02 that ensures signals ENA and ENB can never be asserted simultaneously. The whole bridge switch is assembled on a double-side PCB sized 100 x 160 mm and enclosed in a shielded standard rack unit, measuring 3U x 14HP.

### 5.2.3. Resonant load design

The resonant load is composed by the capacitor C (Figure 18), the step-up transformer, and a high-voltage, full-wave rectifier bridge. The leakage inductance of the transformer is utilized as the resonance inductor L.

The primary is composed of 3 windings of 15 turns each connected in parallel to minimize skin effect losses; wire section is 0.5 mm. The secondary is composed of a single winding of 135 turns of wire with section 0.3 mm; as the wire is wound on a single layer, there is no inter-winding corona. Due to the relatively loose coupling of primary and secondary, the primary exhibits a winding inductance of 0.7 mH and a leakage inductance of 70  $\mu\text{H}$ , as required. The assembled transformer measures 100 x 114 x 25 mm.

Each arm of the full-wave rectifier bridge is composed by a series of seven UF5408 diodes, capable to stand a continuous reverse voltage of 1000 V and an average forward current of 3 A. Each bridge arm is therefore functional up to 7 kV, ensuring a sufficient margin for transients. Due to the relatively high frequency of the pulses to be rectified (100 kHz), a fast rectifier is required to avoid overheating; the UF5408 provides a reverse recovery time of max 75 ns, which is sufficient to fulfill the requirements. The bridge DC output is shunted by a light load composed by the parallel of a 550 pF capacitor and a 40 Mohm resistor. This facilitates an homogenous voltage distribution when more converters are connected in series to reach a 20 kV output voltage.

### 5.2.4. Step-up transformer design

Compromises must be made when designing the transformer to operate under both high-frequency and high-voltage conditions. High frequency requires a small, high-permeability core (e.g. ferrite), tight windings and close proximity between primary and secondary. High-voltage design instead requires a minimum separation between individual turns and between primary and secondary windings, to avoid dielectric breakdown.

Primary and secondary are wound on two different legs of the core, therefore simplifying enormously insulation problems. Dielectric strength required between primary and core is 1.3 kV, while between secondary and core 10 kV is required. Coil formers for both windings are custom made out of 1.5-mm thick acrylic sheet and are covered with one layer of Kapton or Mylar tape before winding. The primary winding includes also an electrostatic shield (which is grounded) to reduce capacitive coupling between primary and secondary and avoid

high-voltage to reach the bridge switch circuitry in case of a dielectric breakdown at the secondary. The transformer requirements are listed in Table 2.

Table 2: Transformer design specification

Symbol	Parameter	Value
$V_1$	Primary RMS voltage	560 V
$V_2$	Secondary RMS voltage	5 kV
$I_1$	Primary RMS current	3.7 A
$I_2$	Secondary RMS current	0.8 A
$f$	Switching frequency	50 kHz
$L_1$	Primary leakage inductance	70 $\mu$ H

To maximize the distance between primary and secondary and taking into account the relative high power transferred, an unconventional approach has been taken for the core selection. Instead to calculate the characteristics of the required core, as usually done, the largest core available has instead been picked and its suitability has been verified. The transformer uses two U-shaped ferrite cores type U100/57/25-3C90 (Philips) having a square cross-section and characteristics as from Table 3 [Phi97].

The winding design is subject to two main constraints:

1. The flux density must be limited to avoid core saturation.
2. Core losses must be limited to avoid excessive temperature rise.

Both of the above requirements translate into a minimum number of turns for the windings.

Table 3: Characteristics of the U100/57/25-3C90 core

Symbol	Parameter	Value
$V_e$	Effective volume	199000 mm <sup>2</sup>
$A_e$	Effective cross section	6.45 cm <sup>2</sup>
$A_w$	Window area	30 cm <sup>2</sup>
$A_L$	Inductance factor	5500 nH
$\mu_c$	Effective permeability	2200

From the product sheet of the 3C90 material, a safe value  $B_{\max}$  of 400 mT is selected for the maximum flux density [Phi99]. To avoid core saturation,  $B_{\max}$  must not be exceeded; the minimum number of primary turns is therefore restricted to satisfy this requirement. The correct calculation of the core flux density requires the application of the Faraday's law [Fla92]:

$$d\phi = \frac{10^4}{N} \int_0^t e \cdot dt \quad (5-13)$$

$$dB = \frac{d\phi}{A_e} = \frac{10^4}{A_e N} \int_0^t e \cdot dt \tag{5-14}$$

where:

- $d\phi$  change in flux [maxwell]
- $dB$  change in flux density [T]
- $N$  number of turns
- $A_e$  core magnetic cross section [cm<sup>2</sup>]
- $e$  voltage applied [V]

The value of the above integral is positive for the half-cycle where the voltage is positive and negative for the other half-cycle of voltage. When the positive half-cycle begins,  $B$  is at its maximum negative value; therefore, its maximum value is only one half of its total change.

$$B'_{\max} = \frac{dB}{2} = \frac{10^4}{2A_e N} \int_0^t e \cdot dt \tag{5-15}$$

The integration interval of interest is defined as one half-period when the voltage is positive, or the other half-period when the voltage is negative; the half-period having the greatest integration area has to be selected, resulting in the maximum  $dB$  value. The solution of the integral is made difficult by the complex waveshape of the voltage applied to the transformer primary (Figure 22) and its profile changing together with the charge evolution.

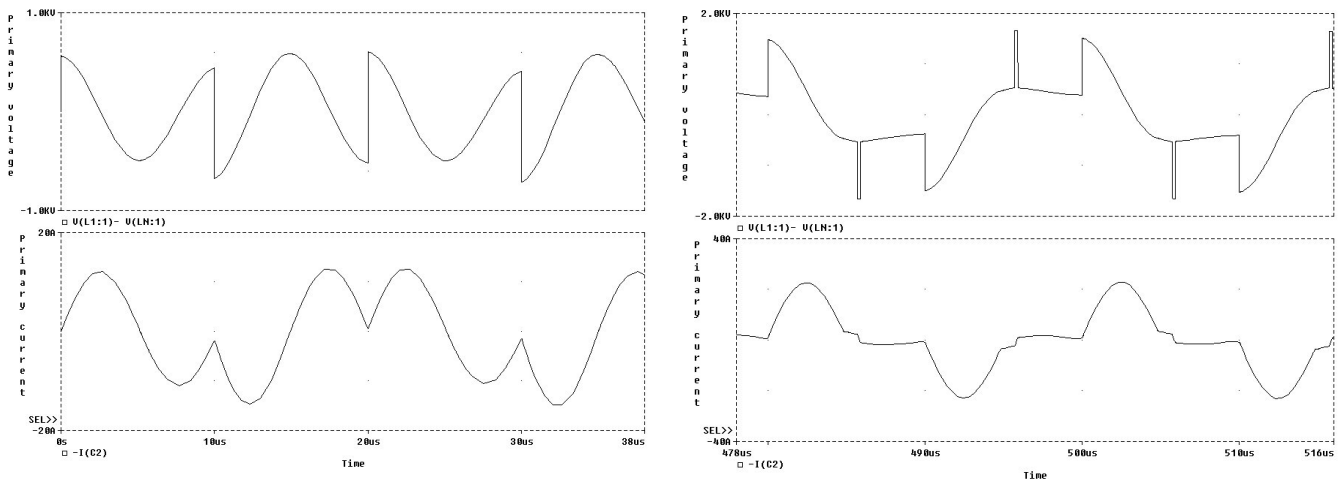


Figure 22: Simulation of transformer primary voltage and current at charge beginning (left) and end (right).

A better approach is to use MicroSim and integrate the primary voltage over the entire charge interval (Figure 23). The resulting measure is directly proportional to the flux density  $B$  instant value and we have:

$$B_{\max} = \text{MAX} \left( \frac{10^4}{A_e N} \int_0^t e \cdot dt \right) = \frac{10^4}{A_e N} \cdot \text{MAX} \left( \int_0^t e \cdot dt \right) \quad (5-16)$$

From the MicroSim simulation the largest integral value can be found near the charge end and it is:

$$\text{MAX} \left( \int_0^t e \cdot dt \right) \approx 3.16 \cdot 10^{-3} \text{ V} \cdot \text{s} \quad (5-17)$$

Then:

$$N_{\min} = \frac{10^4}{A_e B_{\max}} \text{MAX} \left( \int_0^t e \cdot dt \right) = \frac{10^4}{6.45 \cdot 0.4} \cdot 3.16 \cdot 10^{-3} \approx 12 \text{ turns} \quad (5-18)$$

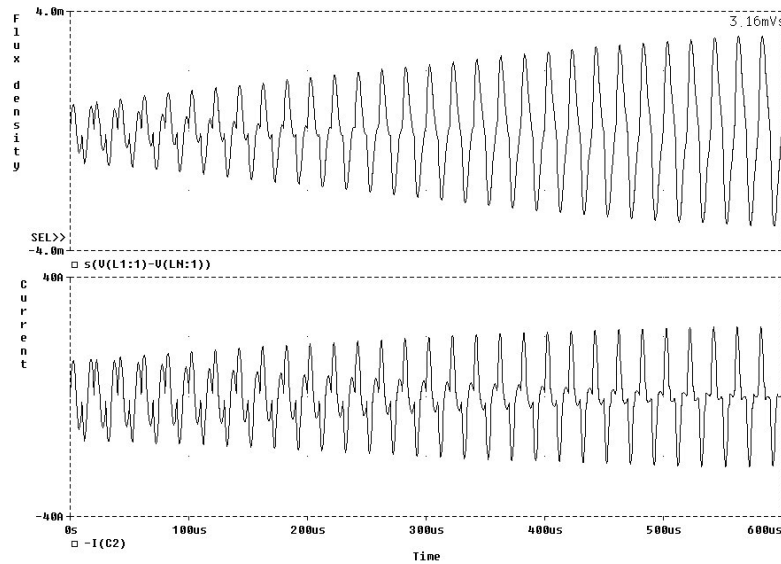


Figure 23: Simulation of the transformer current (lower trace) and of its voltage integrated over time (upper trace).

Power losses in the core due to hysteresis losses and eddy current are directly proportional to the maximum flux density. As seen before, the maximum flux density changes during the charge cycle; a sufficient approximation is given by averaging the peak values of the term

$$\int_0^t e \cdot dt \quad (5-19)$$

over all half-cycles from zero to full charge. This can be done using MicroSim by computing the average of the integral envelope:

$$\int_0^t e \cdot dt \Big|_{\text{av}} = \text{AVG} \left( \text{ENVMAX} \left( \int_0^t e \cdot dt \Big|_{,10} \right) \right) = 2.13 \cdot 10^{-3} \text{ V} \cdot \text{s} \quad (5-20)$$

The thermal resistance  $R_t$  for the core is not published but may be approximately calculated as [Uni93]:

$$R_t \approx 23 \cdot (A_e A_w)^{-0.37} = 23 \cdot (6.45 \cdot 30)^{-0.37} = 3.3 \text{ }^\circ\text{C/W} \quad (5-21)$$

Targeting a maximum temperature rise of 100 °C, the resulting power loss is:

$$P_v = \frac{\Delta T}{R_t \cdot V_e} = \frac{80}{3.3 \cdot 199000 \cdot 10^{-9}} = 152 \text{ kW/m}^3 \quad (5-22)$$

From the product sheet of the 3C90 material, at a switching frequency of 50 kHz, a power loss of 152 kW/m<sup>3</sup> is dissipated when using a peak flux density of about 0.2 T. The corresponding minimum number of primary turns is:

$$N_{\min} = \frac{10^4}{A_e B_{\max}} \cdot \int_0^t e \cdot dt \Big|_{\text{av}} = \frac{10^4}{6.45 \cdot 0.2} \cdot 2.13 \cdot 10^{-3} \approx 16 \text{ turns} \quad (5-23)$$

The design is therefore core-loss limited. Because a pretty thick coil former is used (1.5 mm) and the magnetic coupling is not optimal, it is feasible to use a number of turns slightly lower than  $N_{\min}$ . Practical tests indicate that 15 turns for the primary winding allow achieving exactly the 70 µH of leakage inductance targeted. It is then assumed:

$$N_1 = 15 \text{ turns}$$

$$N_2 = N_1 \frac{V_2}{V_1} = 15 \frac{5000}{560} \approx 135 \text{ turns}$$

Selecting the typical RMS current density of 450 A/cm<sup>2</sup>, the required copper sections for the windings are:

$$S_1 = \frac{I_1}{J} = \frac{3.7}{450} = 8.2 \cdot 10^{-3} \text{ cm}^2$$

$$S_2 = \frac{I_2}{J} = \frac{0.8}{450} = 1.78 \cdot 10^{-3} \text{ cm}^2 \quad (5-24)$$

From the wire tables, AWG18 wire (1 mm diameter) is required for the primary and AWG24 (0.5 mm diameter) for the secondary. At the working frequency, the penetration depth for copper is only:

$$D_{\text{pen}} = \frac{75}{\sqrt{f}} = \frac{75}{\sqrt{50000}} = 0.33 \text{ mm} \quad (5-25)$$

Therefore, the targeted current density cannot be achieved using a single-wire winding. As the number of primary turns is very small and there is plenty of winding space left, the primary is built using 3 windings of 15 turns each connected in parallel, wound using AWG24 (0.5 mm diameter). The secondary wire section choice is constrained by the requirement to have only a single winding layer, in order to avoid inter-winding corona discharges. As the usable core window winding length is about 50 mm, the maximum wire diameter is:

$$d_2 = \frac{l}{N_2} = \frac{50}{135} = 0.37 \text{ mm} \quad (5-26)$$

A single layer with 135 turns of AWG29 (0.3 mm diameter) is used for the secondary. As the core heat dissipating surface area is huge compared with the area of the core window effectively filled, it is believed that current density higher than 450 A/cm<sup>2</sup> can be easily used for the secondary.

### 5.3. High voltage probe

The high voltage probe module is responsible for measuring the voltage developed on the capacitor under charge and providing the controller module with a voltage proportional to it. As the converter module outputs are connected in series but the middle modules are tapped to ground (see Figure 16), the resulting voltage is the sum of a potential max 10 kV positive in respect to ground, plus a second potential max 10 kV negative in respect to ground. As all converter modules are built the same way, their performance is almost identical and a unique control signal pair is sufficient to control all four bridge switch groups. Nevertheless, it is useful to measure the absolute difference of these two voltages: it is a good indicator of a uniform voltage distribution on the converter module outputs and therefore of their functionality.

Two compensated voltage dividers with ratio 1:50000 reduce the potentials measured to 0.2V (at 10 kV input voltage); the dividers are encapsulated in two shells filled with epoxy resin. The signals are then fed to two HCPL-7800 isolation amplifiers (Figure 24); these parts exhibit a non-linearity error of 0.004% and a gain of 8. Their input side is powered by a LME0505S DC-DC converter and, therefore, is completely insulated from the output side. The differential outputs of the isolation amplifiers is buffered to 1.5 V (at 10 kV input voltage) by two EL2444 operational amplifier sections and fed to a summer and a difference amplifier.

The output of the difference amplifier (VSENSE) is proportional to the sum of the absolute value of the two input voltages HV+ and HV- and assumes a maximum value of 3 V when the capacitor is charged to 20 kV. The output of the summer is proportional to the difference of the absolute values of HV+ and HV- and is fed to the input of a window detector composed by two sections of a LM339 OPAMP. The window is centered at 0 V and set to assert the signal VNBIGGER\_ if the sum of HV+ and HV- is less than -100 V or signal VPBIGGER\_ if their sum is greater than 100 V. The FAULT\_ signal is the logical OR of VNBIGGER\_ and VPBIGGER\_ and can be used to detect a fault in the converter modules. A fraction of VSENSE is available for connection to an external LCD voltage meter mounted on the probe module front panel and displaying the capacitor charging voltage, expressed in kilovolts.

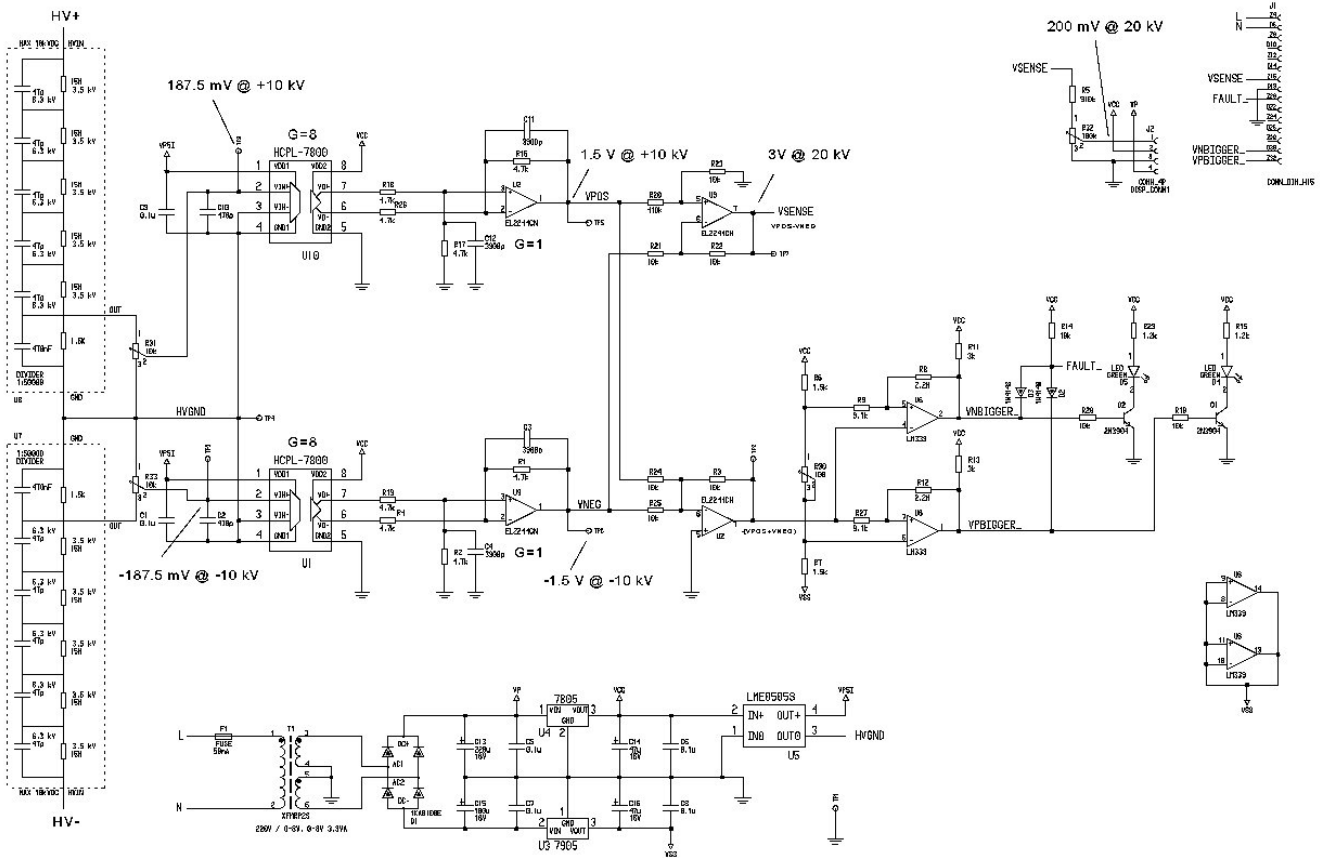


Figure 24: High voltage probe schematic diagram.

The high voltage probe is assembled on a double-side PCB sized 100 x 160 mm and enclosed in a shielded standard rack unit, measuring 3U x 14HP. The HV+ and HV- input leads are available on the module front panel through two high voltage connector sockets (same kind used in the converter modules).

### 5.4. Controller

The CCPS controller module is built around the UC3860 Resonant Mode Power Supply controller chip (Figure 25). Drive pulses for the converter modules are generated on pins 17 and 20 (signals OUTA and OUTB) according to the sequence A, off, B, off.

For a resonance load frequency of 100 kHz (see Chapter 5.2.1), output A must be active for 5 μs, then both outputs must be off for 5 μs, then output B on for 5 μs and finally both outputs off for 5 μs. This sequence translates into a UC3860 switching period of 10 μs (i.e. a switching frequency of 100 kHz). The pulse frequency can be varied from 40 to 110 kHz using trimmer R8. Pulse duration is variable from 3.6 to 8 μs through trimmer R10 and set to the required 5 μs.

The UC3860 is fed with 12V (VP12) and generates a reference voltage of 5V (VP5). An internal Under Voltage Lockout logic turns both outputs off and inhibits the oscillator if VP12 drops below 8V. Operation starts only if VP12 is safely higher than 9.2V.



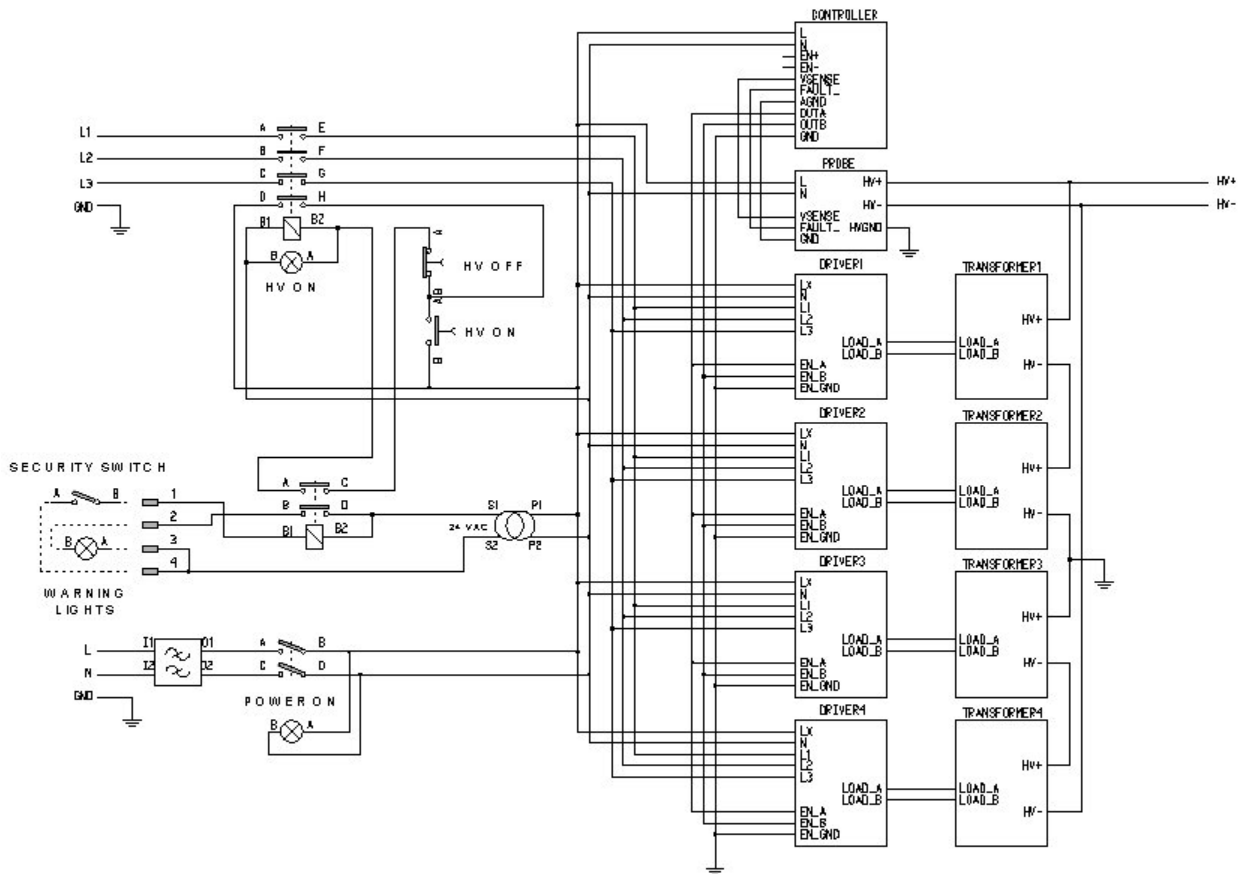


Figure 26: CCPS modules' interconnection.

### 5.5. Module interconnection and auxiliary circuitry

The CCPS modules are connected as from Figure 26. A double switch supplies the device with one single mains phase, powering the control logic part of each module. If the external security switch is closed, the main contactor can be energized by pressing the HV ON pushbutton; the contactor feeds all three phase to the power section of the four converters (named DRIVER modules in Figure 26). Pressing the HV OFF emergency pushbutton or opening the security switch releases the contactor immediately. The outputs of the converters (named TRANSFORMER in Figure 26) are connected in series and center-tapped to ground.

### 5.6. Assembly and mechanics

The whole CCPS together with its auxiliary circuitry is assembled in a standard 19" rack 9 U high (Figure 27). Each module is mounted inside a 14 HP wide plug-in frame box and connections to the other modules are realized through DIN 41612 type H connectors.

As the commutation losses of the SLR topology are very low, the converter modules' IGBT are equipped with a relatively small heatsink ( $3.7 \text{ }^\circ\text{C/W}$ ) which has proven to be sufficient. The three-phase mains has shown to be prone to flashover with the rest of the converter circuitry, due to its floating nature and the potential swinging effect of the Tesla transformer transients. The mains are therefore taken to the module through a second DIN connector different from the one used by the rest of the signals and fed to the PCB only after rectification (Figure 28).

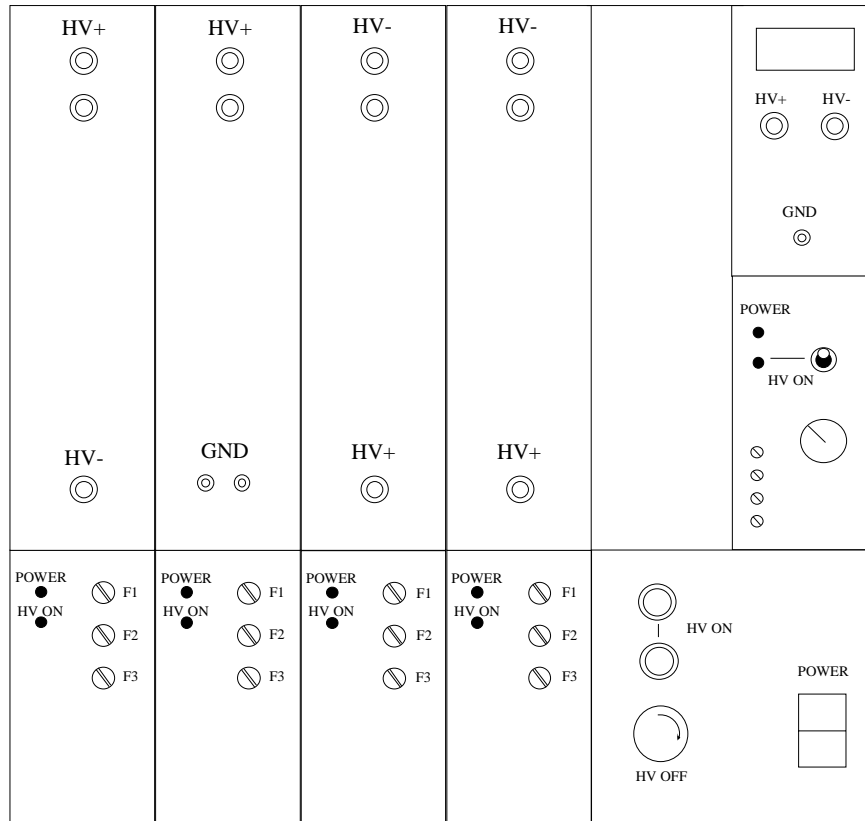


Figure 27: The CCPC rack housing.

All of the resonant load components are assembled on a double-side PCB sized 160 x 232 mm and enclosed in a shielded standard rack unit, measuring 6U x 14HP.

The high voltage terminals from the diode bridge are connected to high voltage connector sockets mounted on the module front panel. These connector sockets and their related plugs have been developed at the HUT High Voltage Laboratory and tested to be functional up to 30 kV DC.

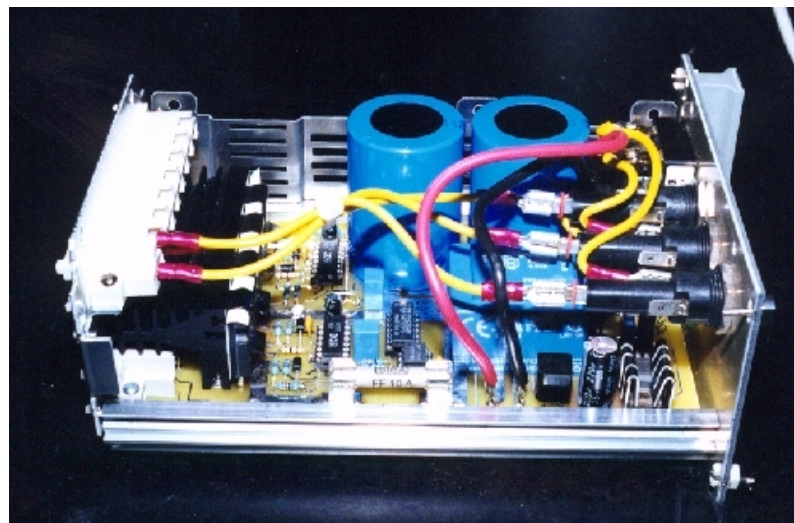


Figure 28: One of the plug-in converter modules.



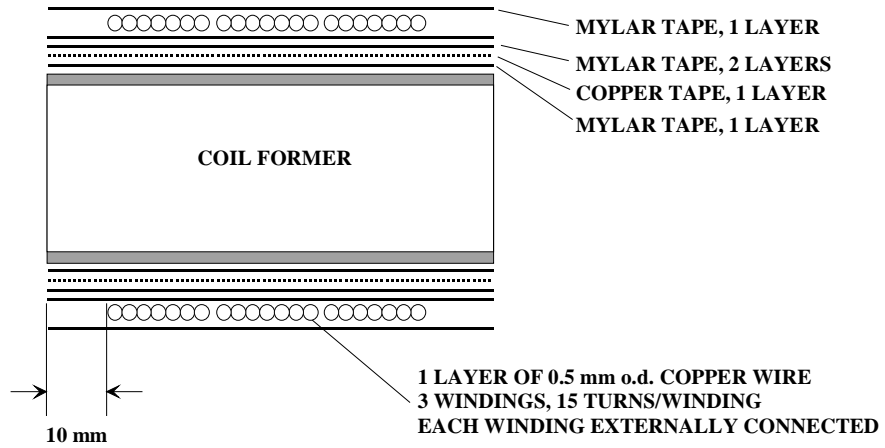


Figure 31: Primary winding organization.

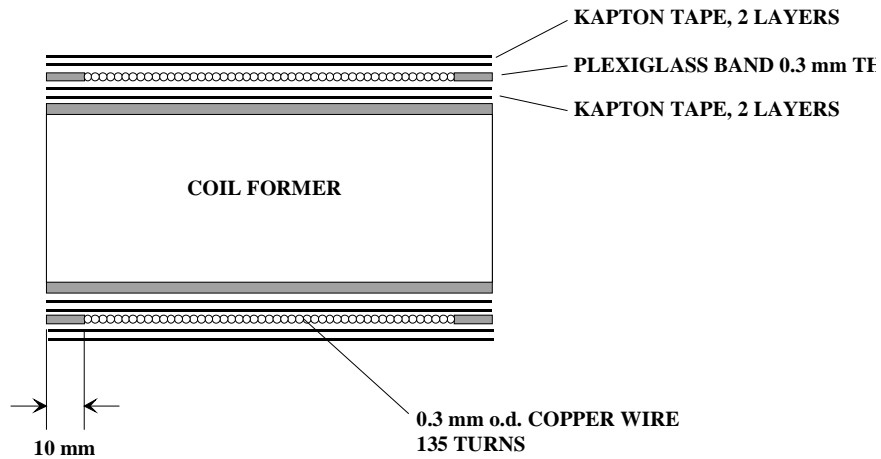


Figure 32: Secondary winding organization.

## 6. TESLA COIL MODELING AND MEASUREMENTS

This chapter describes Thor's modeling process and the measurements performed to validate its model. First, a detailed, classical description of the TC theory of operation is given; the working point optimization is treated according to Phung's work [Phu91], aiming at developing the maximum secondary voltage (see also Chapter 1.5) and according to Finkelstein's work [Fin66], seeking for a complete energy transfer, with some additions. The secondary coil is described abandoning the lumped-circuit view and employing a novel approach [Nic01].

Then the measurements performed on Thor are reported, being the first part of them intended for finding out the values of its components and the last part used to describe its functionality.

Thor is modeled in Chapter 6.3: an equivalent inductance and capacitance are derived for the secondary coil, a simple model for the spark gap is proposed and, finally, a complete model of Thor's primary and secondary circuits is built. The validity of the overall model is proved at the end of this chapter by comparing measured and simulated waveforms.

### 6.1. Detailed theory of operation

#### 6.1.1. Air-coupled resonant circuits

Operation of the Thor Tesla Coil can be regarded as that of two inductively air-coupled, damped resonant circuits (Figure 33). The primary circuit is formed when the spark gap conducts and connects in series the primary capacitor  $C_1$ , the primary winding  $L_1$  and its equivalent resistance  $R_1$ . The secondary circuit is formed by the series of the secondary winding  $L_2$  with its equivalent resistance  $R_2$  and with the top toroid  $C_2$ . The loop is closed through ground, as the secondary coil base is grounded and the top toroid exhibits a lumped capacity in respect to ground too. The primary and secondary coils are inductively coupled with each other with mutual inductance  $M$ .

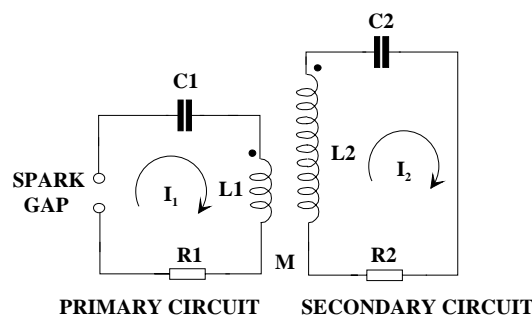


Figure 33: Inductively coupled primary and secondary circuits in a TC.

According to the first Kirchoff law, the sum of the voltages around a closed circuit is zero, therefore [Ter43, Smy50]:

$$R_1 i_1 + \frac{1}{C_1} \int i_1 dt + L_1 \frac{di_1}{dt} + M \frac{di_2}{dt} = 0 \quad (6-1)$$

$$R_2 i_2 + \frac{1}{C_2} \int i_2 dt + L_2 \frac{di_2}{dt} + M \frac{di_1}{dt} = 0 \quad (6-2)$$

If  $q_i$  is the instantaneous charge on the capacitors  $C_1$  and  $C_2$ , for each circuit is

$$i_i = \frac{dq_i}{dt} \quad i = 1, 2 \quad (6-3)$$

Substituting in Equation (6-1) and (6-2)

$$R_1 \frac{dq_1}{dt} + \frac{1}{C_1} q_1 + L_1 \frac{d^2 q_1}{dt^2} + M \frac{d^2 q_2}{dt^2} = 0 \quad (6-4)$$

$$R_2 \frac{dq_2}{dt} + \frac{1}{C_2} q_2 + L_2 \frac{d^2 q_2}{dt^2} + M \frac{d^2 q_1}{dt^2} = 0 \quad (6-5)$$

Rearranging and introducing the operator  $\mathcal{D}$  as the differential operator with respect to time  $t$

$$\left[ \mathcal{D}^2 + \frac{R_1}{L_1} \mathcal{D} + \frac{1}{L_1 C_1} \right] q_1 + \frac{M}{L_1} \mathcal{D} q_2 = 0 \quad (6-6)$$

$$\left[ \mathcal{D}^2 + \frac{R_2}{L_2} \mathcal{D} + \frac{1}{L_2 C_2} \right] q_2 + \frac{M}{L_2} \mathcal{D} q_1 = 0 \quad (6-7)$$

The above equations yield the following auxiliary equation (or characteristic equation) [Hof75]

$$\begin{aligned} (1 - k^2) D^4 + \left( \frac{R_1}{L_1} + \frac{R_2}{L_2} \right) D^3 + \left( \omega_1^2 + \omega_2^2 + \frac{R_1 R_2}{L_1 L_2} \right) D^2 + \\ \left( \frac{R_1}{L_1} \omega_2^2 + \frac{R_2}{L_2} \omega_1^2 \right) D + \omega_1^2 \omega_2^2 = 0 \end{aligned} \quad (6-8)$$

where:

$$k = \frac{M}{\sqrt{L_1 L_2}} \quad (6-9)$$

$$\omega_i = \frac{1}{\sqrt{L_i C_i}} \quad i = 1, 2 \quad (6-10)$$

$k$  is the coupling coefficient ( $0 < k < 1$ ), while  $\omega_1$  and  $\omega_2$  are, respectively, the angular resonance frequencies of the uncoupled primary and secondary circuits (also called open-circuit resonances).

Equation (6-8) is a fourth-order linear homogeneous differential equation that has got four complex roots  $D_i$ ,  $i=1..4$ . If these roots are distinct then the four functions

$$y_i = e^{D_i t} \quad i = 1..4 \quad (6-11)$$

constitute a basis of the space of solutions for the system formed by Equation (6-6) and Equation (6-7). The general solution of this system is therefore

$$q_1 = \sum_{i=1}^4 A_i e^{D_i t} \quad (6-12)$$

$$q_2 = \sum_{i=1}^4 B_i e^{D_i t} \quad (6-13)$$

The constants  $A_i$  and  $B_i$  can be evaluated using the initial conditions at  $t=0$

$$\begin{aligned} q_1 &= 0 \\ q_2 &= q_0 \\ \mathcal{D}q_1 &= \mathcal{D}q_2 = 0 \end{aligned} \quad (6-14)$$

where  $q_0$  is the initial charge on the primary capacitor. The primary and secondary capacitor voltages are simply

$$v_1 = \frac{1}{C_1} q_1 = \frac{1}{C_1} \sum_{i=1}^4 A_i e^{D_i t} \quad (6-15)$$

$$v_2 = \frac{1}{C_2} q_2 = \frac{1}{C_2} \sum_{i=1}^4 B_i e^{D_i t} \quad (6-16)$$

Solutions in a closed form for  $v_1$  and  $v_2$  can be found only for the ideal case of no damping ( $R_1 = R_2 = 0$ ). The roots  $D_i$  of Equation (6-8) have only imaginary parts and the secondary voltage [Cra54] can be expressed as [Phu91]

$$v_2(t) = \frac{2kV_1}{\sqrt{(1-T)^2 + 4k^2 T}} \sqrt{\frac{L_2}{L_1}} \sin\left(\frac{w_2 + w_1}{2} t\right) \sin\left(\frac{w_2 - w_1}{2} t\right) \quad (6-17)$$

where:

$$T = \frac{\omega_1^2}{\omega_2^2} = \frac{L_2 C_2}{L_1 C_1} \quad (6-18)$$

$$\begin{aligned}
 w_1 &= \omega_2 \sqrt{\frac{(1+T) - \sqrt{(1-T)^2 + 4k^2T}}{2(1-k^2)}} \\
 w_2 &= \omega_2 \sqrt{\frac{(1+T) + \sqrt{(1-T)^2 + 4k^2T}}{2(1-k^2)}}
 \end{aligned} \tag{6-19}$$

$T$  is the tuning ratio, defined as the square of the ratio of the uncoupled resonance frequencies, while  $V_1$  is the initial voltage across  $C_1$ .  $w_1$  and  $w_2$  are the resonance frequencies of the primary and secondary circuits when coupled; the physical constraints on the values of  $k$  and  $T$  ensure that  $w_1$  and  $w_2$  are always real.  $w_2 > w_1$  is also assumed.

Equation (6-17) is important and shows that the secondary voltage is a high frequency oscillation  $(w_2 + w_1) / 2$  which is amplitude modulated by another low frequency oscillation  $(w_2 - w_1) / 2$  (for an example, see Figure 7 at page 9).

### 6.1.2. Conditions for maximum voltage gain

From Equation (6-17) in the previous chapter it can be seen that the voltage  $v_2(t)$  at the secondary capacitor  $C_2$  can be greater than the original voltage on  $C_1$  at time zero. This is the basic principle used by the Tesla Coil to generate high voltages at its secondary.

An obvious way to optimize a TC design is to set it for developing the maximum achievable secondary voltage. The maximum voltage gain (from Equation (6-17)) is

$$G = \left. \frac{v_2(t)}{V_1} \right|_{\max} = \frac{2k}{\sqrt{(1-T)^2 + 4k^2T}} G_L \tag{6-20}$$

where:

$$G_L = \sqrt{\frac{L_2}{L_1}} \tag{6-21}$$

Gain  $G$  from Equation (6-20) can be achieved only if both the sine terms in Equation (6-17) are equal to  $\pm 1$  simultaneously, i.e. only if

$$\frac{w_2 + w_1}{2} t = \frac{\pi}{2} + m\pi \quad \text{and} \quad \frac{w_2 - w_1}{2} t = \frac{\pi}{2} + n\pi \tag{6-22}$$

where  $n$  and  $m$  are positive or negative integers. Without losing generality,  $n$  can be set to zero, therefore changing the requirement to

$$\frac{w_2}{w_1} = \frac{1+m}{m} \tag{6-23}$$

Substituting Equation (6-19) into Equation (6-23)

$$k = \sqrt{\frac{\alpha^2(1+T)^2 - (1-T)^2}{4T}} \tag{6-24}$$

where:

$$\alpha = \frac{1+2m}{1+2m+2m^2} \quad (6-25)$$

$k$  can now be eliminated from Equation (6-20) giving [Phu91]

$$G = \frac{v_2(t)}{V_1} \Big|_{\max} = \sqrt{\frac{\alpha^2(1+T)^2 - (1-T)^2}{\alpha^2 T(1+T)^2}} G_L \quad (6-26)$$

The above result has been previously investigated [Ree88,Phu91] striving for maximizing the  $G/G_L$  ratio and pointing out that a value higher than 1 can be obtained for tuning ratios different than unity. Figure 34 shows that this ratio has its maximum for  $T < 1$ , depending on the value chosen for  $m$ ; for instance, if  $m = 1$  then the maximum value achievable for  $G/G_L$  is 1.18 when  $T = 0.541$  and  $k = 0.546$  [Phu91].

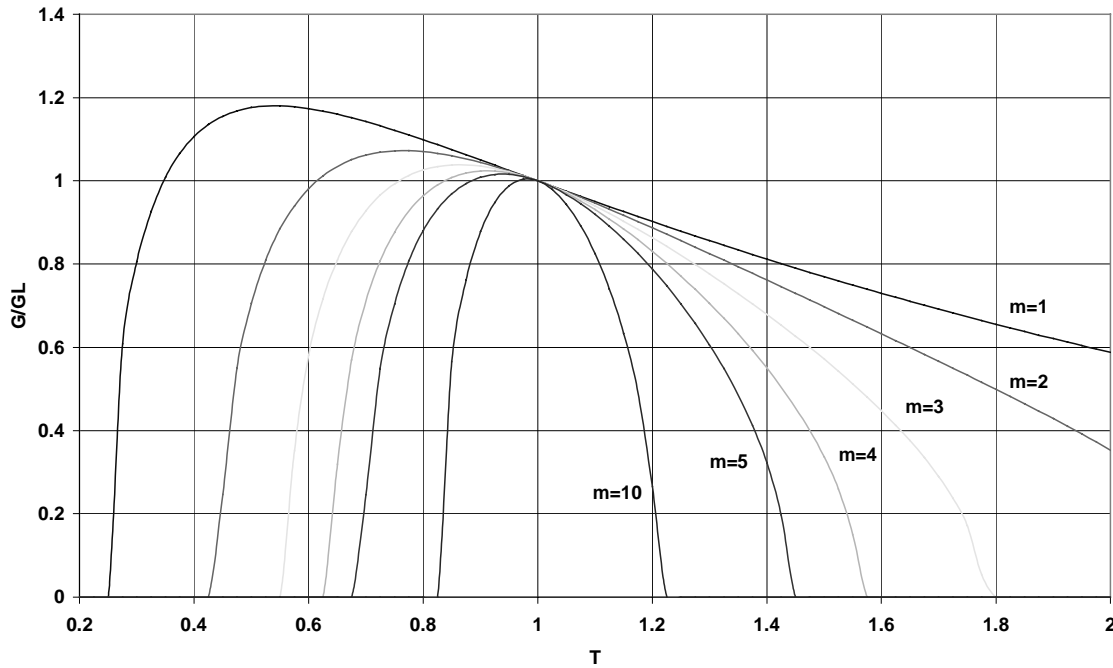


Figure 34:  $G/G_L$  gain vs. tuning ratio  $T$  for different  $m$  values [Phu91].

This analysis is correct and results in a maximized  $v_2(t)$  peak value supposing that the values of  $G_L$  (i.e.  $L_1$  and  $L_2$ ) and of  $V_1$  remains constant. As the tuning ratio  $T$  (Equation (6-18)) can be varied operating on  $C_1$ ,  $C_2$ ,  $L_1$  or  $L_2$ , it is of practical interest to examine each of these cases separately in terms of the overall voltage gain achieved at the secondary. From Equation (6-17) and Equation (6-26)

$$V_2 = v_2(t) \Big|_{\max} = V_1 G = V_1 \sqrt{\frac{\alpha^2(1+T)^2 - (1-T)^2}{\alpha^2 T(1+T)^2}} G_L = V_1 G_T \sqrt{\frac{L_2}{L_1}} \quad (6-27)$$

where:

$$G_T = \frac{G}{G_L} = \sqrt{\frac{\alpha^2(1+T)^2 - (1-T)^2}{\alpha^2 T(1+T)^2}} \tag{6-28}$$

It has to be noted that choosing a value for  $m$ , calculating  $\alpha$  from Equation (6-25), picking a value for  $T$  and calculating  $k$  using Equation (6-24), condition (6-23) is ensured and the sine terms product is maximum ( $\pm 1$ ).

**Optimizing on  $L_1$  or  $L_2$**

From Equation (6-21) and Equation (6-18)

$$T = \frac{L_2 C_2}{L_1 C_1} = G_L^2 \frac{C_2}{C_1} \tag{6-29}$$

Optimizing on  $L_1$  or  $L_2$ ,  $C_1$  and  $C_2$  are constant and, from the equation above

$$G_L = \sqrt{\frac{C_1}{C_2}} T \propto \sqrt{T} \tag{6-30}$$

As also  $V_1$  is constant, from Equation (6-27) and Equation (6-30)

$$V_2 \propto G_T \sqrt{T} \tag{6-31}$$

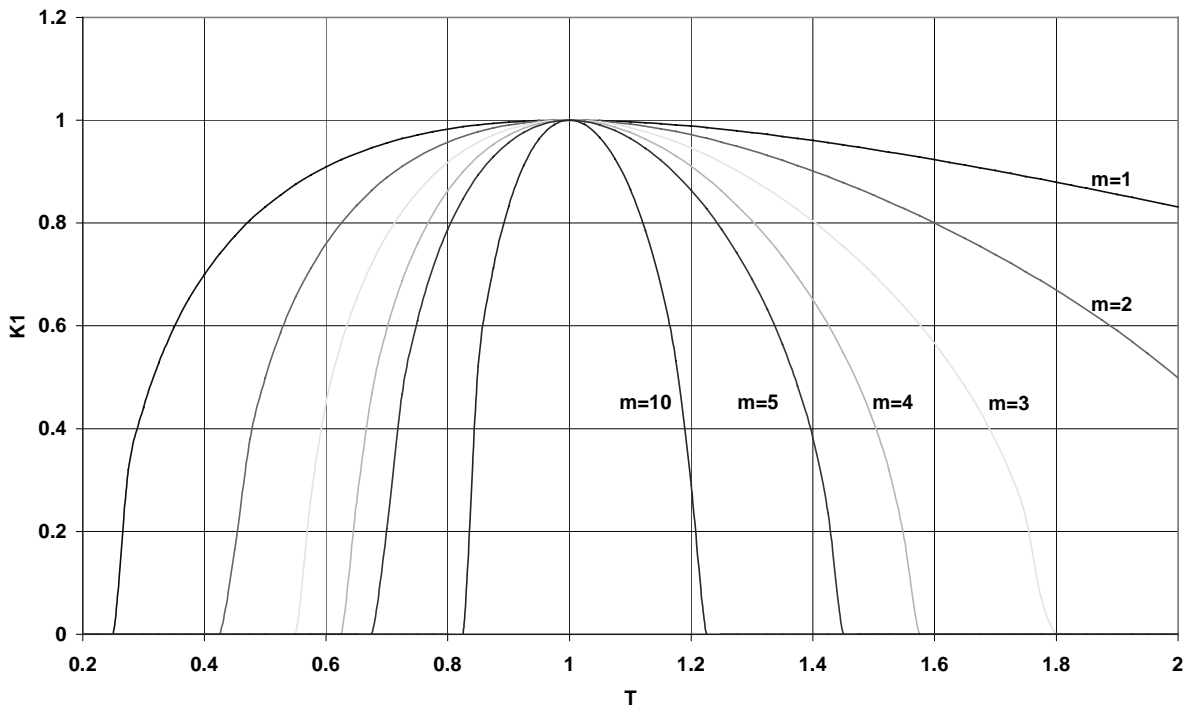


Figure 35:  $K_1$  gain vs. tuning ratio  $T$  for different  $m$  values.

This means that when varying  $T$  by changing  $L_1$  or  $L_2$ , the original graph family from Figure 34 has to be corrected by a factor  $\sqrt{T}$ . Therefore, the variable  $K_1$  can be defined as

$$V_2 \propto K_1 = G_T \sqrt{T} \quad (6-32)$$

From Figure 35 it can be easily seen that the maximum  $V_2$  value is now reached with  $T = 1$ , regardless of the value of  $m$  (anyway,  $m$  has to be an integer as seen before). In practice, on a real Tesla Coil the secondary winding cannot be easily modified but the primary tap can be moved with no problem. At the light of the above considerations, when tuning moving the primary coil tap the best performance can be achieved with a tuning ratio  $T = 1$ .

### Optimizing on $C_1$

When evaluating the benefits of optimizations involving the change of  $C_1$ , it is mandatory to use the same amount of energy  $E_0$  to accumulate the initial charge  $q_0$  on it. Recalling that  $V_1$  is the initial voltage across  $C_1$

$$E_0 = \frac{1}{2} C_1 V_1^2 \quad (6-33)$$

From Equation (6-27) and Equation (6-33), eliminating  $V_1$

$$V_2 = \sqrt{\frac{2E_0}{C_1}} G_T \sqrt{\frac{L_2}{L_1}} \quad (6-34)$$

Substituting Equation (6-18) in the previous equation and eliminating  $C_1$

$$V_2 = \sqrt{2E_0} \sqrt{\frac{L_1 T}{L_2 C_2}} G_T \sqrt{\frac{L_2}{L_1}} \quad (6-35)$$

As  $L_1$ ,  $L_2$ ,  $C_2$  and  $E_0$  are constant,  $V_2$  is now proportional to  $K_2$  defined as

$$V_2 \propto K_2 = \sqrt{T} G_T \quad (6-36)$$

This means that the same results obtained in the previous chapter for  $K_1$  (Figure 35) can be applied also in this case. Therefore, when tuning by changing the primary capacitor value, the best performance can be achieved with a tuning ratio  $T = 1$ .

### Optimizing on $C_2$

Equation (6-27) is influenced by the value of  $C_2$  only in its  $G_T$  term: therefore, the results presented in Figure 34 [Phu91] apply without any correction when the Tesla Coil optimization is performed by varying the top terminal capacity.

All in all, the best improvement (in terms of secondary voltage) from the typical condition of  $T = 1$  can be achieved by decreasing  $C_2$  in order to have  $T = 0.541$  (see Table 4). While the gain improvement is only 18%, the coupling coefficient value required is  $k = 0.546$ , which imposes severe engineering problems to avoid dielectric breakdown between the primary and secondary windings, and makes the practical utility of this result highly questionable.

Table 4: Maximum gain as a function of tuning ratio and coupling coefficient [Phu91]

$m$	1	2	3	4	5	10
$T$	0.541	0.766	0.863	0.912	0.939	0.982
$k$	0.546	0.364	0.271	0.215	0.178	0.095
$G_T$	1.18	1.073	1.039	1.024	1.016	1.005

### 6.1.3. Conditions for complete energy transfer

A slightly different approach is to define a TC optimal functional mode as one where all of the charge initially present on  $C_1$  gets eventually transferred to  $C_2$ , possibly in the shortest amount of time.

Intuitively, a complete transfer of the energy present on  $C_1$  to  $C_2$  implies the developed voltage  $V_2$  to be maximum [Fin66]. As seen in Chapter 6.1.2, this requires Equation (6-22) to be satisfied; this equation can be rearranged as

$$\frac{w_2}{w_1} = \frac{a + 2b + 1}{a} \quad (6-37)$$

It can be shown [Fin66] that a further condition required for the whole charge present on  $C_1$  to move to  $C_2$  is

$$\omega_1 = \omega_2 \quad (6-38)$$

That is, the tuning ratio value must be  $T = 1$ . Substituting Equation (6-38) in the characteristic equation (6-8) the following roots can be easily found

$$\begin{aligned} w_1 &= \frac{\omega_1}{\sqrt{1+k}} \\ w_2 &= \frac{\omega_1}{\sqrt{1-k}} \end{aligned} \quad (6-39)$$

Using the conditions expressed by Equation (6-37) and Equation (6-39), the value(s) of  $k$  needed to ensure complete energy transfer can be found as

$$\frac{w_2}{w_1} = \frac{a + 2b + 1}{a} = \frac{\sqrt{1+k}}{\sqrt{1-k}} \quad (6-40)$$

that is

$$k = \frac{c^2 - a^2}{c^2 + a^2} \quad (6-41)$$

where

$$c = a + 2b + 1 \quad b = 1, 2, 3... \quad (6-42)$$

Summarizing, a tuning ratio  $T = 1$  and a value of  $k$  as given by Equation (6-41) are sufficient to ensure both a maximum voltage at the secondary and a complete energy transfer from the primary. The choice of  $a$  and  $c$  (and therefore of  $k$ ) affects only the position of the time instant when the transfer will be completed.

Table 5: Some of the values of  $k$  that ensure complete energy transfer if  $T=1$  [Deq02]

$a$	$c$	$k$	Notch	Cycles	$a$	$c$	$k$	Notch	Cycles
1	2	0.600	1	1.0	1	4	0.882	2	2.0
2	3	0.385	1	1.5	2	5	0.724	2	2.5
3	4	0.280	1	2.0	4	7	0.508	2	3.5
4	5	0.220	1	2.5	5	8	0.438	2	4.0
5	6	0.180	1	3.0	7	10	0.342	2	5.0
6	7	0.153	1	3.5	8	11	0.308	2	5.5
7	8	0.133	1	4.0	10	13	0.257	2	6.5
8	9	0.117	1	4.5	11	14	0.237	2	7.0
9	10	0.105	1	5.0	13	16	0.205	2	8.0
10	11	0.095	1	5.5	14	17	0.192	2	8.5
11	12	0.087	1	6.0	16	19	0.170	2	9.5
12	13	0.080	1	6.5	17	20	0.161	2	10.0
13	14	0.074	1	7.0	19	22	0.146	2	11.0
14	15	0.069	1	7.5	20	23	0.139	2	11.5

In Table 5 are listed some of the values of  $k$  obtained from Equation (6-41). The notch reported is the one that contains the total transfer instant, while the cycle number refers to the number of primary oscillation cycles (primary current) after what the transfer is complete. Note how this number of cycles is simply  $c/2$ , while the notch number is given by  $b$  (Equation (6-42)).

At the time instant when all the initial charge has been transferred from the primary to the secondary is (see Figure 36)

$$V_{C_1} = 0 \quad V_{C_2} = V_2 \quad I_1 = 0 \quad I_2 = 0 \quad (6-43)$$

Under the condition  $T = 1$ , Equation (6-17) gives

$$v_2(t)|_{T=1} = V_1 \sqrt{\frac{L_2}{L_1}} \sin\left(\frac{w_2 + w_1}{2} t\right) \sin\left(\frac{w_2 - w_1}{2} t\right) \quad (6-44)$$

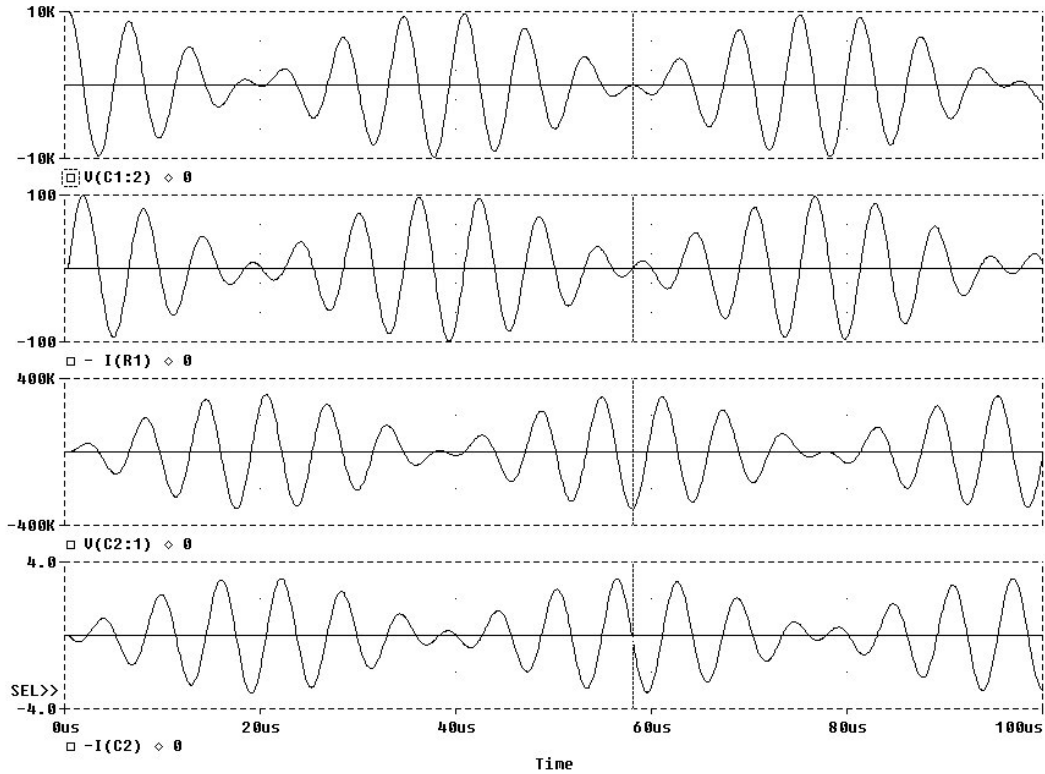


Figure 36: Total energy transfer after 10 primary cycles (see cursor) with  $k=0.161$ , in correspondence of the second notch.

Supposing lossless circuits and  $T = 1$ , varying  $k$  does not influence the maximum value of  $v_2$  achievable, only the time instant when it will be reached. It is therefore interesting to investigate the amount of energy left in the primary when not using the  $k$  values that ensure total transfer.

The following analysis is deliberately limited to  $0.2 < k < 0.6$  as this is the range usually employed on real Tesla Coils. As the energy stored in  $C_2$  is proportional to the square of the voltage upon it, the function  $f(k, t)$  defined as

$$f(k, t) = \left[ \sin\left(\frac{\omega_2 + \omega_1}{2} t\right) \sin\left(\frac{\omega_2 - \omega_1}{2} t\right) \right]^2 \tag{6-45}$$

gives a direct measurement of the percentage of the total energy in  $C_2$ . Figure 37 shows the maximum value assumed by  $f(k, t)$  within its first notch, for different values of  $k$ ; also the time instant when this value was reached is reported.

It can be easily noted that for coupling coefficient values lower than 0.43, the energy left on  $C_1$  is always less than a mere 4%; the same applies for  $0.53 < k < 0.6$ . The worst performance is achieved for  $0.43 < k < 0.53$ , with a maximum of 13% of energy left on  $C_1$ .

In a real TC, the resonant circuits are lossy and it is crucial to reach the maximum voltage at the secondary in the shortest time, to minimize losses. On the other hand, the coupling coefficient cannot be raised at will without causing dielectric breakdown on the secondary winding or between secondary and primary.

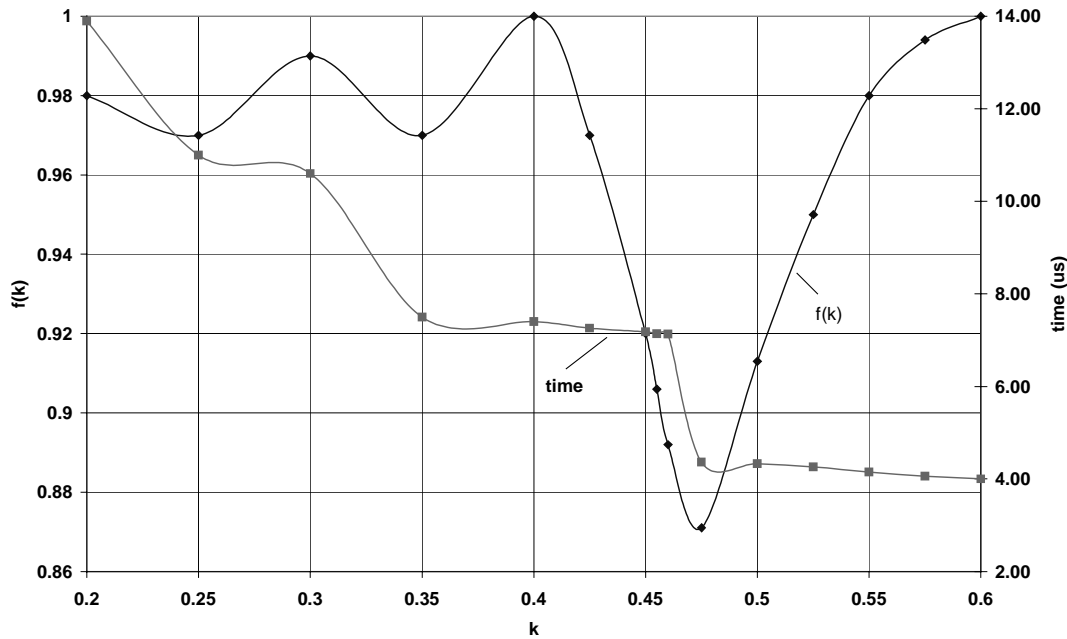


Figure 37: Energy transferred and transfer time vs. coupling coefficient.

In order to achieve the optimal performance, a viable strategy might then be:

- Tune the primary coil to achieve  $T = 1$ .
- Increase  $k$  as much as possible.
- Avoid  $k$  values between 0.43 and 0.53.
- Do not care about catching  $k$  values optimal in term of total energy transfer.

#### 6.1.4. Inductance and capacitance of a close-wound solenoid

A major issue within the modeling of a TC is the ability to predict the resonant frequency (actually *frequencies*) of the secondary coil together with its top-load. This procedure has been roughly approximated in Chapter 4.2 and was based on using the DC equivalent inductance  $L_{dc}$  and the self-capacitance.

The work published by Medhurst [Med47] and applied in Equation (4-3) consists of empirical results of self-capacitance measurements presented in the form of tables. These results apply to solenoids carrying an approximately uniform current at a frequency well below the lowest self-resonance, which is clearly not the case with Tesla coils.

Unloaded coils of large  $h/d$  excited near their self-resonance frequency exhibit a cosinusoidal current distribution profile, with its maximum at the coil base. Therefore, their apparent inductance is less than the one at a lower frequency [Nic01]. As  $h/d$  gets smaller, the location of the current maximum rises towards the middle of the coil and its amplitude grows up to 40% above that of the base current; the result is an effective coil utilization that can be greater than the low frequency value. The equivalent series inductance at resonance can typically vary from  $0.7 L_{dc}$  (at large  $h/d$  and low elevation) to  $1.1 L_{dc}$  (at small  $h/d$  and high elevation).

Breit [Bre21] published the first successful theoretical study of a solenoid near to its lowest self-resonance frequency for the case of a very small height/diameter ratio: the same approach can be extended to any particular height/diameter ratio. The physical reactance distributions can be obtained by means of elliptic integrals over charge rings and current

filament rings, and a differential equation can be formed on the basis of the charge conservation and magnetic induction laws [Nic00].

**Physical capacitance**

Figure 38 shows the main paths of the electric flux radiating from an arbitrary point A on the surface of a coil placed above a ground plane. Each path A-B can be replaced by an equivalent capacitance sized as from the ratio between the charge induced across A-B and the flux connecting the two points. For each infinitesimal section of the coil, its external capacitance  $C_{ext}$  can be defined as the parallel of  $C_{ground}$ ,  $C_{wall}$  and  $C_{infinity}$  as

$$C_{ext}(x)dx \tag{6-46}$$

where the section has got position  $x$  and length  $dx$ . The external capacitance is high at the coil base due to its proximity to the ground plane, and also at the coil top due to its open end. The internal capacitance between two coil sections  $C_{int}$  can be defined as

$$C_{int}(x, y)dxdy \tag{6-47}$$

where the first section has got position  $x$  and length  $dx$ , and the second one has got position  $y$  and length  $dy$ .

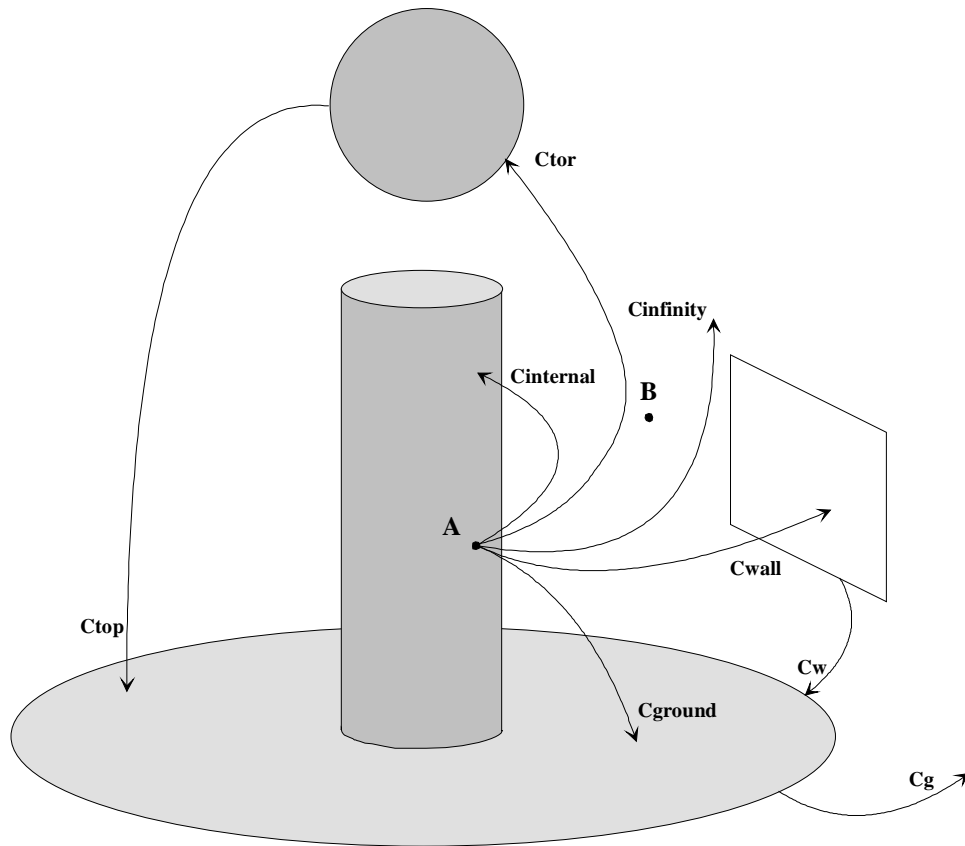


Figure 38: Modeling of the secondary coil capacitances [Nic00].

The top-load (toroid) has got its own capacitance to the ground plane that can be lumped into a single value  $C_{\text{top}}$ , but it also introduces an extra capacitance between itself and any infinitesimal coil section at position  $x$  and of length  $dx$

$$C_{\text{tor}}(x)dx \quad (6-48)$$

### Physical inductance

Every portion of the coil at position  $x$  and of length  $dx$  experiences also an induced EMF resulting from the contributions of all other points on the coil, acting as current sources. The contribution of the current  $I(y)$  passing through a single point at position  $y$  and of length  $dy$  is

$$M(x, y)dx dy \frac{dI(y, t)}{dt} \quad (6-49)$$

where  $M(x, y) = M(y, x)$  is the mutual induction coefficient between  $x$  and  $y$ . The primary winding is operated well below its self-resonance frequency and, therefore, its contribution to the secondary EMF can be reduced to that of a lumped inductor as

$$M_p(x)dx \frac{dI_p(t)}{dt} \quad (6-50)$$

where  $I_p$  is the current traversing the primary winding.

### Coupling equations

Conservation of charge requires that, for each coil section, the net current entering the section matches the increase rate of the charge  $Q$ , i.e.

$$\frac{dQ}{dt} = I_s(x, t) + I_c(x, t) = I(x, t) - I(x + dx, t) \quad (6-51)$$

where:

$$\begin{aligned} I_s(x, t) &= C_{\text{ext}}(x) \frac{d}{dt} V(x, t) dx \\ I_c(x, t) &= \frac{d}{dt} dx \int_0^h C_{\text{int}}(x, y) [V(x, t) - V(y, t)] dy \end{aligned} \quad (6-52)$$

$I_s$  and  $I_c$  are the displacement currents into the external and internal capacitance, respectively, while  $h$  is the coil height. Meanwhile, the total EMF induced in a coil section is given by integrating Equation (6-49) over all source current positions  $y$  along the coil:

$$dV(x, t) = - \frac{d}{dt} dx \int_0^h M(x, y) I(y, t) dy \quad (6-53)$$

Equations (6-51) and (6-53) can be rearranged as:

$$\frac{d\bar{I}(x)}{dx} = -j\omega C_{\text{ext}}(x)\bar{V}(x) - j\omega \int_0^h C_{\text{int}}(x, y)[\bar{V}(x) - \bar{V}(y)]dy \quad (6-54)$$

$$\frac{d\bar{V}(x)}{dx} = -j\omega \int_0^h M(x, y)\bar{I}(y)dy \quad (6-55)$$

where the barred V and I terms represent sinusoidal vectors with angular frequency  $\omega$ . These equations constitute a complete set of differential equations and are satisfied independently for each frequency; their solution, for a given  $\omega$ , provides the current and voltage vector modules for that frequency component.

The operating conditions typical of a Tesla Coil secondary feature the base of the coil connected to ground (inductive feed) or to a low impedance voltage source (base feed), and a toroid placed on the top, resulting in the following additional equations

$$\begin{aligned} \bar{V}(0) &= 0 && \text{(inductive feed)} \\ \bar{V}(0) &= V_{\text{in}} && \text{(base feed)} \end{aligned} \quad (6-56)$$

$$\bar{I}(h) = j\omega C_{\text{top}}\bar{V}(h) + j\omega \int_0^h C_{\text{tor}}(x)[\bar{V}(h) - \bar{V}(x)]dx \quad (6-57)$$

Supposing a situation where base feed is employed, the secondary resonant frequencies can be found by plotting the ratio

$$\frac{\bar{V}(0)}{\bar{I}(0)} \quad (6-58)$$

which is the complex impedance seen between the base of the coil and ground. The resonances are revealed by the peaks and dips of the impedance response. Note that these values are not harmonically related but from the 4<sup>th</sup> resonance upwards exhibit an approximately constant frequency step between consecutive even numbered resonances, and similarly between the odd numbered ones. The Tesla Coil secondary base grounding ( $\bar{V}(0) = 0$ ) results in the suppression of the peaks (odd numbered resonances). Conversely, an open-circuit base condition ( $\bar{I}(0) = 0$ ) would result in the suppression of the dips (even numbered resonances).

At resonance, all the voltages  $\bar{V}(x)$  are in phase with each other and also all the currents  $\bar{I}(x)$  are in phase with each other, being 90 degrees out of phase with the voltages. This means that, applying a sinusoidal excitation to the coil, the voltages measured between the coil base and any two points A and B along the coil have possibly different amplitudes but also constant phase difference equal to zero.

In this situation, during each sinusoidal excitation cycle, there are two time instants when the entire coil voltage is momentarily zero and, simultaneously, the current along the coil assumes its maximum instantaneous value. Thus, at resonance, the stored energy is completely transferred between the electric field and the magnetic field twice in each cycle.

### Equivalent shunt capacitance

The displacement current into the external capacitance can be expressed from Equation (6-52) as

$$\bar{I}_s(x) = j\omega C_{\text{ext}}(x)\bar{V}(x)dx \quad (6-59)$$

where the barred  $I_s$  represents a sinusoidal vector. The total current reaching the ground plane from the coil is given by the integral of all the contributions of  $\bar{I}_s(x)$ . By charge conservation, this current must be equal to the coil base current  $\bar{I}_{\text{base}}$ <sup>9</sup>, therefore

$$\bar{I}_{\text{base}} = \int_0^h \bar{I}_s(x) = j\omega \int_0^h C_{\text{ext}}(x)\bar{V}(x)dx \quad (6-60)$$

It can be imagined that this entire current flow comes from a hypothetical lumped capacitor charged to the top voltage  $\bar{V}_{\text{top}}$ <sup>10</sup>, defined as the *equivalent shunt capacitance*  $C_{\text{es}}$  by

$$\bar{I}_{\text{base}} = j\omega C_{\text{es}}\bar{V}_{\text{top}} \quad (6-61)$$

From Equations (6-60) and (6-61)  $\bar{I}_{\text{base}}$  can be eliminated giving

$$C_{\text{es}} = \frac{1}{\bar{V}_{\text{top}}} \int_0^h C_{\text{ext}}(x)\bar{V}(x)dx \quad (6-62)$$

At the first resonance frequency,  $C_{\text{es}}$  is usually less than 70% of the DC capacitance value.

### Equivalent series inductance

The top voltage  $\bar{V}_{\text{top}}$  can be calculated as the integral of the differential voltage along the all coil, that is

$$\bar{V}_{\text{top}} = \int_0^h \frac{d\bar{V}(x)}{dx} dx \quad (6-63)$$

Using Equation (6-55) to eliminate  $\bar{V}(x)$

<sup>9</sup>  $\bar{I}_{\text{base}} = \bar{I}(0)$

<sup>10</sup>  $\bar{V}_{\text{top}} = \bar{V}(h)$

$$\bar{V}_{\text{top}} = -j\omega \int_0^h \int_0^h M(x, y) \bar{I}(y) dy dx \quad (6-64)$$

It is possible to define an equivalent lumped inductance that induces the top voltage  $\bar{V}_{\text{top}}$  when carrying the same base current  $\bar{I}_{\text{base}}$ , that is

$$\bar{V}_{\text{top}} = -j\omega L_{\text{es}} \bar{I}_{\text{base}} \quad (6-65)$$

where  $L_{\text{es}}$  is the *equivalent series inductance* of the coil at the frequency  $\omega$ . Eliminating  $\bar{V}_{\text{top}}$  using Equation (6-64) gives

$$L_{\text{es}} = \frac{1}{\bar{I}_{\text{base}}} \int_0^h \int_0^h M(x, y) \bar{I}(y) dy dx \quad (6-66)$$

For coils of medium to large  $h/d$ ,  $L_{\text{es}}$  is typically between 70% and 100% of its DC value, while in the case of small  $h/d$  it can exceed it by up to 20%. Addition of top-load tends to make the current profile more uniform and the  $L_{\text{es}}$  value becomes very near to its DC value.

## 6.2. Measurement results

### 6.2.1. Secondary circuit components

The inductance of the secondary coil (neglecting the non-uniform current distribution) was measured using a Fluke PM6306 RLC meter (at 1 kHz and 1 VAC). After subtracting the cables' inductance, the value obtained was 80.22 mH.

Then the following setup was arranged in order to measure the secondary circuit resonance frequencies:

1. The secondary coil base was connected to ground through a HP33120 waveform generator.
2. The top toroid was left into place and connected.
3. One end of the primary coil was grounded, the other end was left open.
4. A distance of at least 3 meters was ensured between Thor and any nearby object .
5. The oscillation amplitude was read from an oscilloscope with its input probe left unconnected.

The frequencies where the oscilloscope reading was at a maximum are reported below:

- $f_a = 65.56$  kHz
- $f_b = 220.2$  kHz
- $f_c = 344$  kHz

In order to estimate the secondary circuit quality factor  $Q$ , also the two frequencies where the oscillation amplitude was halved were measured: their values were  $f_a' = 65.3$  kHz and  $f_a'' = 65.82$  kHz.

Then

$$Q = \sqrt{3} \frac{f_a}{f_a'' - f_a'} = \sqrt{3} \frac{65560}{65820 - 65300} = 218.4 \quad (6-67)$$

The circuit resistive loss  $R_2$  was calculated as

$$R_2 = \frac{2\pi f_a L_2}{Q} = \frac{2\pi \cdot 65560 \cdot 80.22 \cdot 10^{-3}}{218.4} = 151.3 \text{ ohms} \quad (6-68)$$

The correct value of  $Q$  was then found by subtracting the HP33120 output impedance value (50 ohms) from  $R_2$  and recalculating the quality factor with the obtained value

$$Q' = \frac{2\pi f_a L_2}{R_2 - 50} = \frac{2\pi \cdot 65560 \cdot 80.22 \cdot 10^{-3}}{151.3 - 50} = 326 \quad (6-69)$$

### 6.2.2. Primary circuit components

The primary circuit is composed by 9.5 turns of copper pipe (primary coil) and a 0.1  $\mu\text{F}$  pulse capacitor. Coil and capacitor were connected in parallel and driven by a HP33120 waveform generator. The injected current was monitored for maximums in order to find the values of the circuit resonance frequencies. The results are reported in Table 6, for different coil tap positions.

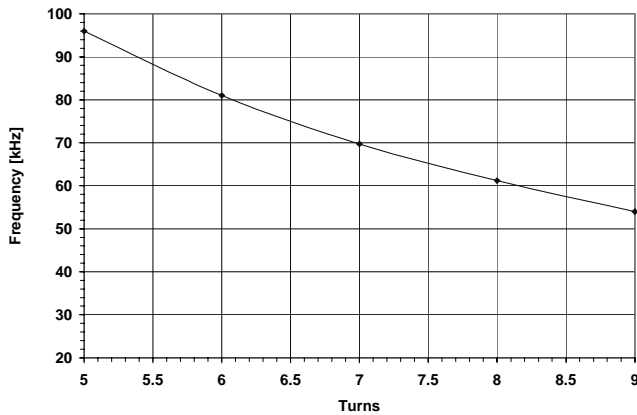


Figure 39: Primary circuit resonance frequency vs. primary coil tap position.

Table 6: Primary circuit resonance frequencies

Primary turns	Freq. (kHz)
9	54
8	61.2
7	69.7
6	81
5	96

Subsequently, in order to calculate the coupling coefficient, the inductance of the primary coil tapped at 9.5 turns was measured using a Fluke PM6306 RLC meter (at 1 kHz and 1 VAC): after subtracting the cables inductance, the value obtained was 99.1  $\mu\text{H}$ .

Primary and secondary coils were then connected in series and the resulting inductance  $L_t$  was measured using the same instrumentation; the elevation of the primary coil in respect of the secondary coil was varied as much as allowed by the mechanics. The mutual inductance  $M$  and the coupling coefficient  $k$  were calculated according to the following equations, assuming  $L_2 = 80.22 \text{ mH}$

$$M = \frac{|L_t - (L_1 + L_2)|}{2} \quad (6-70)$$

$$k = \frac{M}{\sqrt{L_1 L_2}} \quad (6-71)$$

In Table 7 the primary coil elevation is defined as the distance from the underlying PVC table, but also the distance from the secondary coil base turn is given, for reference.

Table 7: Primary and secondary coils coupling coefficient

Height from table (mm)	Height from secondary (mm)	Lt (mH)	M (μH)	k
343	149	79.052	634.05	0.2249
326	132	79.087	616.55	0.2187
286	92	79.170	575.05	0.2039
245	51	79.264	528.05	0.1873
204	10	79.365	477.55	0.1694
164	-30	79.474	423.05	0.1500
125	-69	79.576	372.05	0.1319
85	-109	79.656	332.05	0.1178
65	-129	79.716	302.05	0.1071

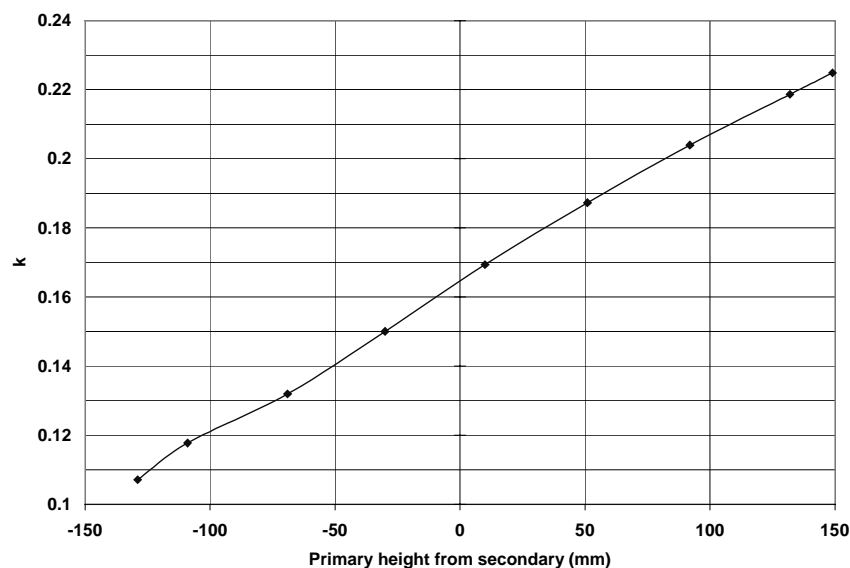


Figure 40: Primary and secondary coils coupling coefficient vs. primary elevation.

The value of the primary capacitor was measured using a Fluke PM6306 RLC meter (at 65 kHz and 1 VAC); the reading was 0.09678 μF, with an equivalent parallel resistance of 5.97

kohms. Based on this capacitance value and the measurements in Table 6, the primary inductance vs. the tap position could be calculated with the following relation

$$L_1 = \frac{1}{C_1(2\pi f)^2} \quad (6-72)$$

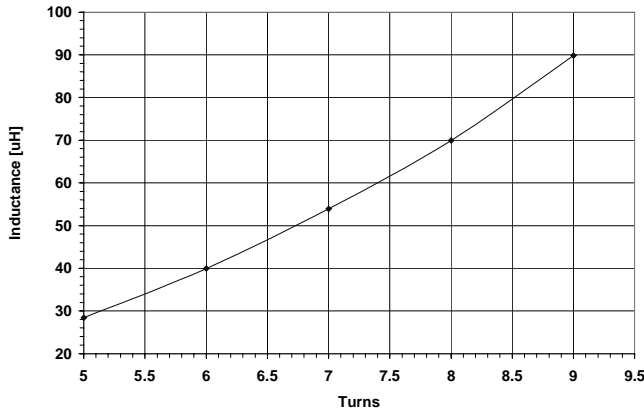


Figure 41: Primary coil inductance vs. tap position.

Table 8: Primary coil inductance vs. tap position

Primary turns	Inductance (µH)
9	89.8
8	69.9
7	53.9
6	39.9
5	28.4

### 6.2.3. Secondary voltage waveform

The secondary voltage waveform is regarded as the most significant indicator to provide an insight into Thor's functionality. Any variation in the primary or secondary circuits components, or of the coupling coefficient, affects noticeably the shape of the voltage generated.

Given that, in this context, the voltage absolute magnitude is unimportant, the voltage on the secondary top electrode can be measured by an oscilloscope with its input probe left unconnected. This method is preferred for its intrinsic simplicity and its non-intrusive characteristic. In all of the following measurements the coupling coefficient was set to 0.187 and the rotating spark gap speed was regulated to provide a constant break rate of 300 Hz; the primary coil was tapped at 7.5 turns.

#### Unloaded condition

The primary capacitor charging voltage was set about 11-12 kV, as suited to obtain a regular triggering of the rotating spark gap, yet without developing any leaders from the top electrode and, therefore, avoiding to load it.

The waveform recorded had a very good repeatability and included a variable number of beats (3 - 4) according to the exact time instant the spark gap stopped conducting (Figure 42 to Figure 45).

#### Leader loading

The primary capacitor charging voltage was set about 14 kV, resulting in continuous emission of leaders from the top electrode and a noticeable loading of the secondary circuit

(Figure 46). The energy originated from the primary capacitor was almost completely dissipated within the first two beats, followed by the spark gap opening and free oscillation in the secondary circuit.

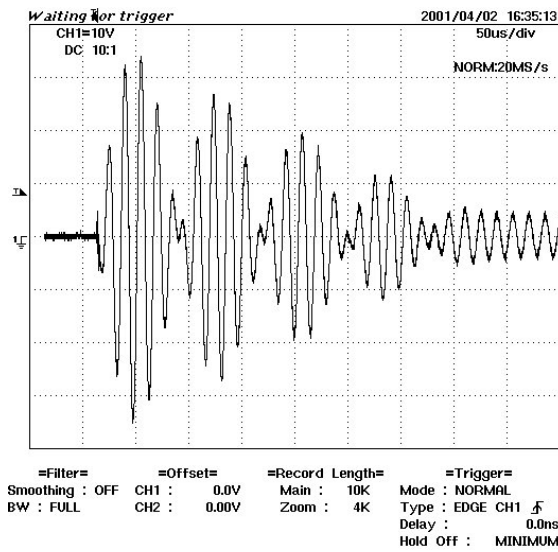


Figure 42: Typical secondary voltage waveform, with four beats.

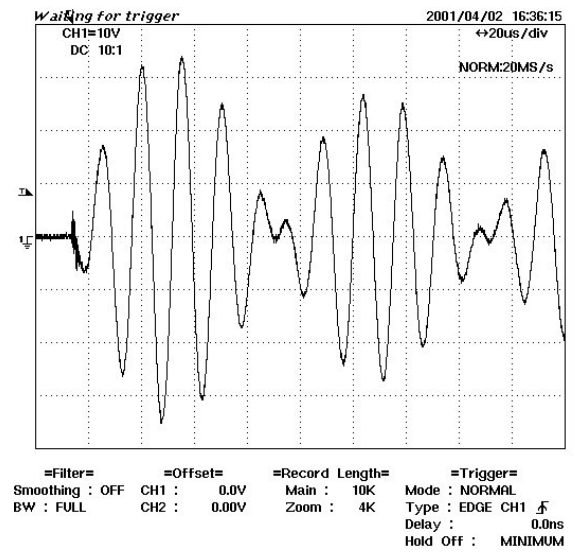


Figure 43: Zoomed first two beats from Figure 42.

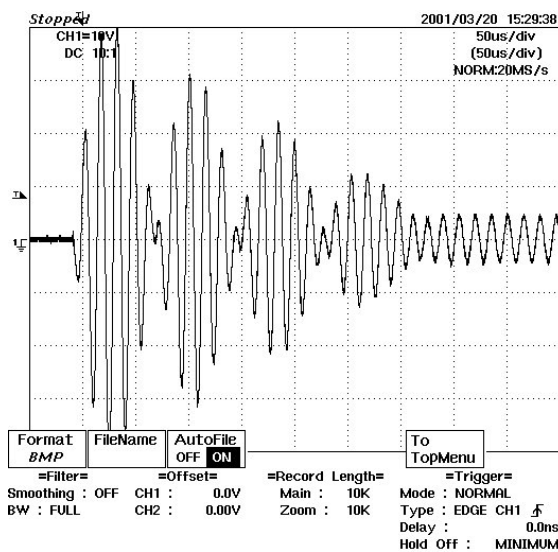


Figure 44: Another secondary voltage waveform sample.

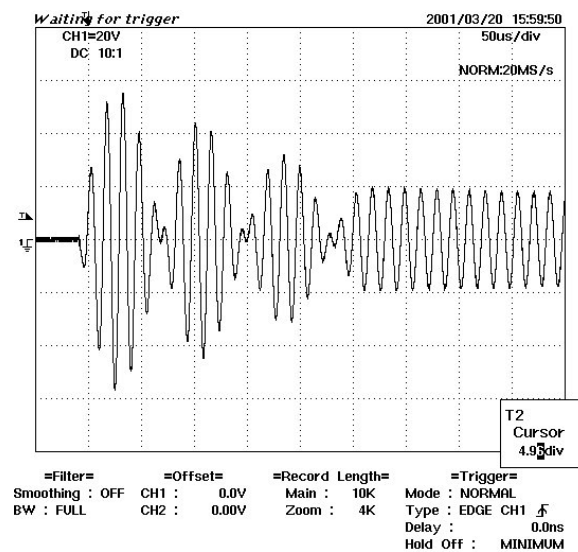


Figure 45: A third secondary waveform sample, with three beats only.

### Ground-discharge loading

The primary capacitor charging voltage was set about 14 kV and a grounded rod was placed at 50 cm from the top electrode. Thor's operation produced a continuous discharge upon the rod and a typical secondary voltage waveform as reported in Figure 47.

The discharge developed within the first beat, resulting in a relatively low impedance loading of the secondary circuit and a complete damping of the oscillations.

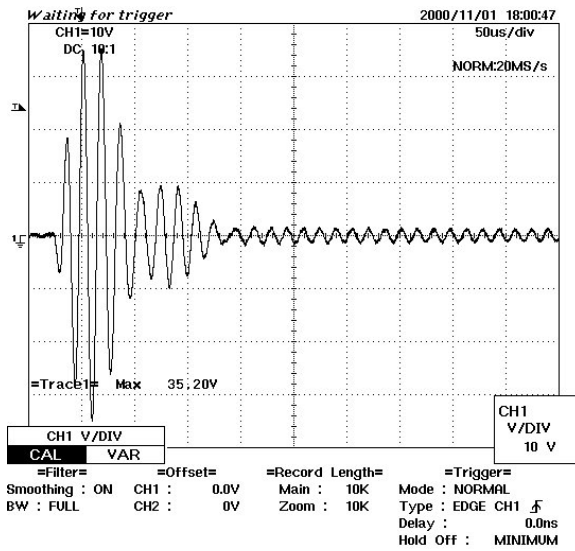


Figure 46: Secondary voltage waveform when leaders are produced.

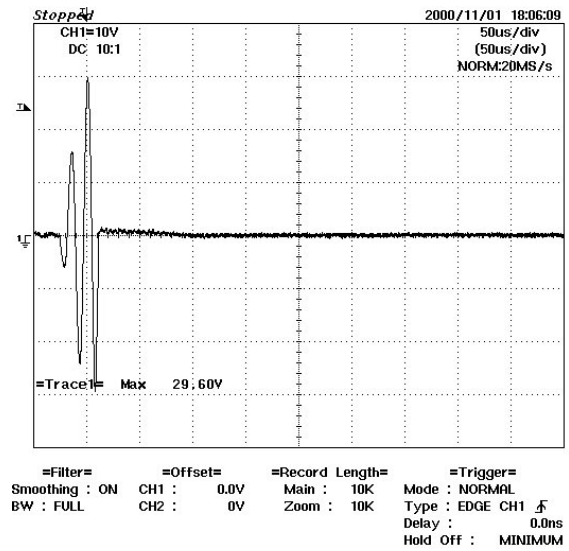


Figure 47: Secondary voltage waveform with a ground discharge.

### 6.3. Simulation model

#### 6.3.1. Secondary coil simulation

The calculation of the physical capacitances mentioned in Chapter 6.1.4 are implemented in C language and performed by a batch program [Nic03]. For the Thor's case, Figure 48 shows the calculated  $C_{int}(x,y)$  for section number 10, being the coil divided in 32 sections numbered from 1 (bottom) to 32 (top).. Each section is supposed to have null capacitance with itself and is symmetrical by definition.

Figure 49 shows  $C_{ext}(x)$ , that rises steeply at the coil base due to the proximity to the ground plane. The capacitance rise at the coil top is smoother, due to the shielding effect of the top-load. The program predicts a toroid capacitance  $C_{top} = 54.25$  pF.

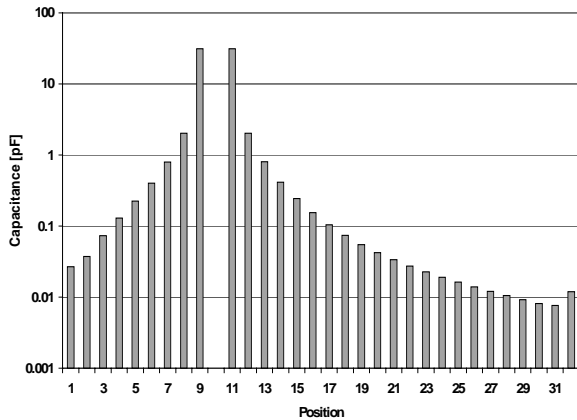


Figure 48:  $C_{int}(x,y)$  for  $y=10$  vs. coil position.

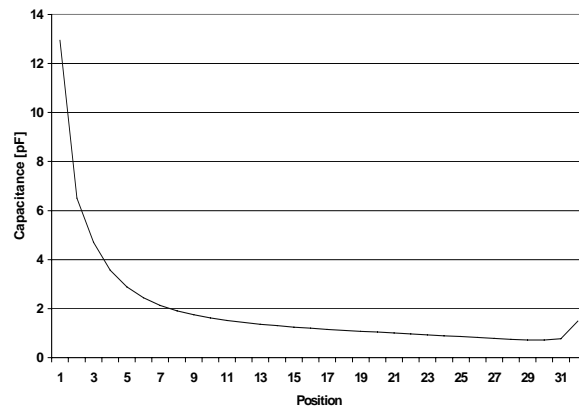


Figure 49:  $C_{ext}(x)$  vs. coil position.

Equations (6-54) to (6-57) in Chapter 6.1.4 are solved numerically by replacing the integrals and differentials with finite sums and differences, and employing a discrete form of the physical reactance distributions. The equations, reduced in matrix form, are then processed by Gaussian elimination. The calculation procedure is implemented in C language [Nic02] and outputs a series of useful results:

- The complex base impedance vs. frequency, useful to find the location of the resonance frequencies.
- The maximum voltage gain vs. frequency.
- The voltage and current distribution profile along the coil, for a specified frequency.
- The equivalent shunt capacitance and series inductance values.

In Thor's case, after a thorough measurement of the coil's actual dimensional data (i.e. not simply using the design data from Chapter 4) the resonance frequencies predicted by the program are:

- $f_a = 66.49$  kHz
- $f_b = 225.2$  kHz
- $f_c = 345.6$  kHz

as can be easily verified from the three dips in Figure 50. Note also the sudden phase shift of the impedance from  $-90$  to  $+90$  degrees in correspondence of the resonances.

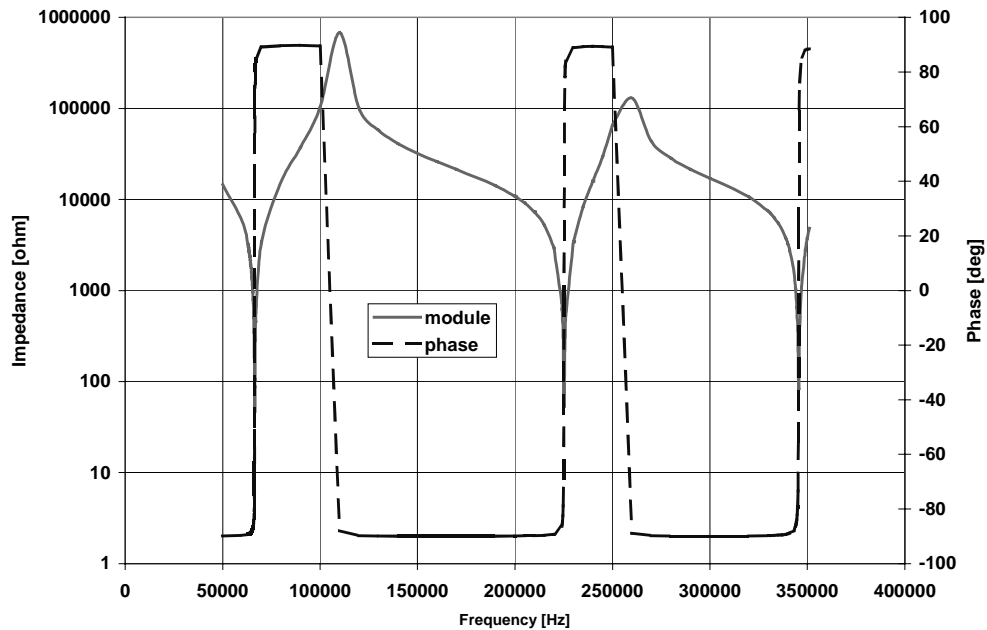


Figure 50: Module and phase of the secondary coil base impedance vs. frequency.

Figure 51 displays the secondary coil voltage gain, intended as the maximum instantaneous voltage value measured on the coil (not necessarily at the top) when applying a nominal sinusoid of  $1 V_{\text{peak}}$  at the base. Note that the voltage gain exhibits local maximums at the resonances, being its global maximum (683) in correspondence of the first resonance (66.49 kHz). These gain values are theoretical and take into account only the coil's wire resistance loss, while in practice additional losses result in a reduced performance.

The voltage and current maximum value along the coil in module and phase are predicted in Figure 52 and Figure 53 for the first resonance frequency; coil turns are numbered from bottom (1) to top (940). The voltage exhibits a sinusoidal profile, with its maximum in correspondence of the secondary coil top.

The phase diagram reveals that the current is always in phase with the coil base drive signal while the voltage is always 90 degrees behind it. The voltage phase swing from  $-90$  to

+90 degrees within the first 50 sections is purely an artifact caused by the simulation program driving the coil with a generator at its base. The actual Thor working condition, where the secondary drive voltage is magnetically induced by the primary winding would show a constant voltage phase shift of +90 degrees on every coil section.

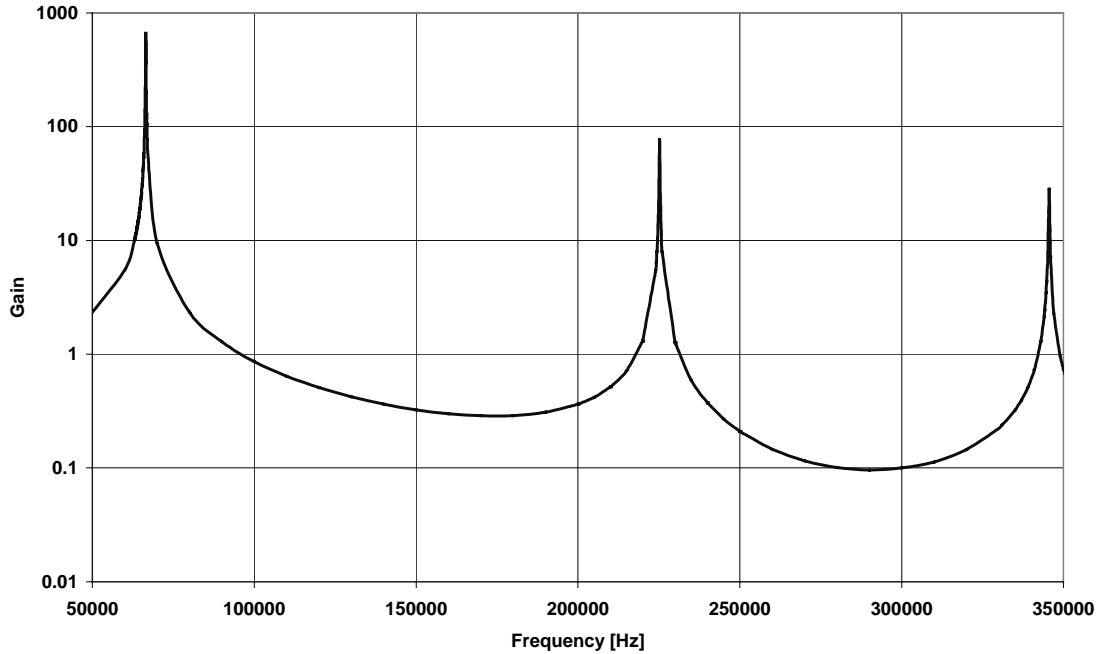


Figure 51: Voltage gain of the secondary coil vs. frequency.

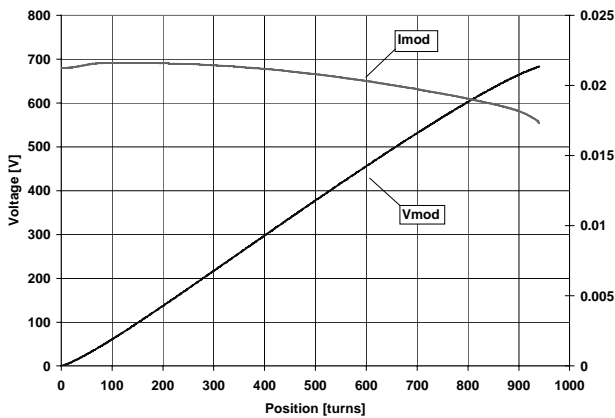


Figure 52: Voltage and current distribution (module) of the secondary coil at 66.49 kHz.

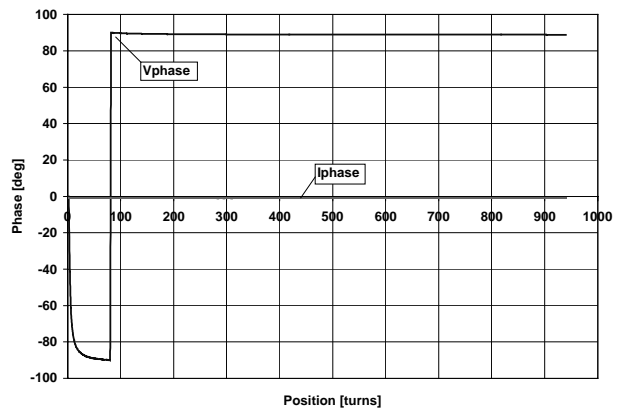


Figure 53: Voltage and current distribution (phase) of the secondary coil at 66.49 kHz.

Figure 54 shows the first derivative of the voltage distribution from Figure 52, i.e. the voltage gradient along the coil. Its maximum is located in the region between turn n. 300 and turn n. 370; this is the secondary location where it is much more feasible to have isolation breakdown with turn-to-turn discharges.

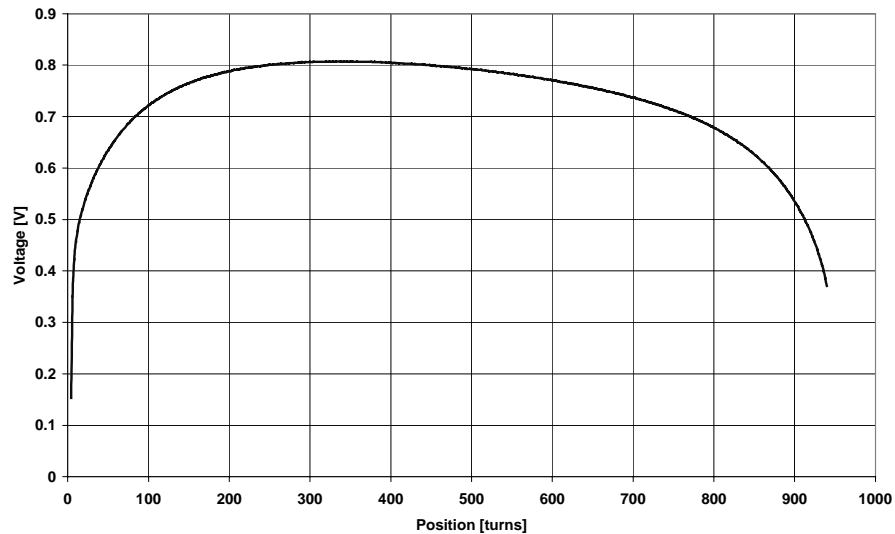


Figure 54: Voltage gradient of the secondary coil along its height.

Table 9: Predicted and measured secondary resonance frequencies

	Predicted (kHz)	Measured (kHz)	Error (%)
$f_a$	66.49	65.56	1.4
$f_b$	225.2	220.2	2.3
$f_c$	345.6	344	0.5

The difference between the predicted resonance frequencies and those actually measured in Chapter 6.2 is relatively small (see Table 9). The secondary modeling procedure outlined in Chapter 6.1.4 is therefore accepted and its results are used to build an approximated model of the coil. This model is sufficiently valid only in the vicinity of the first resonance frequency  $f_a$  and features the series of  $L_{es}$  and  $C_{es}$  predicted (see Table 10).

Table 10: Predicted equivalent reactances at 66.49 kHz

Equivalent shunt capacitance $C_{es}$	74.4 pF
Equivalent series inductance $L_{es}$	76.98 mH

### 6.3.2. Spark gap simulation

In the initial model of Thor's primary and secondary circuits, all losses were accounted by the resistance of the two coils, being the spark gap element simulated by an ideal switch. The resulting waveform of the secondary voltage was the typical double-frequency interference from Equation (6-17), multiplied by exponential decay term introduced by the losses.

Practical measurements, instead, showed a pretty linear decay (e.g. Figure 42), clearly pointing out the presence of a negative-resistance element in one of the circuits. This element

could be easily identified as the spark gap and, therefore, required a model for a correct simulation.

The consulted references proposed a model that either had not performed well in all simulations ([Nar91]), was described with insufficient detail ([Roc77]) or required a large number of parameters to be inferred by characterization and was felt to be too much complex for the purpose ([Bas97]).

The model depicted in Figure 55 was built using MicroSim following a trial and error procedure, keeping in mind the voltage-current relationship of a generic gas discharge. The general requirement was to simulate a resistor whose value was inversely proportional to the amount of current that traversed it; this component would experience an increasing voltage drop in correspondence to a decreasing current.

The spark gap model parameters are:

- Tsw\_on the time instant when the spark gap starts conducting.
- Tsw\_off the time instant when the spark gap stops conducting.
- Iscale a scaling coefficient for adapting the peak value tracker to different current magnitudes.
- Rscale a multiplicative coefficient that affects the spark gap output resistance.

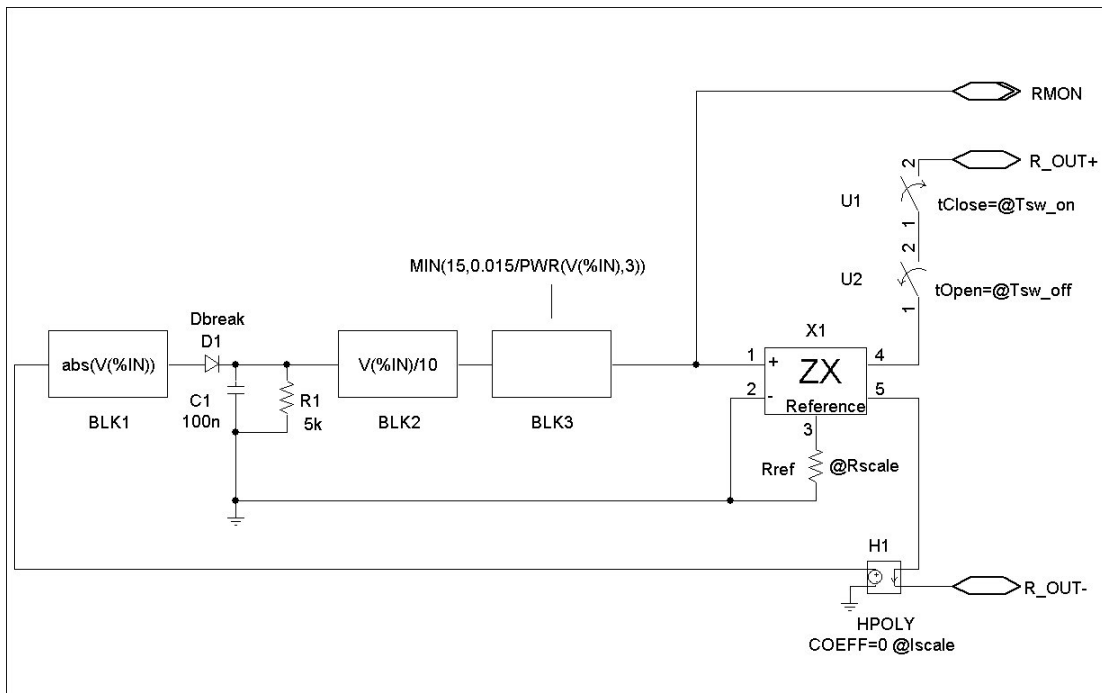


Figure 55: Spark gap simulation model.

The spark gap terminals are named R\_OUT+ and R\_OUT-; U1 closes at time Tsw\_on, allowing the current  $I_{in}$  to flow through the gap. At time Tsw\_off U2 opens, setting the gap into high impedance.

H1 is a current-to-voltage converter, measuring the current passing through the gap; its transfer function is

$$V_{out} = I_{in} \cdot I_{scale} \quad (6-73)$$

Block BLK1 outputs the absolute value of the converted voltage. After it, the group D1, C1 and R1 tracks the peak value of the current waveform; typically, its output resembles the waveform decay trend. After being divided by ten (BLK2), the resulting signal is fed to BLK3, which implements the actual negative-resistance law

$$V_{\text{out}} = \frac{0.015}{V_{\text{in}}^3} \quad (6-74)$$

The MIN function is used to avoid excessive overshoot when the input current is still small. The last block of the chain is the ZX component (a voltage-to-resistance converter part of the *anl\_misc* MicroSim library), which provides a resistance

$$R_{45} = R_{\text{scale}} \cdot V_{12} \quad (6-75)$$

between its terminals 4 and 5. Therefore, the instant value of the resistance  $R_{45}$  (i.e. the resistance between R\_OUT+ and R\_OUT-) can be monitored by measuring the voltage  $V_{12}$  on terminal RMON and multiplying it by  $R_{\text{scale}}$ .

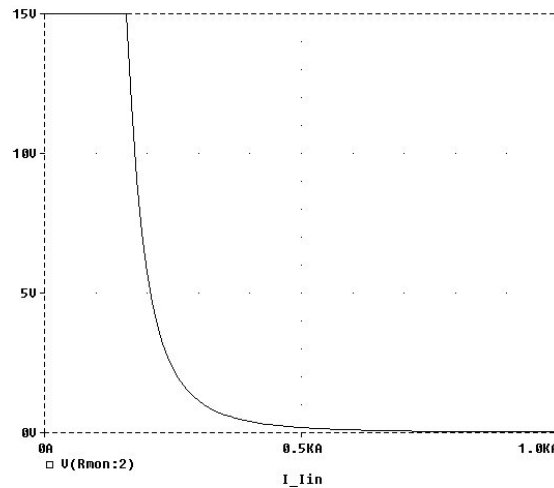


Figure 56: Transfer function of the spark gap simulation model ( $I_{\text{scale}}=0.01$ ,  $R_{\text{scale}}=1$ ).

Figure 56 has been obtained by feeding the spark gap model with a current variable from zero to 1000A and plotting the value of  $V_{\text{RMON}}$ . As the  $R_{\text{scale}}$  parameter was set to 1, the voltage measured gives directly the spark gap resistance.

As it was out of the scope of this work to provide a thorough and fully justified model of a spark gap, the one described above was regarded as satisfactory because it provided simulation results very similar to the actual measurements.

### 6.3.3. Overall simulation model

Thor's overall simulation model is intended to represent the primary and secondary circuits, together with the spark gap; the power supply and its protection filter network are not included. As well, it is assumed that the secondary is not loaded by leaders or discharges to ground, while corona losses are ignored. Simulations are run for single pulses, meaning that pulse repetition rate is not relevant.

The model parameters were derived as follows:

- C1 (primary capacitor): measured directly (Chapter 6.2.2) together with its equivalent parallel resistance  $R_c$ .
- L1 (primary coil): an inductance of  $62 \mu\text{H}$  was interpolated from Figure 41, being the primary coil tapped at 7.5 turns. This value had to be increased to  $65 \mu\text{H}$  in a trial and error fashion in order to achieve waveform match. A justification for this need was found in the long (over one meter) cables used to connect the primary coil to the rest of the circuitry.

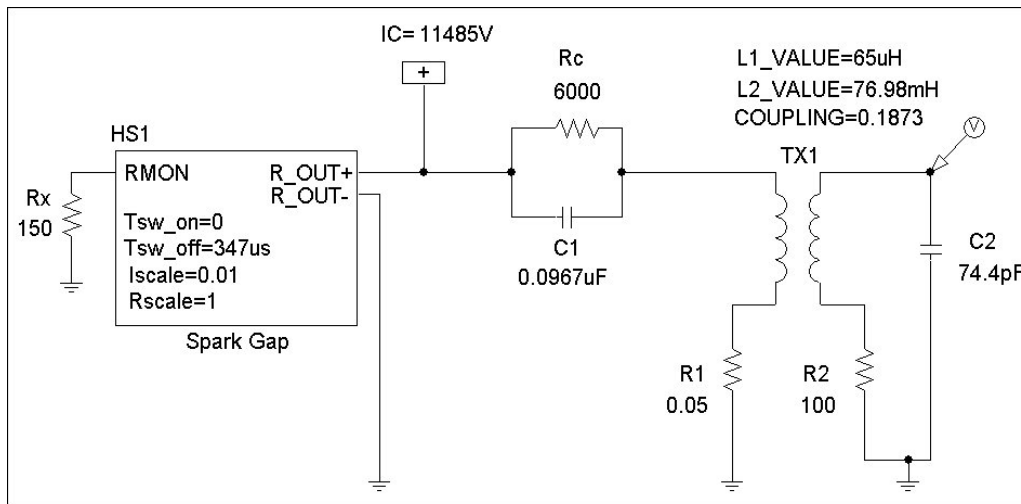


Figure 57: Thor's overall simulation model.

- R1 (primary lumped resistance): this resistance accounted for losses in connections, primary coil DC resistance and AC losses. As its measurement was relatively difficult, its value was derived by trial and error.
- Spark gap: its parameters were derived following trial and error. It was particularly useful monitoring the voltage on  $R_x$  in order to set properly the  $I_{scale}$  parameter. Namely, it was crucial to operate in the non-constant region of the spark gap transfer function to achieve a linear decay similar to the one measured.
- C2 (secondary lumped capacitance): assumed equal to the equivalent shunt capacitance  $C_{es}$  from the secondary coil model (Table 10).
- L2 (secondary coil lumped inductance): assumed equal to the equivalent series inductance  $L_{es}$  from the secondary coil model (Table 10).
- R2 (secondary coil lumped resistance): derived from the  $Q$  factor measurement in Chapter 6.2.1 (Equation (6-68)) after subtracting the meter output impedance. That is,  $151.3 - 50 \approx 100$  ohm.
- Coupling coefficient: its value was read from Table 7, for the used primary height (245 mm).

The value of  $R_x$  is not relevant, because the function of this component is uniquely to provide a connection for pin RMON of HS1. Block IC defines the initial condition for C1, that is, the voltage this capacitor is initially charged to.

#### **6.4. Comparison of measurement against simulation results**

The Thor simulation model was evaluated from its ability to accurately reproduce the secondary voltage waveforms measured and reported in Chapter 6.2.3. The unloaded condition was preferred, as it didn't require taking into account additional secondary loading and, therefore, matched the initial assumptions made for the model design.

In particular, the waveform reported in Figure 42 (reproduced with much more accuracy in Figure 58) was regarded as a representative example, for its clearness and sufficient swing. Model parameters Tsw\_on was set to the default value zero, while Tsw\_off was adjusted following a trial and error procedure. As the measurement system didn't allow to know about the exact voltage scale of the measured signal, the simulation model parameter IC was set to 11485 V for two reasons:

1. The voltage used during the measurement was actually 11 – 12 kV.
2. This value allowed for a simple conversion factor between the measured waveform vertical scale and the simulated one, that is

$$V_{\text{simulated}} \approx 10^4 V_{\text{measured}} \quad (6-76)$$

The simulation result is reported in Figure 59: the model follows the measured data very well. Even if a numeric subtraction of the two waveforms is not possible, for the lack of tabulated data from the measured one, a graphical subtraction shows an almost perfect match.



## 7. CONCLUSIONS AND FUTURE WORK

### 7.1. Conclusions

A medium-sized Tesla Coil has been designed using a mix of approximated and empirical design equations. The finished apparatus measures 3 meters in height, with a base support measuring one square meter. After the assembly completion, the value each component has been directly measured or calculated.

The approximated equations provided a satisfactory degree of precision: the secondary resonance frequency was achieved with an error of about 11%, while the primary coil inductance was measured to be within 4% from the expected. Nevertheless, the secondary coil and its top toroid electrode have also been precisely modeled using a novel procedure; model simulations have shown a very good match with the measurements performed, with errors of around 2%.

The theory describing the functionality of a Tesla Coil has been reported, including the classical treatment, two different views of “optimal” functionality, and some small personal results. A model of the constructed Tesla Coil has been designed using MicroSim. The model includes the components of the primary and secondary resonant circuits, and a simple sub-model simulating the spark gap negative resistance characteristic. The oscillation waveforms produced by simulation runs have shown very good concordance with those recorded by real measurements, therefore validating the modeling procedure and tools.

A byproduct of this study work is constituted by the design and realization of a 5 kW, 20 kV capacitor charging power supply, used to feed the Tesla Coil in a stabilized and repeatable way. The series-loaded resonant topology has proven to be efficient for capacitor charging, thanks to its intrinsic short-circuit tolerance, and also provide minimal losses, allowing for a size shrink of the power supply electronics.

The power-packing advantages of the IGBT devices used for switching have been counterbalanced by their relative facility to get damaged by the transients so abundant in every disruptive Tesla Coil. A considerable amount of time and effort have been consumed in designing a number of protection mechanisms and optimizing the PCB layout to avoid IGBT failures. The design of a power transformer suitable to the series-loaded resonant topology has been tackled in a rather unconventional way: instead of relying on ready-made empirical equations, design data have been calculated from simulations of the switch bridge waveforms, using only basic magnetic circuit laws.

It is also mandatory to report a measurement of Thor’s performance, as usually intended among Tesla Coil hobbyists, as the longest discharge obtained from the toroid. A 3-meter long discharge to a grounded rod was measured when the coil was fed with 18.3 kV, 4.3 kW, at a pulse rate of 260 Hz.

All in all, Thor, together with its power supply, constitutes a functional research workbench where all functional components are of known value, the operating conditions can be replicated precisely, and the effort and uncertainty can all be concentrated on the single parameter object of the measurement.

## 7.2. *Future work*

Thor's functionality allows for generating HV pulses with variable repetition rate and pulse energy: a natural extension would be to generate a series of predefined and variable number of pulses. This would require a proximity sensor mounted on the rotating spark gap to synchronize the first pulse with the electrode position, plus some modification to the power supply controller board. This setup would allow to research on the development of corona, leaders and discharges in relation to the pulses number, repetition rate and energy.

Another possible area of interest is the integration of secondary loading in Thor's model: shunting of the secondary circuit with resistive and/or capacitive loads, including a direct voltage measurement together with the load, would allow to track Thor's output characteristic. This, in turn, would allow connecting known loads to the TC (e.g. dielectric samples, HV components under test, etc.) while being able to compensate for the working point shift introduced.

A model including secondary loading and a proved (i.e. verified by direct measurement) TC magnification factor would allow to calibrate a non-intrusive capacitive voltage probe (equivalent to the flying oscilloscope probe). This kind of secondary voltage measurement would allow to attempt modeling the loading represented by leaders and streamers.

## REFERENCES

- [Bas97] Basso, C: *Spice model simulates spark-gap arrestor*. Design Idea published on EDN Magazine, Cahners Publishing Company, July 3, 1997.
- [Ber96] Bergmann, K., Gruening, H.: *Hard-drive – A Radical Improvement for the Series Connection of GTO's*. Paper presented at the EPRI 96, The Future of Power Delivery, pp. 1 – 10, April 9 – 11 1996.
- [Bie90] Bieniosek, F. M.: *Triple resonance pulse transformer circuit*. Review of Scientific Instruments, pp. 1717 – 1719, vol. 61, no. 6, 1990.
- [Bre21] Breit, G.: *Distributed Capacity of Inductive Coils*. Physical Review, V17, Part 6, pp. 649-677, June 1921.
- [Bru98] Bruckmann, M., Sommer, R. & al.: *Series Connection of High Voltage IGBT Modules*. IEEE Industry Applications Conference, pp. 1067 –1072, vol. 2, 1998.
- [Bur96] Burke, R. A., Gregory, K. & al.: *The use of commercial thyristors in capacitor discharge power supplies*. IEE Colloquium on Pulsed Power '96, pp. 12/1 -12/3, 1996.
- [Bus87] Bussey, J.: *Report of Atlas/Centaur-67/FLTSATCOM F-6 investigation board*. Vol. 2, NASA, 1987.
- [Che96] Chen, J., Lin, J. & al.: *The Techniques of the Serial and Paralleled IGBTs*. Proceedings of the 22nd IEEE International Conference on Industrial Electronics, Control, and Instrumentation, p. 999 -1004, vol. 2 , 1996.
- [Cor87] Corum, K. L., Corum, J. F.: *Vacuum tube Tesla Coils*. Corum & Associates, 1987.
- [Cor99] Corum, K. L., Corum, J. F.: *Class Notes: Tesla Coils and the Failure of Lumped-Element Circuit*. Paper available at <http://www.ttr.com/corum/index.htm>. Accessed 02/27/2001.
- [Cra54] Craggs, J. D., Meek, J. M.: *High Voltage Laboratory Technique*. Butterworth Scientific Publications, London, 1989.
- [Dam87] Damstra, G. C., Pettinga, J. A. J.: *A six pulse kV Tesla transformer*. Fifth International Symposium on High Voltage Engineering, paper 62.13/1-3, vol. 2, 1987.
- [Deq00] de Queiroz, A. C. M.: *Synthesis of multiple resonance networks*. 2000 IEEE ISCAS, Geneva, Switzerland, pp. 413-416, Vol. V, May 2000.
- [Deq01] de Queiroz, A. C. M.: *Designing a Tesla magnifier*. Manuscript available at <http://www.coe.ufrj.br/~acmq/tesla/magnifier.html>. Accessed 03/07/2001.
- [Deq02] de Queiroz, A. C. M.: Email correspondence on the Tesla mailing list on 9 – 12.12.2000.
- [Dru04] Drude, P.: *Über induktive Erregung zweier elektrischer Schwingungskreise mit Anwendung auf Perioden und Dämpfungsmessung, Tesla transformatoren und drahtlose Telegraphie*. Annalen der Physik, pp. 512-561, vol. 13, 1904.
- [Fin66] Finkelstein, D., Goldberg, P. & al.: *High Voltage Impulse System*. Review of Scientific Instruments, pp. 159 – 162, vol. 37, no. 2, 1966.
- [Fla92] Flanagan, W. M.: *Handbook of transformer design and applications*. McGraw-Hill, second edition, 1992.

- [Ger96] Gerster, C., Hofer, P. & al.: *Gate-control strategies for snubberless operation of series connected IGBTs*. 27th Annual IEEE Power Electronics Specialists Conference, pp. 1739 – 1742, vol. 2, 1996.
- [Gir00] Giralt, M., Buret, F.: *Implementation of a discharge propagation model using an electric field map: an attempt toward a design tool for high-voltage overhead insulation*. J. Phys. D: Appl. Phys., vol. 33, pp. 504 - 516, 2000.
- [Gla48] Glasoe, G. N., Lebacqz, J. V.: *Pulse generators*. McGraw-Hill, 1948.
- [God70] Godfrey, R., Mathews, E. R. & al.: *Analysis of Apollo 12 lightning accident*. NASA MSC-01540, 1970.
- [Gub97] Gubanov, V. P., Korovin, S. D. & al.: *Compact 1000 PPS High-Voltage nanosecond pulse generator*. IEEE Transactions on Plasma Science, p. 258 – 65, vol. 25, no. 2, 1997.
- [Gui93] Guildini, R., Chatroux, D. & al.: *Semi-conductor power mosfet devices in series*. Fifth European Conference on Power Electronics and Applications, p. 425 – 30, vol. 2, no. 377, 1993.
- [Ir983] *IGBT Characteristics*. International Rectifier application note AN-983.
- [Ir990] *Application Characterization of IGBTs*. International Rectifier application note INT990.
- [Har98] Hardt, N., Koenig, D.: *Testing of insulating materials at high frequencies and high voltage based on the Tesla transformer principle*. Conference record of the 1998 IEEE International Symposium on Electrical Insulation, p. 517 - 20, vol. 2, 1998.
- [Hit83] Hitchcock, R. N., Stanton, S. J., Levy, et. al.: *Computer modeling of medium coupled resonant air core transformers including resistive losses*. 4<sup>th</sup> IEEE Pulsed Power Conference, Albuquerque, New Mexico, 1983.
- [Hof75] Hoffmann, C. R. J.: *A Tesla transformer high-voltage generator*. Review of Scientific Instruments, pp. 1 – 4, vol. 46, no. 1, 1975.
- [Hul93] Hull, R.: *The Tesla Coil Builder's guide to the Colorado Springs Notes of Nikola Tesla*. Tesla Coil Builders of Richmond Virginia, 1993.
- [Lar98] Larsson, A., Bondiou-Clergerie, A., Gallimberti, I.: *Numerical modelling of inhibited electrical discharges in air*. J. Phys. D: Appl. Phys., vol. 31, pp. 1831-1840, 1998.
- [Les77] Les Renardieres Group: *Positive discharges in long air gaps*. Electra 53, p. 31 – 132, 1977.
- [Les81] Les Renardieres Group: *Negative discharges in long air gaps*. Electra 74, p. 67 – 216, 1981.
- [Lip90] Lippincott, A. C., Nelms, R. M. & al.: *A series resonant converter with constant on-time control for capacitor charging applications*. Proc. Applied Power Electronics Conf., pp. 147-154, March 1990.
- [Lip91] Lippincott, A. C., Nelms, R. M.: *A Capacitor-Charging Power Supply Using a Series-Resonant Topology, Constant On-Time/Variable Frequency Control, and Zero-Current Switching*. IEEE Transactions on Industrial Electronics, vol. 38, no. 6, 1991.
- [Mat82] Matsuzawa, H., Suganomata, S.: *Design charts for Tesla-transformer-type relativistic electron beam generators*. Review of Scientific Instruments, p. 694 – 96, vol. 53, no. 5, 1982.

- [Med47] Medhurst, R. G.: *H.F. Resistance and Self-Capacitance of Single-Layer Solenoids*. Wireless Engineer, pp. 35 – 43, February 1947, pp. 80 – 92, March 1947.
- [Mes95] Mesyats, G. A., Shpak, V. G. & al.: *RADAN-EXPERT portable High-Current accelerator*. Tenth IEEE International Pulsed Power Conference, pp. 539 –543, vol. 1, 1995.
- [Mit95] Mitter, C. S.: *Application Considerations Using Insulated Gate Bipolar Transistors (IGBTs)*. Motorola Semiconductor Application Note AN1540, 1995.
- [Moh89] Mohan, N., Undeland, T. M., Robbins, W. P.: *POWER ELECTRONICS: Converters, Applications and Design*. Wiley, 1989.
- [Nel90] Nelms, R. M., Strickland, B. E. & al.: *High Voltage Capacitor Charging Power Supplies for Repetitive Rate Loads*. Conference Record of the 1990 IEEE Industry Applications Society Annual Meeting, pp. 1281 - 1285, vol. 2, 1990.
- [Nel92] Nelms, R. M., Schatz, J. E.: *A Capacitor Charging Power Supply Utilizing a Ward Converter*. IEEE Transactions on Industrial Electronics, vol. 39, no. 5, 1992.
- [New90] Newton, S. R., Nelms, R. M.: *Simulation of capacitor charging power supplies*. Proc. 25<sup>th</sup> Intersociety Energy Conversion Engineering Conf., vol.1, pp. 386 - 390, August 1990.
- [Nic00] Nicholson, P.: *Secondary Basics*. Document pn2511. Manuscript from the Tesla Secondary Simulation Group. <http://www.abelian.demon.co.uk/tssp/>. 25<sup>th</sup> Nov 2000.
- [Nic01] Nicholson, P.: Discussion from the Tesla Secondary Simulation Group available at <http://www.abelian.demon.co.uk/tssp/misc.html>. Accessed 01/23/2001.
- [Nic02] Program TSIM, available from the Tesla Secondary Simulation Group as C source code. <http://www.abelian.demon.co.uk/tssp/model.html>. Accessed 01/23/2001.
- [Nic03] Program TCAP, available from the Tesla Secondary Simulation Group as C source code. <http://www.abelian.demon.co.uk/tssp/model.html>. Accessed 01/23/2001.
- [Obe95] Oberbeck, A.: *Ueber den Verlauf der electrischen Schwingungen bei den Tesla'schen Versuchen*. Annalen der Physik und Chemie, Vol. 55, 1895.
- [Oka97] Okamura, K., Shimamura, H. & al.: *Development of a semiconductor switch for high power copper vapor lasers*. 11th IEEE International Pulsed Power Conference, p. 975 – 80, vol. 2, 1997.
- [Pal95] Palmer, P. R., Githiari, A. N.: *The Series Connection of IGBTs with Optimized Voltage Sharing in the Switching Transient*. 26th Annual IEEE Power Electronics Specialists Conference, pp. 44 - 49, vol. 1, 1995.
- [Pal96] Palmer, P. R., Githiari, A. N. & al.: *A comparison of IGBT technologies for use in the series connection*. IEE Power Electronics and Variable Speed Drives, Conference publication no. 429, p.236 - 41, 1996.
- [Pal97] Palmer, P. R., Githiari, A. N.: *The Series Connection of IGBTs with Active Voltage Sharing*. IEEE Transactions on Power Electronics, p. 637 – 44, vol. 12, no. 4, 1997.
- [Pal98] Palmer, P. R., Githiari, A. N.: *Analysis of IGBT modules connected in series*. IEE Proc. –Circuit Devices Syst., p. 354 – 60, vol. 154, no. 5, 1998.
- [Phi97] *U100/57/25 Product Specification*. Philips components, 21 Nov 1997.
- [Phi99] *3C90 Material grade specification*. Philips components, 23 Dec 1999.

- [Phu91] Phung, B.T., Blackburn, T.R. & al.: *Tesla Transformer Design and Application in Insulator Testing*. Seventh International Symposium on High Voltage Engineering, p. 133 – 36, vol. 5, 1991.
- [Pod91] Podlesak, T. F., Carter, J. L. & al.: *Demonstration of Compact Solid-State Opening and Closing Switch Utilizing GTO's in Series*. IEEE Transactions on Electron Devices, p. 706 – 11, vol. 38, no. 4, 1991.
- [Ree88] Reed, J. L.: *Greater voltage gain for Tesla-transformer accelerators*. . Review of Scientific Instruments, pp. 2300 – 2301, vol. 59, no. 10, October 1988.
- [Ric??] Rickley, M., Belling, M., Hitchcock, R. N., et. al.: *A large, 500 kV double resonant transformer for testing HV probes and HV resistor materials ???*
- [Roc77] Rockwell International Electronics Operations: *An electrical surge arrestor (ESA) model for electro-magnetic pulse analysis*. IEEE Transactions on Nuclear Science, vol. NS-24, December 1977.
- [Smy50] Smythe, W. R.: *Static and dynamic electricity*. McGraw-Hill, 1950.
- [Sne88] Snelling, E. C.: *Soft Ferrites Properties and Applications*. Butterworths, second edition, London, 1988.
- [Str90] Strickland, B. E., Garbi, M. & al.: *2 kJ/s, 25 kV high-frequency capacitor charging power supply using MOSFET switches*. Proc. 1990 19<sup>th</sup> Power Modulator Symp., pp. 531-534, June 1990.
- [Tak95] Takesuye, J., Deuty, S.: *Introduction to Insulated Gate Bipolar Transistors*. Motorola Semiconductor Application Note AN1541, 1995.
- [Ter43] Terman, F. E.: *Radio Engineers' Handbook*. McGraw-Hill, 1943.
- [Tes14] Tesla, N., *Apparatus for transmitting electrical energy*. Patent n. 1119732, 1 December 1914.
- [Tes78] Tesla, N., manuscript edited by Marincic, A.: *Colorado Springs Notes 1899-1900*. Nolit, 1978.
- [Tes91] Tesla, N., *System of electric lighting*. Patent n. 454622, 23 June 1891.
- [Tes94] Tesla, N., *Means for generating electric currents*. Patent n. 514168, 6 February 1894.
- [Uma87] Uman, M. A.: *The lightning discharge*. Academic Press, 1987.
- [Uni93] *Power Transformer design for Switching Power Supplies*. Unitrode Seminar Manual SEM900, Topic M5, rev. 7/86, 1993 (originally published in SEM100, 1986).
- [Wat96] Waters, R.T.: *The long spark and lightning simulation*. IEE Colloquium on Advances in HV Technology, pp. 4/1 - 4/3, no. 173, 1996.
- [Whe28] Wheeler, H. A.: *Simple Inductance Formulas for Radio Coils*, Proceedings of the I.R.E., Vol. 16, pp. 1398-1400, October 1928.